

41 0628840 6



426317

PHD/2004 TYL

ProQuest Number: 10183038

All rights reserved

INFORMATION TO ALL USERS

The quality of this reproduction is dependent upon the quality of the copy submitted.

In the unlikely event that the author did not send a complete manuscript and there are missing pages, these will be noted. Also, if material had to be removed, a note will indicate the deletion.



ProQuest 10183038

Published by ProQuest LLC (2017). Copyright of the Dissertation is held by the Author.

All rights reserved.

This work is protected against unauthorized copying under Title 17, United States Code
Microform Edition © ProQuest LLC.

ProQuest LLC.
789 East Eisenhower Parkway
P.O. Box 1346
Ann Arbor, MI 48106 – 1346

GROUND CONDITION MONITORING USING FRICTION GENERATED ACOUSTICS

TRISTAN TYLER

A thesis submitted in partial fulfillment of the requirements of The Nottingham Trent
University for the degree of Doctor of Philosophy

December 2004

Abstract	i
Acknowledgements	ii
Nomenclature	iii
List of Figures	iv
List of Tables	ix
1.0 Introduction.....	1
1.1 Aims and Objectives.....	3
1.2 Overview of the Thesis.....	3
2.0 Literature Review.....	7
2.1 Current Methods of Ground Investigation.....	7
2.1.1 Trial Pits.....	7
2.1.2 Coring and Bore Hole Techniques.....	8
2.1.3 Penetration Techniques.....	8
2.1.4 Seismic Simulation.....	10
2.1.5 Ground Penetrating Radar.....	10
2.1.6 In-Situ Testing: Parameter Summary.....	11
2.2 Classification of Soils and Physics of Granular Materials.....	11
2.2.1 Granular Packing.....	13
2.2.2 Particle Shape and Size.....	14
2.2.3 Granular Shear.....	15
2.2.4 Granular Compaction/Consolidation.....	18
2.2.5 Granular Flow.....	19
2.3 Friction.....	20
2.3.1 Surface Topography.....	20
2.3.2 Frictional Processes.....	21
2.3.3 Real Area of Contact.....	22
2.3.4 Wear.....	25
2.4 Granular and Solid Interactions.....	25
2.4.1 Friction of Smooth Particles at Solid Boundaries.....	25
2.4.2 Friction of Rough Particles at Solid Boundaries.....	26
2.4.3 Particle-Solid Friction for Particulate Assemblies.....	27
2.4.4 Geometric Relationships for Granular-Solid Friction....	29
2.4.5 Friction Involving a Rough Solid Surface.....	31
2.4.6 Friction Involving a Smooth Solid Surface.....	32
2.5 Acoustic Emission.....	32
2.5.1 Friction Generated Acoustic Emission.....	33
2.5.2 Parameters of Friction Generated Acoustics.....	34
2.5.3 Solid Acoustic Wave Guides.....	38
2.5.4 Wave Reflection and Transmission.....	39

2.5.5	Wave Propagation in a Cylinder.....	40
2.5.6	Analysis of AE and Acoustic Parameters.....	41
3.0	Experimental Development.....	43
3.1	Initial Experimental Development.....	43
3.1.1	The Drilling Mechanism.....	45
3.1.2	The Probe.....	45
3.1.3	The Signal-Coupling Device.....	49
3.1.4	Preparation of the Geotechnical Medium.....	50
3.1.5	The AE System.....	51
3.1.6	Data Acquisition System.....	51
3.2	Initial Investigations.....	53
3.2.1	Acoustic Signal Characteristics.....	54
3.2.2	Preliminary Experiments.....	55
3.3	Development of a New Experimental Test System.....	60
3.3.1	Probe Design.....	63
3.3.2	Probe Performance Investigation.....	65
3.3.3	Improvements of the Testing System.....	67
3.3.4	Standard Methods for Studying Granular Materials.....	71
3.3.4.1	Standard Shear Box Test.....	71
3.3.4.2	Ring Shear Test.....	75
3.4	AE and the Mechanical Parameters for Monitoring Friction	77
4.0	Theoretical Consideration.....	78
4.1	The Source of the Acoustic Emission.....	78
4.2	Relating the Acoustic Parameters to the Friction Pair.....	78
4.3	Summary Comments.....	86
5.0	Presentation of Results.....	87
5.1	Investigation of the Count Rate and the Acoustic Energy	89
5.2	Abrasive Paper: The Controlled Granular Medium.....	98
5.2.1	Abrasive Paper: Effects of the Applied Load.....	98
5.2.2	Abrasive Paper: Effects of the Sliding Velocity.....	105
5.3	The Steady State Count Rate and the Acoustic Energy....	109
5.4	Development of a Novel Signal Processing Technique...	112
5.5	Characteristic Count Rate Investigation.....	117
5.5.1	Effects of Particle Size and Type.	117
5.5.2	Effects of Particulate Water Content.	121
5.5.3	Using Different AE Systems.	123
5.6	Investigation of the Acoustic Energy.	130

Contents

5.6.1	The Effect of the Particle Size	131
5.6.2	The Average Energy Per Oscillation	135
5.6.3	The Effects of Density on the Acoustic Energy	138
4.6.4	The Effects of Water Content on the Acoustic Energy.....	141
5.7	Standard Shear Box Investigation.....	144
5.8	Ring Shear Investigation.....	147
6.0	Discussion.....	154
6.1	The Count Rate	154
6.2	The Acoustic Energy	161
6.3	The Frictional Properties of the Granular Material	165
6.4	Summary	169
7.0	Conclusions	171
7.1	Experimental Conclusions.....	171
7.2	Theoretical Conclusions.....	175
8.0	Further work.....	178
References	180
Appendix 1	Classification of Particle Size	
Appendix 2	Publications	

Abstract

The development of a novel technique used to characterise ground structures from the acoustic emission generated during a drilling process is presented. Existing ground evaluation techniques were investigated, providing an insight to the relevant parameters, which are useful to the engineer. The literature review considers areas of soil mechanics, granular physics, frictional interactions between solids and solid-granular interfaces as well as the acoustic emission associated with frictional mechanisms. The drilling process was simplified by using a rotating probe, which maximised surface interactions as well as reducing other frictional mechanisms associated with material removal and penetration depth. An experimental apparatus was developed, which consisted of a conical tipped rotating probe that was pushed into granular samples at a controlled feed rate, thus simulating a typical drilling process. The drill string acted as an acoustic wave guide and the acoustic signal was recorded using a suitable coupling device. Preliminary investigations were used to optimise the experimental apparatus for further investigations. Investigations focused on determining the effects that the applied load and sliding velocity had on the acoustic parameters. The effects of varying particulate density, particle size and water content were also considered. A series of standard soil investigation techniques have been conducted to provide information directly associated with the soil samples used in this study. Both peak shear and residual shear forces were considered and the analysis focused on varying grain size, density and water content. Frictional interactions between the probe-tip and different grades of abrasive paper were also considered. Results obtained from the abrasive paper investigations led to the development of an unusual thresholding technique which was used to determine a characteristic signal of the friction pair. Investigations identified a repeatable correlation between the characteristic signal and the average particle size. Further investigations highlighted that the acoustic energy could be used in conjunction with the characteristic signal to obtain more information about the granular material being investigated. Results presented in this thesis provide evidence that ultrasonic monitoring of drilling has potential for real time ground condition monitoring applications.

Acknowledgements

This study was carried out at the Nottingham Trent University from 2000 to 2004. I wish to express my sincere gratitude to the following co-workers.

I am deeply grateful to my Supervisors Dr Eugene Lai and to Dr Roger Hill, for the opportunity to study for this PhD. Without them, this thesis would have not been accomplished, especially Dr Eugene Lai who provided me with a lot of much needed critical advice especially in the final stages of writing this thesis.

I want to thank Professor Glen Mc Hale, Dr Mike Newton and Steve Elliot from the Department of Physics and Chemistry for their support while I was based in their department.

I am deeply grateful to Judith Prest, from the Department of Civil Engineering for her help with using the laboratory equipment, and the regular cups of coffee she made during many hours of tediously sieving sand.

I would also like to thank my fellow researchers, Dr Simon Stanley, Dr Nahn Pham, Dr Fabrice Martin, Rebecca Clinton, Jo Wint, Andy Taylor and Ken O'hara, who provided support, advice and friendship throughout my study.

I would like to thank all the staff at Nottingham Trent University who have been involved with helping me carry out my research.

Finally, I express my sincere thanks to my partner Kara for her, support and understanding as well as my two sons Charley and Sam who provided much needed love and happiness throughout my studies.

Nomenclature

A	Signal amplitude
a	Radius of contact spot
A_a	Apparent area
AE_{RMS}	Root-mean-square of the acoustic signal
A_r	Real are of contact
α	Friction angle
D	Contact modulus
D_{50}	Mean particle diameter
ϵ	AE pulse energy
e_e	Elastic potential energy
F	Total applied force
F_c	Force at a single asperity contact
F_f	Frictional force
h	The closeness of two elastic bodies in contact
\dot{N}_{AE}	Count rate
N_c	Number of asperity contacts
N_p	Number of acoustic pulses generated by a single asperity interaction
η	A Function of surface roughness
θ_i	Incidence angle
θ_r	Reflection angle
P	Pressure
δp	Mean contact pressure
R	Particle radius
R_a	Particle roundness ratio
R_n	Normalised roughness
R_p	Reflection coefficient
s	Spacing parameter
τ	Interfacial shear strength/Radiation time
τ_0	Intrinsic shear strength at no load
T_p	Transmission coefficient
v	Sliding speed
ν	Poisson's Ratio
Z	Acoustic impedence

List of Figures

- Fig 1. Two surfaces during sliding friction.
- Fig 2. Two spherical bodies in contact pressed together by an applied force (a) before loading and (b) is during loading.
- Fig 3. Square packing arrangement.
- Fig 4. Geometrical relationship for the normalized roughness and the particle roundness ratio
- Fig 5. Geometric relationship for the friction angle α
- Fig 6. Schematic diagram of the initial probing system.
- Fig 7. An illustration of the interaction between the probe and a granular material.
- Fig 8. A cross section of the probe, with the insulating sleeve and coupling joint.
- Fig 9. The acoustic signal-coupling device, displaying half a cross section.
- Fig 10. Data acquisition arrangement.
- Fig 11. A typical example of the raw acoustic signal generated from the probe-granular interaction.
- Fig 12. An example of the un-submerged probe's acoustic signal (Noise) and the submerged probe's acoustic signal (signal)
- Fig 13. The variation of the acoustic RMS signals during probe penetration using granular samples of varying grain size.
- Fig 14. Applied load variation during probe penetration using granular samples of varying grain size.
- Fig 15. The acoustic RMS signal against the applied load for a continuous probing penetration to a depth of 50mm using granular samples of varying size.
- Fig 16. Diagram summarising the required improvements to the experimental system.
- Fig 17. Three probe designs used for experimentation

List of Figures

- Fig 18. Two new designed probes with different apex angles. Probe velocity 8Hz (Granular particle diameter 655E-6).
- Fig 19. Variation of AE signal energy against the load using the multi-tip probe. Probe velocity 8Hz (Granular particle diameter 655E-6).
- Fig 20. Schematic diagram of the improved experimental arrangement.
- Fig 21. Experimental arrangement using abrasive paper as an alternative to granular materials.
- Fig 22. The principle of a shear box test.
- Fig 23. Illustration of the relationship between the shear stress and displacement in a shear box test for three different loads.
- Fig 24. An Illustration of the functional relationship between the peak shear stress and the normal stress using results from a shear box tests (Coulomb envelop relationship).
- Fig 25. A ring shear apparatus, (a) displays a cross section of the ring sample box, (b) displays a top view of the ring shear
- Fig 26. The change in the acoustic signals due to an increase in the applied vertical load using Leighton Buzzard sand (655 μ m average particle diameter) and a rotational sliding velocity of 7Hz , a) the count rate, b) the acoustic energy.
- Fig 27. The count rate against the vertically applied load for four different rotational velocities. Data considers full probe particle contact from an initial depth of 30mm.
- Fig 28. Acoustic energy against vertically applied load for four rotational velocities using Leighton Buzzard sand (655 μ m average particle diameter).
- Fig 29. Acoustic energy against count rate for four different rotational velocities using Leighton Buzzard sand (655 μ m average particle diameter).
- Fig 30. Acoustic energy against count rate, for four different grain sizes. Leighton Buzzard sand samples, rotational velocity set at 6.5Hz.
- Fig 31. Count rate against applied vertical load using P1200 abrasive paper for four angular velocities.

List of Figures

- Fig 32. Count rate against applied vertical load using P1200 abrasive paper for an angular velocity of 10Hz.
- Fig 33. Count rate against applied vertical load using P800 abrasive paper for four different angular velocities.
- Fig 34. Count rate against applied vertical load using P400 abrasive paper for two different angular velocities.
- Fig 35. Acoustic energy against count rate using three grades of abrasive paper and 4 sliding velocities.
- Fig 36. Count rate against angular sliding velocity using P400 abrasive paper for three constant vertically applied loads.
- Fig 37. Acoustic energy against count rate using P400 abrasive paper for three constant vertically applied loads.
- Fig 38. Acoustic energy and count rate against vertically applied load for a single penetration into the test sample of 50mm at 5mm/min feed rate. Leighton Buzzard sand particle size 850-1000 μ m.
- Fig 39. Acoustic energy and count rate against vertically applied load for a single penetration into the test sample of 50mm at 5mm/min feed rate. Leighton Buzzard sand particle size 850-1000 μ m.
- Fig 40. An example of the signal generated by the probe-granular interaction for a time period of 20 μ s sampling at 1.5GHz using a 250-500 kHz band pass filter.
- Fig 41. An example of an un-submerged probe's acoustic signal (noise) and a submerged probe's acoustic signal (signal). Data shown for a time period of 20 μ s sampling at 1.5GHz using a 250-500 kHz band pass filter.
- Fig 42. The effects of varying angular velocity on the count rate for a submerged probe (friction generated signal) and an un-submerged probe (system noise).
- Fig 43. Count rate against applied load for the Leighton Buzzard sand samples at an angular sliding velocity of 8Hz.
- Fig 44. Count Rate against applied load for the Sharp sand samples at an angular sliding velocity of 8Hz.

List of Figures

- Fig 45. Average characteristic count rate against average particle size for the sharp sand and Leighton Buzzard sand samples.
- Fig 46. Count rate against vertically applied load using compacted and loose granular samples at an angular sliding velocity of 8Hz
- Fig 47. Count rate against water content for different particle sizes of sharp sand.
- Fig 48. Count Rate against vertically applied load using a lower frequency narrow band-pass system (125-250 kHz) for sharp sand granular samples.
- Fig 49. Average characteristic count rate against average particle diameter using sharp sand of graded particle size for two band-pass frequency ranges.
- Fig 50. Characteristic count rate against particle size for three band-pass filter settings, using sharp sand samples
- Fig 51. The variation of signal amplitude for two band-pass filter settings.
- Fig 52. Count rate against vertically applied load using the broadband BN225 transducer and sharp sand granular samples.
- Fig 53. Average characteristic count rate against average particle size, using the broadband BN225 transducer, and sharp sand granular samples.
- Fig 54. Acoustic energy against applied vertical load using Leighton buzzard sand samples a 375 transducer and a 250-500kHz band pass filter.
- Fig 55. Acoustic energy against applied vertical load for sharp sand granular samples a 375 transducer and a 250-500 kHz band pass filter.
- Fig 56. The change of acoustic energy due the applied load against average particle diameter for two types of granular material.
- Fig 57. Average oscillation energy against average particle contact force for sharp sand granular samples (375 transducer, frequency range 250-500kHz).
- Fig 58. Average oscillation energy against the average particle contact force, using Leighton Buzzard granular samples (375 transducer, frequency range 250-500kHz).

List of Figures

- Fig 59. The contact energy functions against the average particle diameter, for both sharp sand samples and Leighton Buzzard sand samples.
- Fig 60. Acoustic energy against applied load, for sharp sand with an average particle size of 256 μ m.
- Fig 61. Average particle size against the characteristic count rate for compacted and loose granular samples of sharp sand.
- Fig 62. Average oscillation energy against estimated average contact force, for sharp sand samples with an average particle size of 256 μ m.
- Fig 63. Average particle diameter against the average characteristic count rate using samples of sharp sand with varying water content.
- Fig 64. Average acoustic energy per oscillation against average estimated contact force, for sharp sand with an average particle diameter of 655 μ m.
- Fig 65. The contact energy function against the water content using a range of different sized granular samples.
- Fig 66. Shear stress against the linear displacement using a standard shear box, for a 256 μ m particulate sample having 12% water content.
- Fig 67. Friction angle and contact energy function against the water content for two samples of sharp sand with different particle diameter.
- Fig 68. Residual shear friction angles against the average particle diameter data shown for wet and dry samples of sharp sand and Leighton Buzzard sand
- Fig 69. The average count rate against the applied vertical load using a ring shear experimental apparatus, for Leighton buzzard sand samples.
- Fig 70. The average count rates against applied vertical load using a ring shear experimental apparatus, for Leighton buzzard sand samples.
- Fig 71. Average oscillation energy against the shear force using sharp sand samples in a ring shear machine.
- Fig 72. Average oscillation energy against shear force using Leighton Buzzard sand samples in a ring shear machine.

List of Tables

- Table 1. Comparison of the surface roughness values before and after testing using the three new probes.
- Table 2. A comparison of the power law and linear relationships, showing the mean average error and the R^2 values for each trend line.

1.0 Introduction

In Civil Engineering, knowledge of the ground structure and condition is essential for many engineering applications. Ground investigation provides a range of information on which to base proposals for the design and construction of structures. It is also common for ground or embankment structures to suffer from long-term degradation, especially those subjected to dynamical loading in the case of a rail track bed or the foundations of a highway bridge. The existence of material degradation highlights the necessity for ground condition monitoring as a method to effectively predict potential failure [1].

If a simple drilling operation of a geotechnical structure is considered, it is perceptible that the frictional characteristics between the drill tip and the soil structure at a known depth could correspond to changes in the soil structure. Acoustic monitoring of friction pairs is known to provide a sensitive method for determining changes in frictional mechanisms and is a popular condition monitoring tool for many industrial processes involving solid-solid friction pairs [2]. The solid-granular interaction that occurs at the drill tip generates ultrasonic strain waves that will propagate along the drill shaft. The drill shaft would act as a solid acoustic wave guide and is considered to have non-degrading acoustic characteristics. Therefore, monitoring the ultrasonic emission developed by a drilling process may provide a sensitive tool to determine the parameters of the granular material being drilled at a known depth and could provide a novel methodology for ground condition monitoring. This thesis presents a study concerning the sliding frictional interactions between solid and granular surfaces, the generation of acoustic emission caused by these friction pairs as well as providing experimental evidence that could lead to the development of a novel real time technique for

characterising ground structures using the ultrasound generated by drilling interactions. The research considered here arises from fieldwork carried out by Hill [3] where it became apparent that acoustic monitoring of drilling had potential for ground condition monitoring. However, the technique was underdeveloped and this study discusses the progress made towards using ultrasonic monitoring of drilling and assesses its potential as a viable future alternative to current ground evaluation techniques.

Attention was focused on the physical contact between individual granular grains and a flat solid surface in order to develop an understanding of the source of the ultrasonic emission. The parameters related to the mechanical deformation at the points of actual contact were studied with the aim of establishing the effect that these parameters might have on the generated ultrasonic signal.

The experimental development involved simplifying a drilling process so that the parameters relating to sliding friction between solid-granular interfaces could be investigated. Due to the complexity involved with drilling interactions the drill was replaced by a rotating probe, which provided a uniform and stable contact area between the probe and the granular material. The probe was pushed into various granular samples at a controlled feed-rate thus simulating a typical simplified drilling process. Experimental research involved studying and optimising the ultrasonic signal generated between the probe and the geotechnical material being probed, as well as developing an understanding of the parameters that directly influence the ultrasonic signal such as the applied load or rotational speed. Controlled geotechnical media were studied to determine how changes in the friction pair affected the acoustic emission (AE) signal. The acoustic signal generated might be described as acoustic, ultrasonic (although this

really relates to the monitoring frequency used) or perhaps acoustic emission, (although this form of AE does not conform to the usual definition). These terms will be used interchangeably throughout this thesis.

1.1 Aims and Objectives

The main aim of the project is to develop a novel method for characterising ground structures using the acoustic emission generated during drilling interactions. To achieve this aim the following objectives have been set:

- Research methods of characterising ground structures.
- Identify the parameters associated with ground structures, which are useful to the engineer.
- Develop an experimental rig for the investigation
- Define suitable acoustic parameters and the techniques used to analyse them.
- Understand the physics behind the generation of the AE.
- Investigate the parameters that affect the generated acoustic signal.
- Develop empirical correlations relating the AE to the parameters of the ground structure.

1.2 An Overview of the Thesis

The thesis begins with a review of existing techniques, which are used to characterise ground structures and will form a base on which to identify the relevant parameters that are of interest to the engineer. Attention is focused on the various types of ground evaluation procedures that are used, the parameters investigated as well as highlighting the advantages and disadvantages of each technique. Using the information obtained

from the review allowed the focus of this investigation to be associated with the parameters that are of practical use to the engineer.

A review of laboratory techniques used to classify soils will be presented to highlight the number of parameters that exist as well as developing an understanding of the physics surrounding granular materials. The review will discuss the principal physical characteristics of soil particles that determine their classification including the effects of the individual particle's physical characteristics on complete soil systems. The particle packing density and soil saturation will also be addressed particularly focussing on their effects on the soil strength parameters, considering both shear and compression forces.

The novel technique considered here simulates a typical drilling process and the AE is due to the interaction between the drill tip and the granular medium at the depth of penetration. The AE occurs as a result of the frictional interactions between the surface asperities of the drill tip and the granular particles that it is in contact with. A review addressing the physics of frictional contact is presented to provide an understanding of the physical interactions that occur during sliding friction, which produces AE. Surface topography is discussed highlighting that contact only occurs at asperity interactions and that the real area of contact is small compared to the apparent area of contact. Discussion will be focused on the asperity contacts, their deformation, which as a consequence leads to the generation of acoustic emission.

Friction between solid surfaces and granular surfaces are investigated to provide an overview of the frictional characteristics that occur at these interfaces. The investigation considers the parameters associated with granular materials and how they relate to the

frictional properties concerning a granular-solid interface. The behaviour of granular particles at the solid-granular boundary is discussed, which helped optimise the frictional interaction between the drill-tip and the granular material.

The applications of using AE are considered in order to provide an overview of how AE has become a popular and useful tool in many NDT techniques. Attention was focused on friction generated acoustic emission, such as condition monitoring techniques, which has more relevance to the AE considered in this study. The aim was to provide an understanding of the physical parameters that play an important role concerning friction generated acoustics.

The development of an experimental rig, the method of recording the acoustic signal and the acoustic parameters used is described. Preliminary investigations were carried out to test the performance of the probing system; investigate the typical data trends recorded and highlight any areas of concern which were used for experimental redevelopment. The data obtained from these investigations helped improve the experimental arrangement for further in-depth investigations. Standard laboratory experimental techniques were done to provide information relating to the soil properties of the test soil samples used in this investigation.

A theoretical discussion is also provided relating the acoustic emission to the frictional contact. The discussion is based on existing models associated with solid-solid friction pairs and an attempt to relate these models to solid-granular friction pairs is provided. These models were later considered during the discussion of the experimental results.

The experimental results focus on the effects that the applied load and the sliding velocity had on the acoustic emission. Changes in the particle size and the packing density were investigated as well as variations in saturation level of the granular material. The results highlight a novel thresholding technique that was developed, which provided a method for differentiating between granular samples of varying grain size. Using the estimated particle size and geometry it was possible to investigate the average contact force and provided a sensitive method of identifying changes in the granular particle size. An evaluation of using acoustic monitoring of drilling interactions as a potential tool for identifying changes in soil structures is discussed.

2.0 Literature Review

The aim of the literature review was to provide a methodical and structured approach for an investigation relating to the acoustic emission generated during drilling interactions.

2.1 Current Methods of Ground Investigation

Ground investigations are usually in-situ although some investigations are carried out within a laboratory on the soil samples collected from the site investigation. The aim of a site investigation is to gather information regarding the ground condition and evaluates any potential problems that may be encountered during both the construction and life of the project. The following sections provide an overview of the in-situ techniques used by engineers and highlight the relevant parameters that are of interest to the engineer.

2.1.1 Trial Pits

A trial pit provides a simple but effective method of identifying shallow ground conditions. The pit is produced typically by an excavator and can determine ground condition up to 4m below the ground level. Advantages of this method include simplicity, speed and cost. The disadvantages include the difficulty in producing pits lower than the water table due to the instabilities generated by saturated granular flow and therefore only shallow ground conditions can be determined. Trial pits allow a physical examination of the soil where strata type and thickness can be determined as well as enabling the procurement of soil samples for further laboratory testing. The trial pit also allows further in-situ tests to be carried out including coring as well as the

installation of instruments including for instance piezometers or extensometers that are used for other methods of ground evaluation [4].

2.1.2 Coring and Bore Hole Techniques

In coring, a tubular cutter is used to extract a physical sample of the soil for detailed examination. The test cores are taken over small depths and the soil samples are retained within the cylinder for laboratory analysis. During this sampling procedure a degree of mixing is inevitable and changes in the strata type are only considered accurate within a 0.1m range. The samples taken are usually referred to as disturbed samples but for cohesive fine-grained soils the level of disturbance is small and are usually considered undisturbed. Coring is an accurate technique and produces less soil disturbance than trial pits. Coring can also provide undisturbed samples (cohesive fine grained soil) for detailed laboratory analysis to determine other parameters such as shear strength and permeability. However, in-situ examination is usually used to determine strata type and thickness [4, 5].

2.1.3 Penetration Techniques

There are two common forms of penetration techniques, the standard penetration test (SPT) and the cone penetration test (CPT). Penetration techniques investigate the general soil characteristics by measuring the change in the shear resistance of the soil at different depths to determine the thickness and lateral extent of various strata. The shear strength and compressibility may also be estimated while checking the density of ground fills. The SPT is mainly used to estimate the relative stiffness and bearing capacity of a soil as an empirical function of the penetration resistance, which is measured by counting the number of controlled blows for a probing rod to reach a

specified depth. Using predetermined empirical correlations, the deformation of granular soils and the shear strength of cohesive soils can be estimated. However, the quality and reliability of the test results depend upon the experience of the operator [4]. The CPT is a further development of the SPT and consists of a steel rod with a conical tip (apex angle 60° and a diameter of 35.7mm) that is pushed into the ground at a rate of 20mm s^{-1} . The diameters of the cone and the rod are the same with the penetration resistance at the tip of the cone and the sleeve-friction along a section of the shaft being measured. Both the shear resistance and the sleeve-friction are used to determine the soil profile, type and bearing capacity using empirical correlations. This technique provides a rapid method of determining soil structure, but the cone tip only responds to changes in the soil structure within 5-10 probe tip diameters above and below the cone tip, which can lead to some imprecision in locating soil interfaces. Further developments of the CPT incorporate a pore water pressure sensor to help determine any soil saturation and hydraulic properties of the soil including permeability and conductivity [6]. In practice CPT and SPT are usually used as an intermediate profiling tool between a number of strategically placed bore holes. The results collected from the bore holes are correlated with the results obtained using the penetration technique, both of which improve data interpretation. Bore hole data is also used to investigate the ground layers of low resistance where penetration techniques usually fail, as well as exploring below the depths that are attainable by penetration techniques [4]. CPT results are essentially based on empirical correlations although research is available involving theoretical and finite element approaches for determining shear properties of soils [7, 8]

2.1.4 Seismic Simulation

There are many methods of seismic investigations but a common method (seismic reflection method) utilises a seismic source (a sudden impact or a vibration generator) and vibration sensors that are mounted on the ground surface. The propagation time of the seismic wave is monitored to allow the determination of the shear wave velocity using the phase information for each frequency contained within the waveform. The wave velocity can be recorded up to depths of 20m and a large volume of soil can be investigated rapidly. The change in wave velocity can give an indication of the soil properties or changes within the soil strata, as different host materials will change the seismic wave propagation speed. However, the seismic data is usually correlated with borehole data to improve the interpretation of the results and therefore, seismic simulation is mainly used as a profiling tool [4].

2.1.5 Ground Penetrating Radar

In ground penetrating radar (GPR) electromagnetic energy is transmitted through the ground at typical frequencies between 1-2500 MHz and has the capability of monitoring depths up to 30m. Signal interpretation can either be done simplistically using first arrival time analysis although other complex methods are available involving spatial distributions of the velocity attenuation fields. Grandjean [9] provided an extensive evaluation of current GPR techniques used in civil engineering applications and compared many different signal analysis methods for a single site investigation. GPR is generally used as a profiling tool in conjunction with bore holes (to aid image interpretation) and can identify changes in soil strata (providing there is sufficient contrast between the soil layers) as well as identifying large bodies such as boulders, landmines [9, 10] and tunnels [11]. GPR has also been investigated as a tool to monitor

root systems, which have been reported to have a direct effect on the strength of soil structures [12].

2.1.6 In-Situ Testing Parameter Summary

The main aim of a site investigation is to identify the soil types, where changes in the soil strata occur and hence the structural strength of the soil. Bore holes and coring techniques provide the most reliable method of identifying the soil types that are present within the ground. However, producing many of these holes can be time consuming, expensive and causes further disturbance to the natural soil structure. Therefore, profiling techniques are used in conjunction with a number of strategically placed boreholes to provide an indication of how the soil layers change in-between them. A profiling tool provides a method of identifying the changes in the soil layers. However, identifying changes in a soil structure can be a difficult task as many natural factors can affect the physical properties of the soil such as random soil density, saturation levels and vegetation roots, which highlight the necessity for borehole data. Other parameters such as shear strength are usually carried out on undisturbed samples in a laboratory although the bearing capacity is usually evaluated in-situ using a penetration technique as the bearing capacity is dependent on the in-situ conditions.

2.2 Classification of Soils and Physics of Granular Materials

For Civil Engineering purposes a soil can be described as any loose sedimentary deposit as the organic matters (a geologist's definition of soil) are usually removed before any ground investigation is carried out. The principal characteristics of a soil are the particle size distribution and the plasticity, which are typically classified according to the British standard 5930 [13]. The basic soil types are: gravel, sand, silt and clay classified in

terms of their particle size distribution, (Appendix 1). Other parameters used to classify a soil include, geological origin, mineral content. These properties describe the characteristics of the individual grains, but engineers will require information relating to the behaviour of a complete soil structure.

Soil systems are essentially composed of an assembly of grains that interact through frictional contact. The spaces in-between the grains are voids and in a typical soil structure the voids are filled with water (fully saturated), air (completely dry) or a mixture of both (partly saturated) and these conditions are referred to as the phase characteristics of the soil [14]. The packing density, particle size and particle shape govern the void spaces within a soil structure and the random nature associated with particle sizes and shape can cause an unpredictable network of particle contacts to occur within the soil structure. The behaviour of particle-particle contacts and particle boundary contact can affect the strength of the soil as well as other factors such as the confining pressure. Therefore, many parameters of the soil can influence the soil strength including the particle size, shape, surface roughness and particle composition, in addition to packing density, soil phase characteristics and boundary conditions. The deformation of soil is usually in the form of shear or consolidation but the nature of the deformation is largely dependent upon the state and condition of the granular system being deformed. Granular materials can seem very simplistic but modelling such materials is very complicated due to their unusual physical properties, as a granular material can have either solid-like or fluid-like characteristics depending upon the boundary conditions and the incidence of external forces such as vibration or gravity. Every granular system has unique behavioural properties due to random composition of particle assemblies. The limited understanding of such systems means granular physics

remains as an area for further research. The following sections will provide a review of the important features relating to granular parameters although, a detailed description regarding the soil mechanics involved will not be presented.

2.2.1 Granular Packing

Jaeger et al [15] states that a fundamental issue concerning granular systems is the packing arrangement of the grains. The volume fraction of a filled container can fluctuate considerably due to the random packing arrangement of the grain structure. Jaeger highlights that each configuration of a particle ensemble has its own unique properties and the efforts needed to reproduce a similar granular structure on a large scale is complex, especially when approaching the static limit where inter-granular friction plays a major role. Kwan and Mora [16] analysed the shape characteristics of aggregate samples and evaluated the effects of different shape classification parameters (see also section 1.2.2) on the packing density. Their results suggested that the shape factor and the convexity ratio are the two most important shape parameters, which can affect the packing density.

Granular materials form a stable condition when constrained by rigid boundaries such as container walls or neighbouring grains. Therefore the physical condition of a granular mass can only change by the application of an external force: vibration, compression or shear. A change in temperature has a negligible effect on granular materials meaning any thermo dynamic effects can be ignored. For densification of granular materials to occur, co-operative motion of other grains is required to allow a space for a new grain to slide into place, assuming no granular crushing takes place. Another unique property of granular assemblies is that vertical pressure due to gravity is not height dependent. This

is due to particles at lower levels supporting the particles above them as a result of a bridge forming between the boundary walls and a network of inter-connecting particles [15]. Vanel and Clement [17] measured the pressure distribution at the bottom of a granular column and discussed the heterogeneous and anisotropic character of the force network due to inter-granular contact geometry as well as the frictional properties of these forces.

2.2.2 Particle Shape and Size

The size and shape of the particles are not uniform (spherical or ellipsoidal) and will have a direct effect on the granular packing. The randomness of the particle shapes requires that a suitable method of classification is needed to quantify the general shape characteristics. The shape of a particle can be characterised in terms of the overall shape, roundness and the surface texture. The overall shape is defined by a ratio of three main dimensions, length, breadth and depth. The roundness involves two aspects: the roundness of the corners and the roundness of the outline of the particle. The roundness of the corners is considered important when dealing with the abrasive properties of the grains and is commonly associated with the grain sharpness, while the roundness of the particle outline is measured in terms of its convexity [16].

Particle size is usually a statistical measure of the particle size distribution of a soil sample and the distribution characteristics will have an effect on the packing density. Distribution curves illustrate the range of particle sizes within a particular soil sample and the size fractions of coarse particles are determined by sieving while fines are determined using Stoke's law of settlement [14]. Silty sands tend to have finer particles trapped between the voids of the larger particles thus creating a much denser material

(although a level segregation usually occurs), which explains why the particle distribution dramatically affects the packing of a granular system.

2.2.3 Granular Shear

The following section covers a brief review of granular shear, highlighting the effects of the multiple soil parameters on the shear strength of a granular material/soil. The shear strength of a soil may be defined as the maximum resistance of soil to shearing stress under any given conditions. Many factors can affect the shear strength of a soil such as grain size, shape, packing arrangement and pore-water pressure (which is directly related to the effective stress) [18]. For shear to occur it is common for the soil to dilate allowing a shear plane to develop, although dilation can be minimised by grain breakage [19]. The packing density determines whether or not a granular material will compact or dilate during shear. Loose granular materials have a tendency to initially compact during shear and dense materials will dilate [20]. In general it is conceived that increased density produces a higher shear resistance due to an increase in inter-granular contacts at the slip plane [21].

A sheared granular material displays a phenomenon termed banding, which involves a weak zone that develops within the granular material where the deformation (shear) is concentrated over a length of a few particle diameters [22]. The concentration of the deformation yields a plug effect that is seen as a displacement of a block where little or no movement occurs between the particles within the block [15]. The development of a shear band occurs after the peak failure of the granular sample and is analogous to the static friction coefficient of a sliding solid [23]. The friction angle of a shear band is referred to as the internal coefficient of friction and is usually determined using the well

known Coulomb relationship, which expresses proportionality between the shear stress and the normal stress. Shear test results presented by Schellart [24] highlight non-linear behaviour for low stresses and a linear relationship (Coulomb relationship) for larger stresses. Atkinson [25] focused on the non-linear soil stiffness and highlighted the fact that in order to characterise the non-linearity, it is necessary to consider both the stiffness strength and the strain at failure. Wolf et al [26] monitored the shear band patterns developed in a shear box experiment using x-ray investigation techniques and provided evidence that the shear band pattern develops in the early stages of shear and even at high strains no further shear bands occur.

Jewell [27, 28] investigated the effect of different boundary conditions (governed by the dimensions of a shear box) had on the measured results of a shear test and discussed the practical implications of using direct shear tests. Lade [23] states that the soil strength is primarily proportional to the confining pressure, i.e. the soil strength is related to the environment of the soil sample and has a dependency on the boundary conditions. Pouliquen and Chevoir [29] investigated a variety of shear regimes using different boundary conditions for a range of applications and showed that granular shear is sensitive to many parameters including shear flow geometry, wall roughness, flow-rate and pore-water pressure.

It has already been mentioned that particle shape and roughness characteristics have a significant effect on the strength properties of the soil. Tholen [30] used transmission electron microscopy to investigate the finer details of particulate adhesion contacts by monitoring the stress fringes at adhesion contacts as well as the particle surface and subsurface deformation. Schellart [24] suggested that the coefficient of internal friction

is mainly dependent on the sphericity and rounding of the individual grains and less dependent on the grain size. The shear force also induces a rotation of the grain along the shear plane as well as particle translation. The velocity of the moving grains reduces with increasing distance from the shear plane and movement is due to the stick phase incurred by stick slip friction [31]. Bocquet et al [32] studied the shear flow dynamics and highlighted that low shear rates induce short rapid slip phases while high shear rates cause steady sliding with reduced sticking phases.

Yoshida et al [33] studied the effects of the soil saturation ratio (a ratio between the volume of voids and the volume of water of a given soil sample) on the shear strength of soil. Results indicated that the internal friction and cohesion coefficients decrease significantly with increasing saturation; the reduction in deviatoric stress due to saturation was also dependent on soil type and density. The effective stress in partly saturated soil is affected both by the pore water pressure and pore air pressure. Later work by Kumar and Prakash [34] highlighted an increase in granular cohesion with water contents up to 6% while a reduction occurred between 6% and 20% water content and stated that pore fluid initially promotes hydrogen bonding between particles. Results also indicated that no definite relationship existed between the friction angle and the water content.

An important issue concerning granular materials is the large number of non-linear variables that interact with each other such as grain size, shape and packing density. The difficulty of understanding the behaviour of granular systems has led to many different modelling. Deregeas and Joserand [35] presented a model to describe steady state shear flows using the motion of granular clusters and stress distribution caused by granular

sliding friction. Chang et al [36] considered the mechanism of sliding and separation of particles under large deformation. The model considered non-linear strain fields, particle rotation and the interlocking of grains, which was assumed to contribute to a large portion of the shear strength. Models relating to other granular characteristics as a result of granular shear such as dilatancy [37, 38] cluster formation [39, 40] and the non-linear irreversible behaviour of dense sands [41] have also been developed. The multivariate problems encountered within geotechnical engineering have seen research directed to the use of neural networks and finite element methods, in an attempt to provide a simpler approach to identifying soil characteristics [42, 43].

2.2.4 Granular Compaction/Consolidation

Granular compaction refers to the process involved in physically changing the density of a granular sample by the application of an external force. Consolidation refers to the natural settlement of soil structures caused by natural variations in the inter-particle stresses due to environmental changes. Compaction is an important process when trying to improve the strength of a granular medium, as denser granular materials inherit a larger shear resistance. Compaction or consolidation can occur through two main procedures: granular rearrangement and granular breakage. For granular rearrangement to occur a number of grains would have to move a small distance and the combination of each grain's movement would allow a new grain to fill the space developed in the granular plane. Josserrand et al [44] investigated densification due to induced vibrations and stated that the change in density from an initial time depended on the history (the number of induced vibrations during a specific period of time). Therefore, the rate of compaction would be a function of the granular system's initial density. McDowell [19] studied the mechanical behaviour of crushable soils stating that the tensile stress of the

particles govern the compaction characteristics. The fracture of individual particles was monitored and the results highlighted that larger particles inherited larger grain tensile strength and suggested that the grain tensile strength was a function of the particle size. It was also noticed that for a one dimensionally compressed sand (compressed under uniaxial load), classic yielding occurred to be followed by a region of plastic hardening where the stress applied to the sample must increase for further compaction to occur. Snoeijer et al [45] focused on the packing geometry and the force networks that are produced through a granular material. A granular material under compaction causes the grains nearest the applied force to form a denser state until they become jammed, which consequently transfers some of the applied force to the next layer of particles. However, not all the grains in each layer carry an equal amount of the applied force, leading to complex network of forces, which are distributed throughout the granular material.

2.2.5 Granular Flow

Adams [46] described two types of flow regimes when considering granular dynamics: rapid flow and quasi-static flow. During rapid flow, inertia effects dominate and energy dissipation occurs via particle collisions and is accounted for using a coefficient of restitution. Quasi-static flow concerns a denser array of particulate material, which transmits stresses through an assembly of particle-particle contacts. Therefore, the friction at these contact points profoundly influences the behaviour of the particulate assembly.

2.3 Friction

Amontons and Coulomb developed the first friction laws in the early 17th Century [47]:

- Frictional force is proportional to the applied load.
- Frictional force is independent of the body contact area.
- Frictional force acts in the opposite direction to the relative sliding velocity.

Although these relationships hold for many engineering applications there are many cases where this is not so [48]. Singer [49] provided an in-depth review of the current methodologies of investigating asperity contact and energy dissipation during friction and highlighted many different approaches for studying frictional mechanisms.

2.3.1 Surface Topography

Most materials when observed on a macroscopic scale will have rough surface characteristics. The roughness is due to the existence of surface asperities, which can generally have slopes in the range of 5-10 degrees [50]. The surface profiles are quantified by a surface roughness parameter, calculated by determining the mean deviation from a flat reference line. The existence of surface asperities of two bodies in contact permits two descriptions of contact area: the apparent area of contact and the real area of contact. The dimensions of the body in contact define the apparent area of contact, while the number of interacting asperities and their associated contact areas define the real area of contact.

2.3.2 Frictional Processes

A common method of describing friction is based on the idea of asperity interactions, which considers the formation and destruction of micro/macro contacts. Figure 1 shows two surfaces during sliding friction. Surface two is stationary and surface one is allowed to slide over the top of surface two. The diagram highlights how the area of real contact is a small fraction of the apparent area.

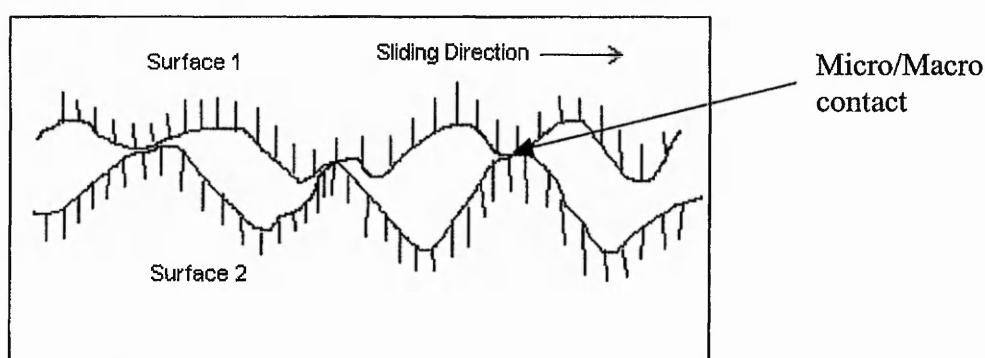


Fig 1. Two surfaces during sliding friction.

The three main stages of asperity interactions are:

1. Adhesive bonding between asperities of the materials in contact.
2. Elastic deformation followed by plastic deformation resulting in shearing or ploughing of the softer surface.
3. Shearing of junctions followed by elastic recovery.

Deformation of asperities generates a contact area that is dependent on the applied load. Sphere and flat surface experiments conducted by Tabor [48] showed that the geometric area deformed plastically under load. The deformation was said to be uniform and that

the area of real contact was proportional to the applied load. The frictional force generated due to sliding is described in the following form:

$$F_f = \tau A_r \quad (1)$$

Where F_f is the frictional force, τ is the interfacial shear strength and A_r is the real area of contact. The three stages of friction discussed earlier would result in characteristic stick-slip behaviour. Adhesive bonding and the elastic/plastic deformation of the contacting asperities generate the stick phase, while the slip phase results from the destruction of the asperity bonds causing a macroscopic slip phase.

2.3.3 Real Area of Contact

The real area of contact is determined by the interaction of contacting asperities between two solid bodies. Therefore, the real area of contact is a function of the number of asperity contacts and the summation of their individual contact areas. Hertz (1882) originally solved the contact problem of two homogeneous and isotropic solid bodies in contact at a single point. A full discussion of a Hertzian contact can be found in the book by Landau and Lifshitz [51]. A general description of Hertzian contacts will be considered here, as this is important when discussing the parameters of acoustic emission. Hertzian contact involves two spherical bodies in contact with radii R_1 and R_2 (Figure 2a), pressed together by an applied force. Deformation will occur symmetrically around the original point of contact and produce a finite contact area over a proportion of their surfaces. Producing this contact area has also produced a linear displacement, h , which is the distance between the undeformed outer surfaces of the solid bodies, assuming no deformation has occurred and both bodies move into each other (Figure 2b).

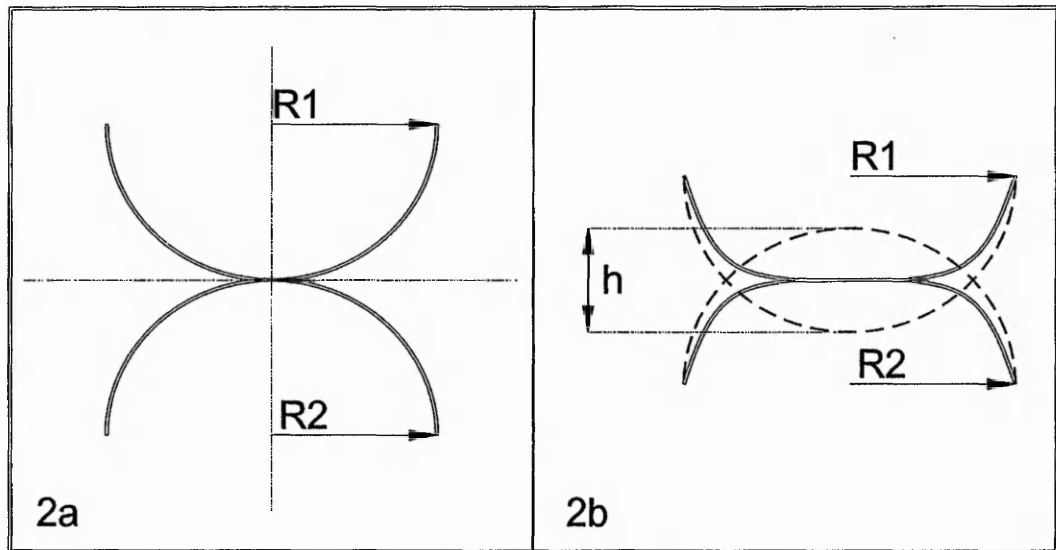


Fig 2. Two spherical bodies in contact pressed together by an applied force (a) before loading and (b) is during loading.

The two main parameters of interest are: the area of contact generated between the two bodies 1 and 2, along with the potential energy generated due to the elastic deformation of the contacting bodies. When two spherical bodies are pressed together a circular area of radius a is formed. Using Hertzian contact laws the radius a of the real area of real contact A_r is given by:

$$a = F_c^{\frac{1}{3}} \left(\frac{DR_1R_2}{R_1 + R_2} \right)^{\frac{1}{3}} \quad (2)$$

Where F_c is the contact force and D is termed the contact modulus, which accounts for the elastic properties of the materials in contact.

The contact modulus is given by:

$$D = \frac{3}{4} \left(\frac{1-\nu_1^2}{E_1} + \frac{1-\nu_2^2}{E_2} \right) \quad (3)$$

Where E and ν are Young's modulus and Poission's ratio respectively of the bodies in contact.

The displacement of the bodies in contact, h , is given by:

$$h = F_c^{\frac{2}{3}} \left(D^2 \left(\frac{1}{R_1} + \frac{1}{R_2} \right) \right)^{\frac{1}{3}} \quad (4)$$

The potential energy, e_e , of bodies in contact can be found using the relationship:

$$-F_c = -\frac{\partial e_e}{\partial h} \quad (5)$$

Therefore e_e is given by:

$$e_e = \frac{2h^{\frac{5}{2}}}{5D} \sqrt{\frac{R_1 R_2}{R_1 + R_2}} + C \quad (6)$$

Where C is constant resulting from the infinite integral and can be determined by experimental investigation. Equations (2)-(6) relate to a single asperity contact and one of the common problems with friction pairs is determining how many of these contacts occur within the apparent area of contact. However, methods using electrical resistivity and heat transfer between the points of real contact have been used to measure the real area of contact [52].

2.3.4 Wear

During the process of sliding friction, wear is inevitable and results from the destructive forces that occur within the areas of real contact. Wear is attributable to plastic deformation and asperity fracture, which in some circumstances can be a useful mechanism especially when “running in” sliding components such as engine cylinders. The amount of wear can dramatically affect the number of asperity interactions and thus affect the nature of the contact between two sliding surfaces, which can lead to mechanical failure (the undesirable case) [52].

2.4 Granular and Solid Interactions

The friction pair considered in this study involves the interaction between a solid surface and a granular layer. Adams et al [53] considered a contact mechanics approach for describing the frictional contact at walls for both smooth and rough particles. The following sections provide an overview of the frictional contact for smooth and rough particles at solid boundaries.

2.4.1 Friction of Smooth Particles at Solid Boundaries

Friction of particles in contact at a solid interface is generally based on adhesive junctions formed between the contacting particle and solid surface. The frictional force is given in equation 1 and the magnitude of the shear strength is given by [53]:

$$\tau = \alpha P + \tau_0 \quad (7)$$

Where α is the coefficient of the pressure P and τ_0 is the intrinsic shear strength at no load.

Combining equations 1, 2 and 7 the frictional force for a single asperity contact is given by:

$$F_f = \pi\tau_0 F_c^{\frac{2}{3}} \left(\frac{DR_1 R_2}{R_1 + R_2} \right)^{\frac{2}{3}} + \alpha F_c \quad (8)$$

Considering the particle friction that occurs at a wall, a sphere flat model is assumed. Referring to equation 4, R_1 is the particle radius and R_2 becomes the flat, which is represented by an infinitely large radius. Therefore, the component involving the radius of curvature R_2 is infinitely small and is omitted from the equation. The particle radius R replaces R_1 to form the following equation representing the frictional force for a sphere and flat sliding interaction [53]:

$$F_f = \pi\tau_0 (F_c DR)^{\frac{2}{3}} + \alpha F_c \quad (9)$$

2.4.2 Friction of Rough Particles at Solid Boundaries

Considering rough particles, it is assumed that the particle in contact has surface asperities and that the real area of contact is defined by the summation of these asperity contacts within the nominal particle contact area. Therefore as the particle creates a nominal contact area described by Hertzian contact laws, further contacts are formed by the particle's surface asperities. The frictional force for rough particles has the following form [53]:

$$F_f \propto (\tau_0 + \delta P) F_c \quad (10)$$

Where δP is the mean contact pressure at the particle's asperity contact. The equation highlights the fact that the frictional force is directly proportional to load, since the number of load bearing contacts will increase with increasing load.

2.4.3 Particle-Solid Friction for Particulate Assemblies

For a given particulate assembly many contacts can occur within a nominal area. The number of contacts depends on the spacing of the particulate material and when dealing with bulk particulates, a spacing parameter has to be addressed. Adams [53] considered this problem (for smooth particles) by assuming the particles form a square packing arrangement (Figure 3) and the spacing is assumed to be constant between adjacent particles. As the spacing is assumed constant the total length in one dimension for a single particle is, sR . Therefore a single particle in a square packing arrangement has an area of s^2R^2 and the number of particles determine the total area of the square packing arrangement. The number of particles, N , within a nominal area, A , is given by:

$$N = \frac{A}{s^2 R^2} \quad (11)$$

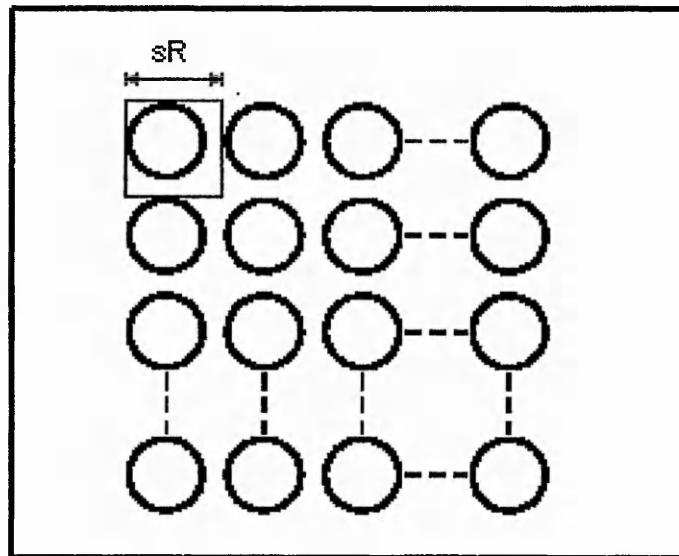


Fig 3. Square packing arrangement.

Using a spacing parameter allows the total frictional force to be determined by summing all of the frictional forces at every particle contact. Therefore, using equations 9 and 11 the total frictional force is given by:

$$NF_f = \pi\tau_0 \left(\frac{AF^2 D^2}{s^2} \right)^{\frac{1}{3}} + F \quad (12)$$

In this case F is the total applied force, which is the sum of all the contact forces F_c :

$$F = NF_c \quad (13)$$

It is interesting to note that for smooth particles in contact, the frictional force is independent of particle size. The reduction in the number of contacts with increasing particle size is counterbalanced by an increase in the Hertzian contact area due to higher contact pressures. Adams also presented an equation for the frictional force for rough particles which was originally derived by Archard [54]:

$$F_f = k \left(\frac{AF^8 D^8}{s^2} \right)^{\frac{1}{9}} + \alpha F \quad (14)$$

Equation 14 reveals that as the roughness increases, the frictional force becomes less dependent on the nominal area and is more dependent on the applied load and would therefore eventually behave according to Amonton's and Coulomb's friction law.

2.4.4 Geometric Relationships for Granular-Solid Friction

Paikowsky, et al [55] stated that the major parameters, which contribute to the interfacial friction, are the grain shape (granular material) and the surface roughness (solid surface). Particles can be considered ellipsoids with a circular cross section along one axis, where the variation in grain shape is accounted for using the average roundness ratio R_a , which is the ratio of the grain's length, L , over its breadth, B , ($R_a = (L/B)$) (Figure 4). Therefore, perfectly rounded particles have $R_a = 1$ and for angular shaped particles, $R_a = 1.25$. Linear relationships were found between the normalised roughness and the product of the roundness ratio and the friction coefficient. The following diagrams (Figures. 4 and 5) describe the geometrical relationships established for the normalised roughness and the friction angle α .

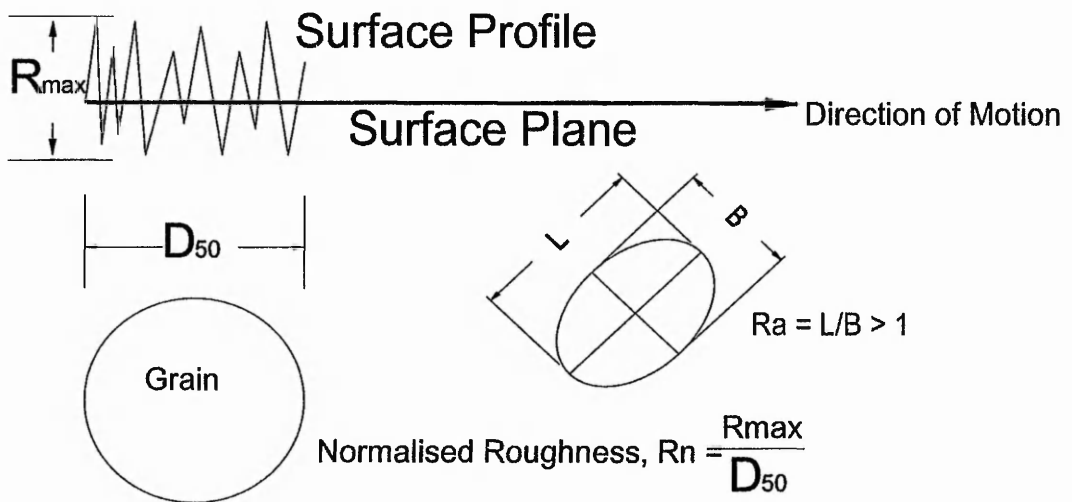


Fig 4. Geometrical relationship for the normalized roughness and the particle roundness ratio

D_{50} is the mean particle diameter as described by Paikowsky [55].

The normalised roughness value, R_n value is the overall surface profile parameter R_{max} divided by the mean grain size diameter D_{50} .

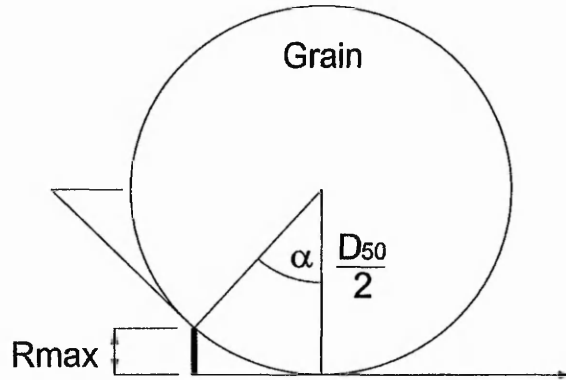


Fig 5. Geometric relationship for the friction angle α

$$R_{\max} = \frac{D_{50}}{2} - \left(\frac{D_{50}}{2} \cos \alpha \right) \quad \therefore R_{\max} = \frac{D_{50}}{2} (1 - \cos \alpha) \quad (15)$$

$$R_n = \frac{R_{\max}}{D_{50}} \quad \therefore R_n = \frac{(1 - \cos \alpha)}{2} \quad \therefore \alpha = \cos^{-1}(1 - 2R_n) \quad (16)$$

The roughness angle α (Figure 5) describes the surface roughness and represents the angle between the plane of movement and the plane of contact. The roughness angle is derived from the normalised roughness and relates to the ratio of the grain size relative to the surface profile (Figure 4). When the surface is smooth compared to the grain size (R_{\max} is small) the frictional resistance lower and is shown by a reduction of the friction angle, despite having a variation of grain sizes. This highlights the fact that the grain size has little or no effect on the frictional coefficient for a smooth solid surface and grains of the same sand type have similar coefficients of friction. Therefore, considering a smooth solid surface, the main parameter that affects the frictional resistance is the grain

shape and the affect on the friction coefficient is accounted for using the modification parameter, R_a .

If there is little contrast between the grain size and the surface roughness the frictional resistance will change according to a change in the surface profile or in the diameter of the particle and occurs due to dilatancy effects i.e. deformation within the granular sub-layers.

2.4.5 Friction Involving a Rough Solid Surface

Uesugi [56] monitored the displacements of granular particles for both rough and smooth solid surfaces. For rough surfaces the displacement of the particles should slip accompanied by grain rolling, along the interface. During sliding, the particles moved in both parallel and perpendicular directions to the interface. The study highlights the dilation that occurs when the surface is rough compared to the grain size and was shown by shear occurring within the sub-surface layers of the particulate material. Dilation occurs due to the shear plane developing within the granular material, as the grains become trapped in the ravines associated with large surface roughness. The entrapment of the grains due to surface roughness was emphasised by Aguirre et al [57] who investigated particles rolling down a rough incline. Subba Rao et al [58] stated that the orientation of the shear plane had an effect on the frictional characteristics. Subba Rao monitored two regimes of sliding; regime 'A' involved the solid material on top of the particulate material while regime 'B' was the opposite. Results indicated that regime 'A' created no peak shear resistance regardless of surface roughness (solid surface) and variations in surface roughness had little effect on the generated friction angles. Results

from regime 'B' indicated that a definite shear resistance peak occurred for the rough surface indicating that dilation of particulate material occurred.

2.4.6 Friction Involving a Smooth Solid Surface

Uesugi [56] demonstrated that for a smooth steel surface there was no rolling of the sand particles and only granular slip was evident along the surface. The displacements of the sand grains were mainly tangential to the sliding interface due to small adhesion forces occurring between the particles and the steel surface during sliding. Therefore, the shear deformation within the granular mass was negligible as the shear plane developed at the steel-sand interface. Subba Rao [58] stated that for a smooth solid surface no shear resistance peaks occurred during sliding, regardless of the shearing regime, highlighting the fact that no granular deformation occurs and also indicating that the frictional resistance is not attributable to granular dilation. It was also found that the friction angles obtained for the shear regime 'A' produced similar friction angles regardless of the surface roughness characteristics of the solid interface.

2.5 Acoustic Emission

Acoustic emission (AE) is a growing technique used in non-destructive testing, primarily for detecting crack extensions and plastic deformation in metal and composite materials [2,59]. Acoustic emission is also becoming a popular condition-monitoring tool for many industrial machines, as AE is generated by sources such as mechanical impacts, friction and cavitation [60-65]. The AE generated by the frictional process between a drill bit and a granular medium provides the source of the acoustic emission being investigated in this study. Monitoring friction-generated acoustics has found a niche in condition monitoring because of its ability to identify signs of potential

mechanical failure in components such as bearings and machine tools. Holroyd and Randall [66] highlighted the sensitivity of AE when detecting changes in lubrication, overloading, wear and provided an overview of the different techniques available for analysing the “acoustic signatures” generated. Dong et al [67] monitored a drilling process using AE techniques. Their results indicated that material shear, plastic deformation, tool deformation, friction between the tool and chip as well as the friction between the work piece and the tool were all sources of acoustic emission. A drilling mechanism is a dynamic process, with strong tribological features and the contribution of the friction between chips and the hole at larger depths had a significant affect on the acoustic signal.

2.5.1 Friction Generated Acoustic Emission

An inevitable characteristic of non-lubricated sliding surfaces is the frictional force and the associated dissipation of energy due to their relative motion. Akay [68] provided an in-depth review of the many aspects of friction-generated acoustics from the ringing of a wine glass to the complex mechanisms involved with brake squeal. Friction generated sounds are generally unsteady and transient. The transient components originate from sudden deformations of the near surface contact area and are related to the stiffness component of the oscillating asperities [69]. Continuous sliding produces a broad range of responses where changes in the radiated sound are governed by variations in the contact force [68]. In contrast Briscoe et al [70] presented results where the spectral content appeared to be unaffected by the contact pressure except for an increase in the overall acoustic energy. They stated that spectral content was dependent on the mechanical properties of the friction pair such as the asperity stiffness and damping. Hinrichs et al [68] mentioned that during the slip phase, frictional forces exhibit

stochastic components, which involve the number of active asperities and the number of times they become excited during sliding. For example, when an asperity is deformed to the extent that the bond is destroyed, the deformed asperity will attempt to reach a state of equilibrium moving some distance before it bonds with another surface asperity therefore, consequently the same surface asperity can be excited many times during sliding.

The source of acoustic emission results from the release of strain energy generated by surface asperity deformation at the real area of contact as described in Section 1.3. When considering sliding friction asperity adhesion is continuously formed and destroyed. The deformation of the asperities creates an elastic energy potential that is suddenly released when the asperity bonds are destroyed. The nature of asperity interactions yield a stick slip mechanism whereby the stick phase is a result of asperity bonding while the slip phase corresponds to the release of strain energy. The sudden change in strain yields a pressure pulse at the point of contact resulting in elastic wave propagation through the friction pair materials. Briscoe et al [70] noticed that the stick slip frequency increased with increasing sliding velocity, which is in agreement with the observations of Akay [68] where corrugated (rough) surfaces produced impulsive contact forces at the corrugation frequency. Therefore, a change in speed would proportionally affect the number of asperity interactions per unit time. It was also highlighted by Briscoe et al [70] that varying load did not affect the stick slip frequency.

2.5.2 Parameters of Friction Generated Acoustics

Jiaa and Dornfield [71] mentioned two types of responses that occur at asperity interactions: deformation of the surface and near surface layers; and asperity fracture.

Both of these responses can potentially be a source of AE. The research considers sliding metals and highlights friction as the source of acoustic emission in the form of impulsive shock due to asperity collisions and micro-vibrations excited by stick-slip phenomena. The outcome of the research agrees with earlier work by Diei [72] who monitored the AE generated by tool wear in face milling and showed that the root-mean-square AE increases as a linear function of the increasing load, with a power law relationship between the sliding velocity and AE_{RMS} . The power law relationship between the AE_{RMS} voltage and the energy dissipation caused by sliding frictional processes is given by:

$$AE_{RMS} = (k\eta\tau A_a v)^{\frac{m}{2}} \quad (17)$$

Where k is a constant depending on the AE measuring system, m is a function of the material properties of the contacting pair, τ is the shear strength of the interfacial material, A_a is the apparent area of contact, η is a function of both the surface roughness and the elastic properties of the friction pair (this parameter defines the actual area of contact $A_r = \eta A_a$) and v is the relative surface sliding speed.

Early research carried out by Sarychev and Shchavelin [73] investigated the influence of the sliding velocity, the applied load, the surface roughness and the mechanical properties of a friction pair on the parameters of AE. Their work states that AE arises from the formation and destruction of the adhesive bond on the site of actual contact as well as the elastic interaction of micro asperities of coarse surfaces. The work outlines a model, which takes into account the discrete nature of frictional contact. Friction is considered an incident process, produced by the formation and destruction of asperity

bonds. Therefore, AE is the propagation of the materials reaction to the pressure pulses generated at the surface by their respective asperity contacts. An expression is obtained for the count rate \dot{N}_a , a measure of the acoustic activity in-terms of a function of the elastic contact between the roughness asperities produced by a sliding frictional process:

$$\dot{N}_a = k \left(\frac{W^{0.71} \theta^{0.71} A_c^{0.71}}{r^{0.9} R_a^{1.6}} \right) v \quad (18)$$

Where W is the normal load, θ is the elastic modulus, A_c is the apparent area of contact, r the surface asperity tip radius, R_a the surface roughness parameter, v the sliding velocity and k is a coefficient of proportionality.

The relationship shown in equation (19) considers the effect of sliding velocity on the acoustic count rate. The relationship describes a general rule for the count rate and the constants A and B would be determined experimentally. Factors such as the material type and surface roughness can affect the index, but in general the index is greater than one. Therefore, considering two sliding bodies in contact, the dependence of the count rate \dot{N} on sliding velocity usually follows the following form [73]:

$$\dot{N} = A + Bv^x \quad (19)$$

Where A and B are constants and $x \geq 1$.

A similar relationship to equation 19 exists between the count rate and the applied load, although $x \leq 1$.

Recent studies examined by Baranov, Kudryavtsev and Sarychev [74] used the stress distribution in the area of real contact as a method for estimating the parameters of acoustic radiation. Attention was focused on describing the amplitude of the signal in terms of the potential energy produced by asperity deformations during sliding friction. Their work provided the following equation relating the amplitude of the acoustic signal, A , to the elastic potential energy generated as a result of asperity interaction:

$$A \approx \left(\frac{\varepsilon}{\tau} \right)^{\frac{1}{2}} \quad (20)$$

Where “ ε ” is the acoustic emission pulse-energy and “ τ ” is the radiation time of the AE pulse. The elastic energy “ ε ” refers to the potential energy generated by the elastic deformation of the contacting asperities and depends on their closeness (the distance between contacting asperity centres), which has been previously described by equation 6 in Section 1.3.3.

The number of acoustic emission pulses generated as a result of sliding friction was considered by Baranov et al [74]. Equation 21 was based on the assumption that the number of acoustic pulses generated during sliding friction is directly proportional to the number of contact spots formed per unit time (analogous to the corrugation frequency suggested by Akay [68]). The following expression was derived relating the number of acoustic pulses generated per unit time \dot{N}_{AE} to the material properties of the friction pair:

$$\dot{N}_{AE} = N_p \frac{L\sigma^2}{8\pi^2\sigma_1^2\eta} \frac{F}{F_0} v \quad (21)$$

N_p is an empirical coefficient that indicates the number of pulses generated for a single contact spot. L represents the characteristic dimensions of nominal area, σ is a normalised function of the two surface profiles represented by a random continuous function $Z_i(r)$ and the subscript, i , represents one of the surfaces within the friction pair. $\eta = 1 + \alpha^2$ whereby α is the measured mean plane of one of the surfaces in contact. F/F_0 is the normalised force pressing the two surfaces together and v is the sliding velocity.

2.5.3 Solid Acoustic Wave-Guides

A waveguide is any structure that causes waves to follow a certain path instead of spreading out into a larger volume of space. The propagation of a strain wave in an elastic solid can also be controlled with a waveguide. The boundaries of the propagating medium are formed by materials of different elastomechanical properties. Depending on the waveguide geometry and the difference in the magnitude of the elastomechanical properties between the propagating medium and its boundary material, the travelling wave in the waveguide may show dispersion as well as mixed polarization, i.e., partly transverse and partly longitudinal. In this study the friction generated elastic wave propagates from the source (drill tip) to a stationary piezoelectric transducer. The drill string acts as a solid acoustic wave-guide and provides a method of transferring the acoustic signals to a stationary transducer. Wave-guides essentially control the directional propagation of a wave by limiting the transmission of the acoustic wave to a predetermined dimension. The following sections will briefly describe the transmission of acoustic waves as well as considering the types of waves that propagate in solid materials. A description concerning the characteristics of wave propagation will be covered although the derivations of the wave equations will not be included since they are available in many standard texts (see for instance [75-77]).

2.5.4 Wave Reflection and Transmission

When an acoustic wave strikes a boundary between two media, some energy will be reflected back into the first medium while the rest of the energy will be transmitted into the second medium. The energy transmitted into the second medium depends on the difference between the acoustic impedance Z of the two materials. The equations for the pressure transmission, T_p , and reflection coefficients, R_p , are:

$$T_p = \frac{2Z_2}{Z_1 + Z_2} \quad (22)$$

$$R_p = \frac{Z_2 - Z_1}{Z_1 + Z_2} \quad (23)$$

Therefore if $Z_1=Z_2$ the reflection pressure will be zero and all the pressure will be transmitted into the second medium. If Z_1 was very different to Z_2 a large impedance mismatch would result and most of the energy is reflected. However, if Z_1 is larger than Z_2 a phase change will occur. The coefficients are independent of incident angle but the intensity I of the transmitted and reflected waves are dependent on angle of incidence given by:

$$I_i \cos \theta_i = (I_r \cos \theta_r + I_t \cos \theta_t) \quad (24)$$

Wave-guides use the impedance mismatch to restrict the transmission of acoustic waves into the surrounding environment [78]. However, the transmission of elastic waves at boundaries becomes important when considering the transfer of the acoustic signal from a drill string to a stationary piezoelectric transducer mounted above.

2.5.5 Wave Propagation in a Cylinder

A drill string can act as a solid acoustic waveguide with non-degrading acoustic characteristics (low acoustic attenuation) that can be simply represented as a finite cylindrical rod. The classical theory such as that of Pochhammer [79] and of Chree [80] considers a continuous wave input and the generation of modes within an infinitely long cylinder. In this study the drill string is analogous to a cylinder of finite length. The excitation due to the frictional contact between the drill tip and a granular medium is assumed to generate stress wave impulses with fluctuating duration, amplitude and time separation. The pressure pulses arising at the drill tip surface will excite complex modes of propagation. Solid acoustic wave-guides also display multimodes with dispersion characteristics, which can make the wave analysis difficult. In this study, broadband multiple modes will be generated, which represent the most complicated case. Therefore, it is not possible to describe with clarity the relationship between the signal responses of the detection transducer and the input frictional excitation. The acoustic emission is generated by an unknown frictional contact source and will excite variable waves of different type, which ultimately excites the transducer in a complex manner. The limited literature directly related to this problem emphasises the limited understanding that exists. Although a variety of literature is available to provide a general understanding of the problems that exist in multi-mode wave propagation as well as the different analysis techniques available (see for instance [81-87]). Due to the complexity of the broadband multi-modal wave propagation problem, finite element modelling is being used increasingly due to its ability to visualise the propagating wave characteristics for the actual structure under investigation [88-90].

2.5.6 Analysis of AE and Acoustic Parameters

There are many different techniques available for monitoring and investigating the acoustic emission generated during sliding friction. This section provides an overview of these methods as well as identifying the acoustic parameters usually used for investigating friction generated acoustics.

The methods of recording acoustic signatures and the type of data analysis depend on the physical system being monitored, the frequency range of the acoustic signal and the equipment available to the engineer. Methods of analysing AE signals can be grouped into two main areas, broadband and narrow band. A broadband system allows for instance the investigation of the AE frequency spectrum, obtained using the Fourier transform. Other techniques include analysing the mode arrival times of acoustic waves between an array of sensors, used for determining the AE source characteristics. Recent studies have used neural networks to identify characteristic patterns within the frequency spectrum, which can be related to the physical parameters of AE generation [91-92]. Bukkapatnam et al [93] presented a methodology for AE signal analysis, based on chaos theory, wavelets and neural networks. Broadband analysis requires large data sets, which can incur large data processing times although advances in computational power have dramatically improved the processing speed of complex data sets.

A narrow bandwidth system narrows the frequency range of the AE system under investigation. Using this method, thresholding techniques can be used to monitor parameters such as, the count rate, the event count as well as analysing time differences between AE events. Other parameters include event amplitude distributions, RMS power and energy, which is determined by integrating the RMS of the voltage signal.

Using a narrow bandwidth system can dramatically reduce processing time and electronic systems are available that can extract the relevant AE parameters required. Scruby [94] provided a good overview of the different acoustic analysis techniques that can be used to monitor AE. Holroyd et al [66] also provided an in-depth overview of the various AE methods used in condition monitoring.

3.0 Experimental Development

The work described in this chapter considers the development of the system used for an experimental investigation of the parameters associated with a sliding granular-solid friction pair. An initial study was conducted to determine the characteristics of the acoustic signal being monitored and to develop an understanding of how the main test parameters might affect the acoustic signal. This chapter also discusses the redevelopment of the experimental arrangement, as a result of the initial study.

3.1 Initial Experimental Arrangement

The initial experimental system (shown in Fig 6) was designed to provide a simplified but controlled drilling process. A probing process, using a rotating probe, replaced the normal drilling motion to improve surface interactions between the geotechnical medium and the probe's surface. The acoustic signal, vertical load, angular velocity and linear displacement were monitored and recorded.

The experimental system consisted of six main components:

- The drilling system
- The probe
- The acoustic signal-coupling device
- The geotechnical medium
- The AE system
- The Data acquisition system

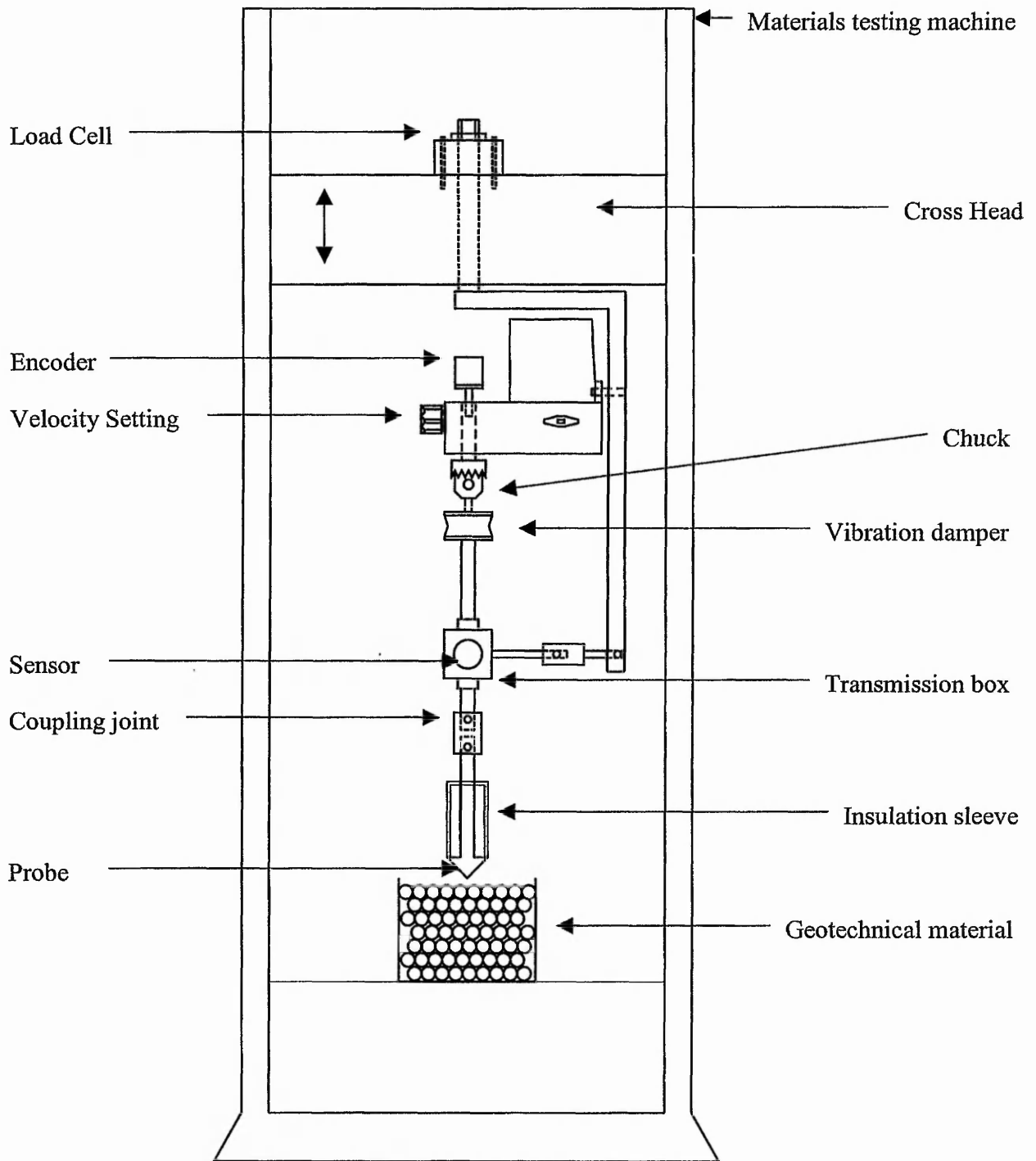


Fig 6. Schematic diagram of the initial probing system.

3.1.1 The Drilling Mechanism

The drilling system provided the rotation and the linear displacement of the probe tip. A Shimadzu AG-100kNE materials testing machine was adapted to house a mechanical drill and a fixture was designed and constructed to attach the drill to a load cell situated on the crosshead. The testing machine provided a controlled linear crosshead speed ranging from 0.1-1000 mm/min, which allowed the probe penetration depth to be controlled by the user. The drilling system was mounted directly to the load cell, which was attached to the cross head on the materials testing machine. The load cell was calibrated to account for the weight of the drilling system to provide a 5V signal output corresponding to a preset full-scale load. The full-scale load could be adjusted on the testing machine control panel, which had a load range between 1-100 kN. The accuracy of the load cell was 0.01% of the full-scale load (selected by the control panel). The drilling system was fitted with an encoder, which produced 100 pulses per rotation. A frequency to voltage converter was used to convert the pulse frequency into a signal voltage between 0-10V.

3.1.2 The Probe

The initial probe was constructed of four components; the adapter for the drill chuck, a rubber damper (to reduce noise generated by the drill vibrations), the main shaft (incorporating a connector to allow the probes to be interchanged) and the probe. The probe was made of stainless steel with a smooth conical tip to increase the surface contact and reduce the level of compaction during probe penetration. The smooth probe tip promoted a suitable sliding interface between the geotechnical medium and the probe tip face. Figure 7 illustrates why the frictional contact cannot be improved by increasing the roughness of the probe. Rough surfaces would generate an unsuitable

sliding plane due to entrapment of the granular particles within the surface asperities. Therefore, a smooth probe surface compared to the granular particle size maximises the probe-granular interaction. The smooth solid-granular interaction is preferred as the AE generated is a direct result of the granular grains sliding against the solid probe. Whereas the rough surface would produce AE due to impulses transmitted through inter-granular contacts from a shear plane occurring within the sub surface layers of the granular material.

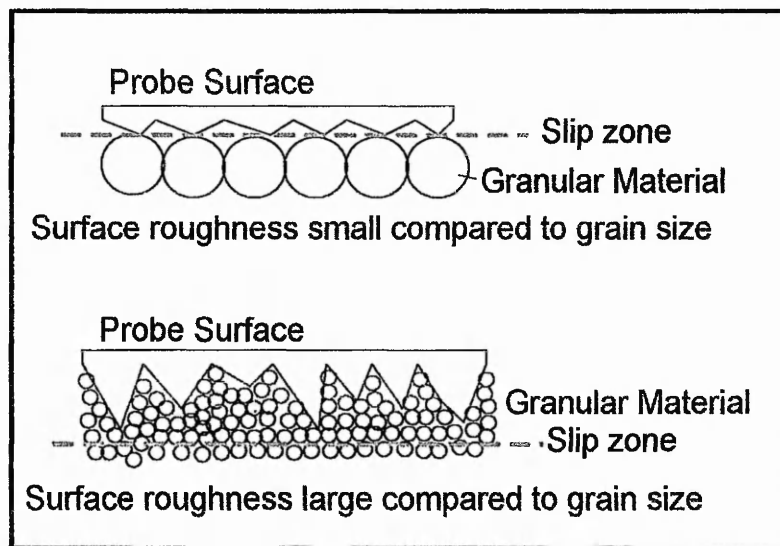


Fig 7. An illustration of the interaction between the probe and a granular material.

Close to the probe head an acoustic insulation sleeve was placed over the probe shaft, with the sleeve permanently fixed using suitable adhesive. The insulation sleeve made contact with the probe in only two places to reduce the transmission of any noise generated by the friction produced between the insulation sleeve and the geotechnical test material (see Figure 8). The air gap between the probe and the sleeve provided a large acoustic impedance mismatch and minimised the transmission of the acoustic signal between the probe shaft and the sleeve, while any transmission via the insulation sleeve was considered negligible. The probe was connected to the main shaft using a

coupling device just below the signal transmission box. The coupling device allowed quick probe inter-changeability although the system had experienced acoustic wave transmission losses due to the air gaps generated between the probe and the main shaft. The acoustic transmission was subsequently improved at this interface by machining the ends of the probe and the main shaft flat and then applying a thin layer of silicon grease, to act as an acoustic coupling fluid.

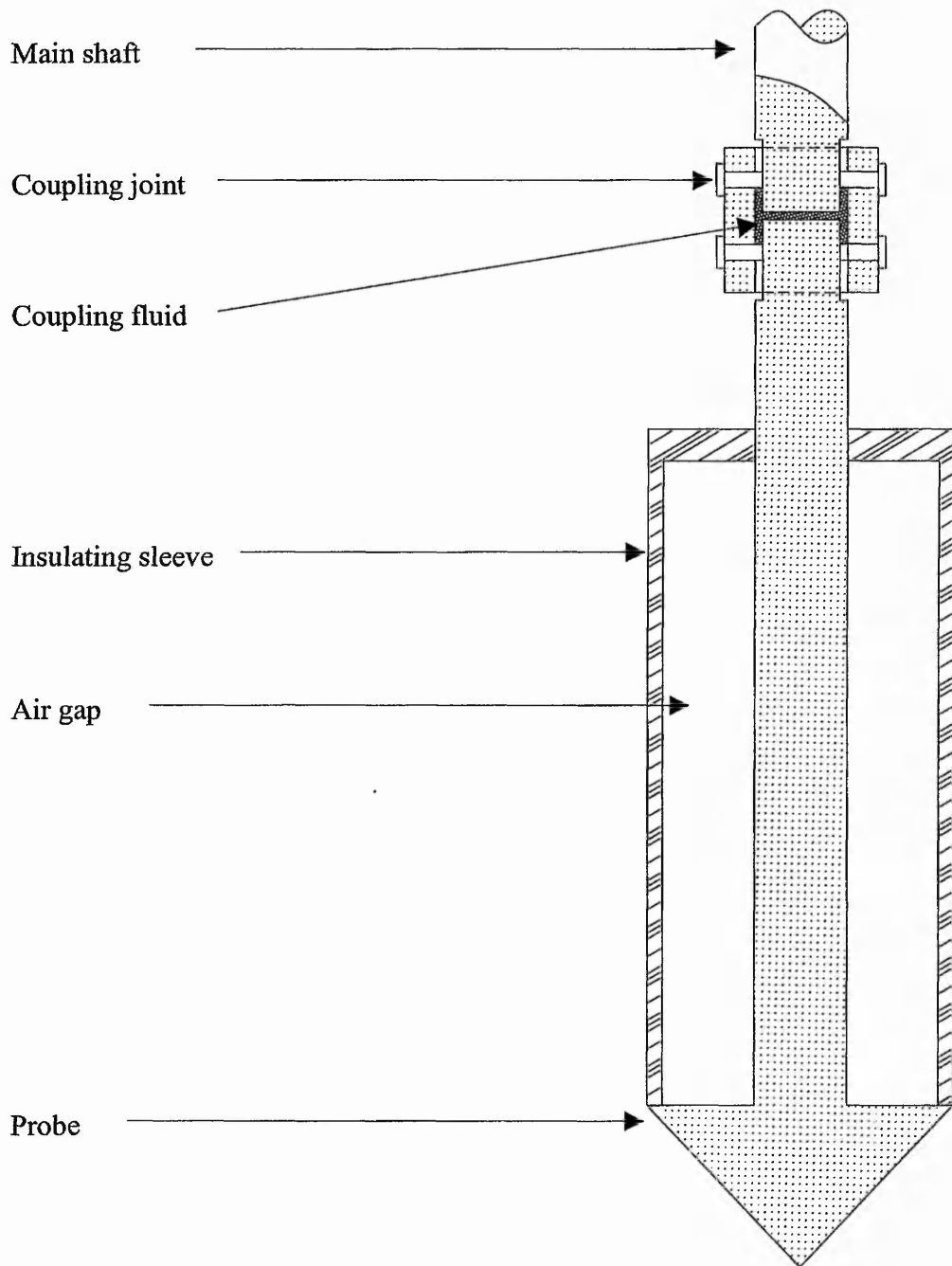


Fig 8. A cross section of the probe, with the insulating sleeve and coupling joint.

3.1.3 The Signal-Coupling Device

The AE transducer cannot be directly attached to the probe shaft due to the continuous rotation of the probe. Therefore the probe shaft is passed through a sealed box (transmission box), filled with oil using sealed bearings (Figure 9). The aim of the transmission box was to couple the transducer to the probe shaft. The lower boundary impedance mismatch between these two materials allows some of the acoustic energy to be transmitted between the probe and the oil. The acoustic waves propagating within the probe shaft will be refracted into the oil followed by the acoustic waves propagating in the oil medium being refracted in the transmission box casing. The acoustic signal transferred to the transmission box casing was detected by the transducer. For illustration purposes (not an exact representation) an example of wave propagation in the coupling device is highlighted with a red dotted line (Figure 9). The transfer box is secured to the main drill-mounting frame using a loose push fit adapter and a rubber sleeve is used as a vibration damper between the transfer box and the drill-mounting frame to restrict any AE noise generated from the drill's operation being transferred to the transfer box.

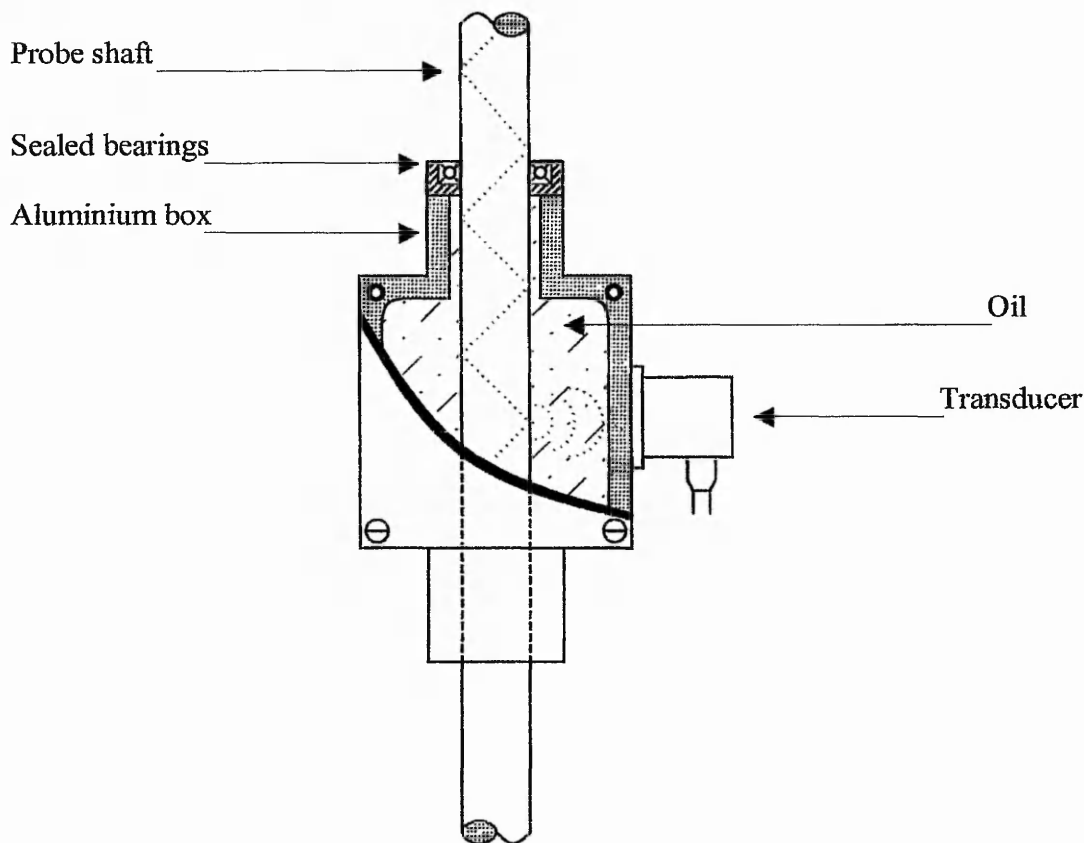


Fig 9. The acoustic signal-coupling device, displaying half a cross section.

3.1.4 Preparation of the Geotechnical Medium

Dry granular materials were sieved to provide a controlled geotechnical medium and different particle size ranges will represent different granular structures. Leighton Buzzard sand was selected for its uniform grain size (data from the work of Kavanagh [95]). Sharp sand (collected from RMC aggregates, Attenborough Nottingham) was also used providing samples having smaller grain size as well as being of a different material composition. All granular samples were placed in containers of similar size and shape to provide consistent boundary conditions for each medium under investigation. The containers were carefully filled by using a layering technique where layers of similar

size and mass were stacked throughout the container creating a uniform density throughout the whole granular sample.

3.1.5 The AE System

The acoustic emission system used was an AECL 2100.M modular range of acoustic emission equipment supplied by Speedronics UK. A piezoelectric transducer with a resonant frequency of 375 kHz was connected to a 60dB preamplifier with a band pass filter range of 250-500kHz. The transducer was fixed to the transfer box (see Section 2.1.3) using a G-clamp with a thin layer of oil was used as a coupling fluid. The amplified acoustic signal was processed using an analogue processing unit, which facilitates the extraction of a number of acoustic parameters. The acoustic count rate, event count and the acoustic energy were the main parameters provided by the AE processing unit. The acoustic energy E is determined using the following relationship:

$$E \propto V^2 \quad (25)$$

Where V is the signal voltage.

The processing unit provides a voltage output (between 0-10v) proportional to the acoustic energy.

3.1.6 Data Acquisition System

A schematic diagram of the full data acquisition system is shown in Figure 10. A DAS 50 data acquisition board provided the interface between the hardware and the software. The DAS 50 board had a maximum A/D conversion rate of 1MHz, while Viewdac software was used to implement the data acquisition sequences and analysis. The

Viewdac software was programmed to meet the requirements of the application. The DAS 50 is a four-channel acquisition board with input voltages up to $\pm 10V$. The load cell provided a full-scale voltage of 5V, which represented a full-scale load of 1000N for measurement of the applied load. A frequency to voltage converter was connected to an encoder, providing a 10V full-scale signal voltage corresponding to a full-scale pulse frequency of 2000Hz. The angular velocity of the probe was determined by calibrating the pulse frequency generated from the encoder rotation. The AE parameters used in this study were the RMS signal voltage, the acoustic count rate and the acoustic energy. The count rate was converted into a signal voltage with a full-scale frequency of 1000Hz corresponding to a full-scale voltage of 10V, with a scaling option available.

Viewdac software was used to control the data acquisition procedures. A sequential sampling program was designed to scan the four input channels at a set interval time and for a predefined period. The change in the signal voltages were used to determine the count rate as well as the change in signal energy. Also the applied load and angular velocity were continuously monitored. The program scaled the signals received by the input channels to represent the desired units and magnitude, as well as storing the data in ASCII format for further analysis. The intervals used for data sampling procedures were adjusted to match the time required for the probe to reach a certain depth, thus maintaining a specified number of data points per millimetre of probe penetration (typically six data points per millimetre).

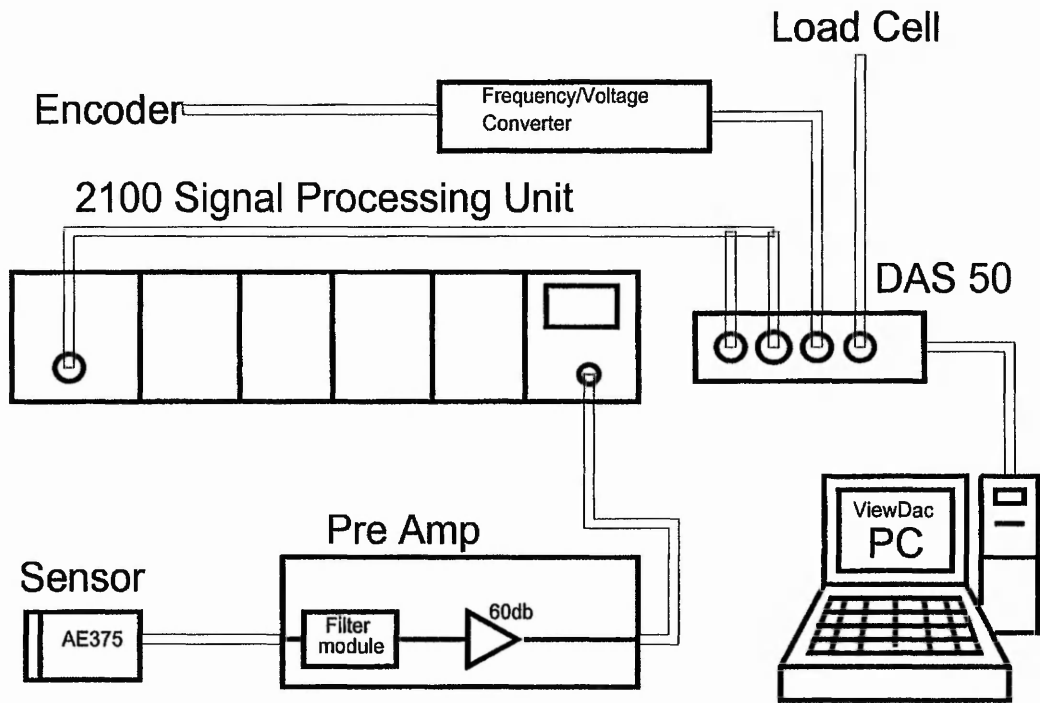


Fig 10. Data acquisition arrangement.

3.2 Initial Investigations

The initial experiments were designed to study the force generated by the probe, the stability of the measured signals and the general stability of the drilling mechanism. Initial work also studied some of the characteristics of acoustic signals being generated and the effect of the dynamic test parameters such as the applied load, the rotational velocity and their functional relationships. The stability, reliability and quality of the monitored signals were evaluated and used to redevelop the experimental design that would allow a thorough parameter investigation. Improving the experimental design increased data quality, which was used to investigate any empirical relationships between the granular material parameters and the associated acoustic emission.

3.2.1 Acoustic Signal Characteristics

The preliminary investigation focused on the raw signal generated by the probe, when it interacted with a granular sample. The acoustic signature was recorded using a Lecroy oscilloscope, with a data sampling speed of 1.5GHz. Figure 11 highlights a typical example of the raw signal generated from the probe-granular friction pair interaction, using 0.2 ms sampling period. The acoustic signal is continuous but with fluctuating amplitude. Changes in load and sliding velocity directly affected the signal amplitude although no identifiable change in other characteristics of the acoustics signature occurred overall.

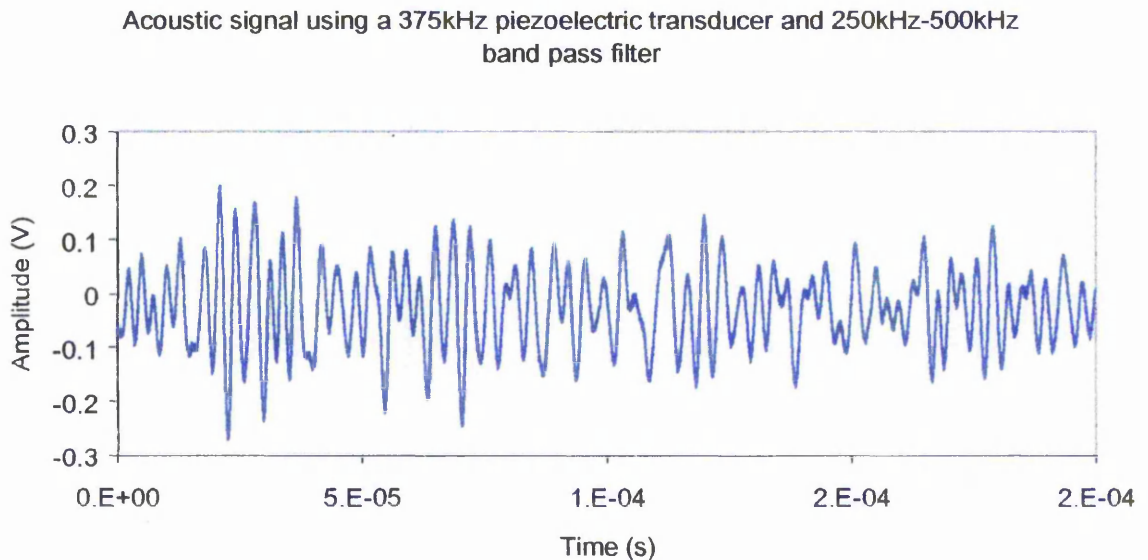


Fig 11. A typical example of the raw acoustic signal generated from the probe-granular interaction.

Figure 12 demonstrates a comparison between the background noise signal (probe un-submerged) and the friction generated signal resulting from the granular-probe

interaction (probe submerged). The investigation identified a change in the acoustic signal due to frictional contact between the granular material and the probe face. This highlighted that the probe-granular sliding interface dominated the generated acoustic signal and outweighed the noise produced from the mechanical drilling system.

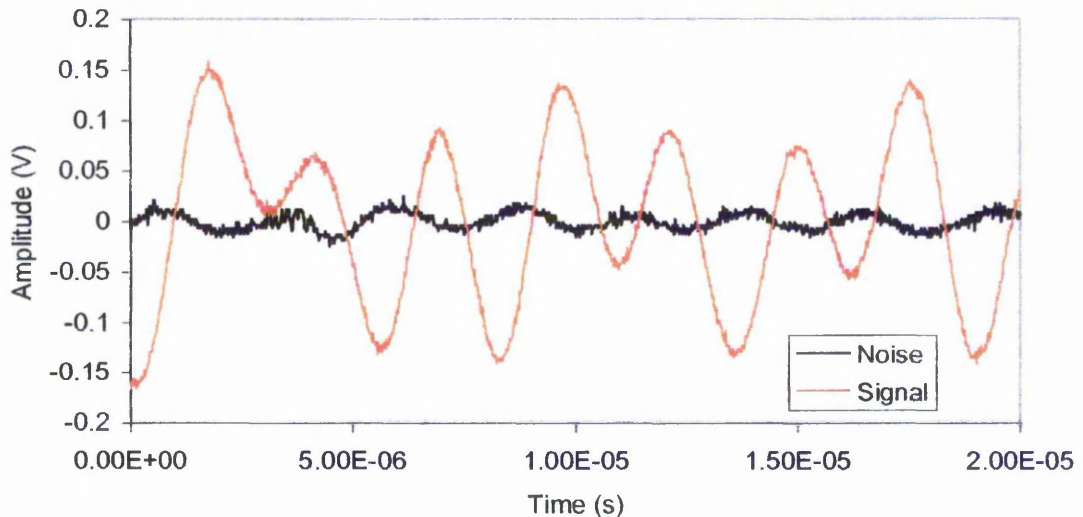


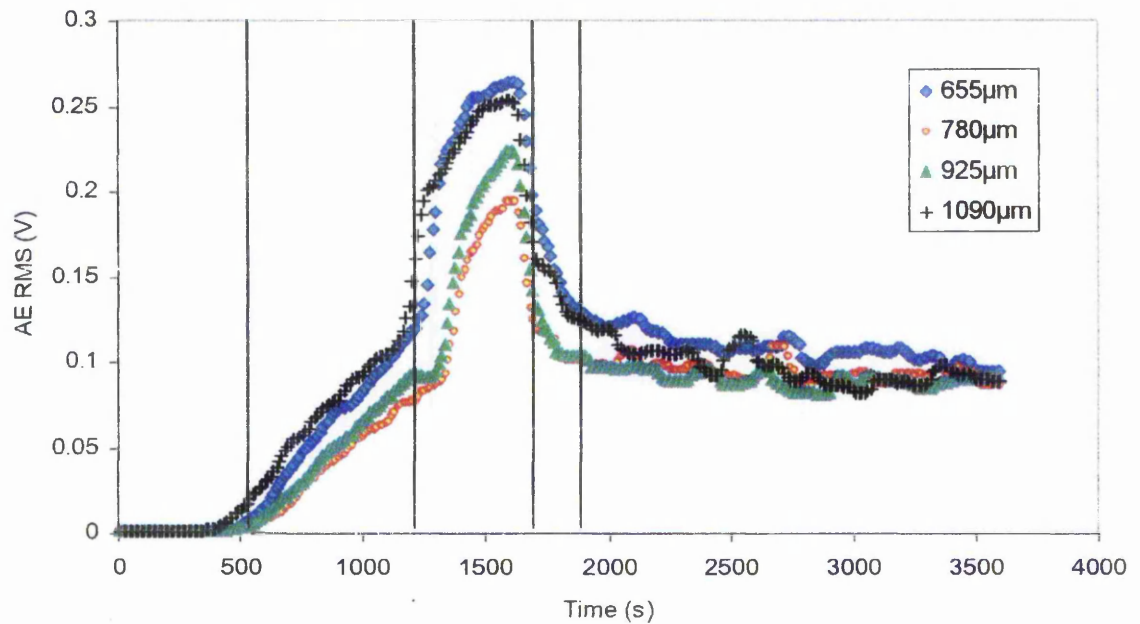
Fig 12. An example of the un-submerged probe's acoustic signal (Noise) and the submerged probe's acoustic signal (signal)

3.2.2 Preliminary Experiments

The effect of the applied load on the RMS acoustic signal was investigated using a constant probe rotational velocity. The acoustic signal was sampled at 1 MHz and the root-mean-square value of the signal could be calculated using the Viewdac software. Experiments indicated that the RMS AE signal appeared to be noisy compared to the load signal. Therefore, a moving average applied over 5 data points was used to smooth the signal and to generate more stable results. Experiments were conducted by pushing the probe into different samples of granular material to a depth of 50mm while continually monitoring the RMS acoustic signal. When the probe reached a depth of 50mm it was left to rotate for a period of time, allowing the stability of the acoustic

RMS signal to be monitored. Sampling the input signals every 6 seconds provided 5 data points per millimetre of penetration.

Fig 13. The variation of the acoustic RMS signals during probe penetration using granular samples of varying grain size.



The results shown in Figure 13 can be broken down into five parts, which are indicated by the five distinct changes in gradient. The first section (0-500s) corresponds to the situation where the probe approaching the test medium is making initial contact with the granular medium (at approximately 500s). Even though there is probe-granular contact, the granular material only applies a small reaction force in response to probe penetration as the grains are unrestrictive and able to move freely. The second part (500-1200s) of the plot suggests that the reaction force increases due to probe penetration. At deeper depths the granular structure is stronger and therefore increased applied forces are needed to deform the granular structure thus increasing the resistance to the vertical movement of the probe. The third section (1250-1700s) corresponds to a sharp increase

in the granular reaction force, indicating that the bulk granular system is more stable (behaving like a solid), which is possibly attributable to granular compaction caused by probe penetration or an increase in confining pressure due to changing boundary conditions. The fourth section (1700-1800s) corresponds to the probe reaching its final depth of 50mm and resulting in a reduction of the reaction force. The reduction in the reaction force occurs because granular systems plastically deform and will not attempt to regain its original shape. However, the reaction force does not completely disappear after the probe has reached its final depth, as the confined granular system behaves like a solid and the force bearing down on the granular system (by the probe) is not large enough to cause deformation. The fifth section (1800-3500s) shows the generated acoustic RMS signal while the probe is rotating in the granular medium highlighting that a small variation in the RMS signal occurs, probably due to the structural instability of the probe.

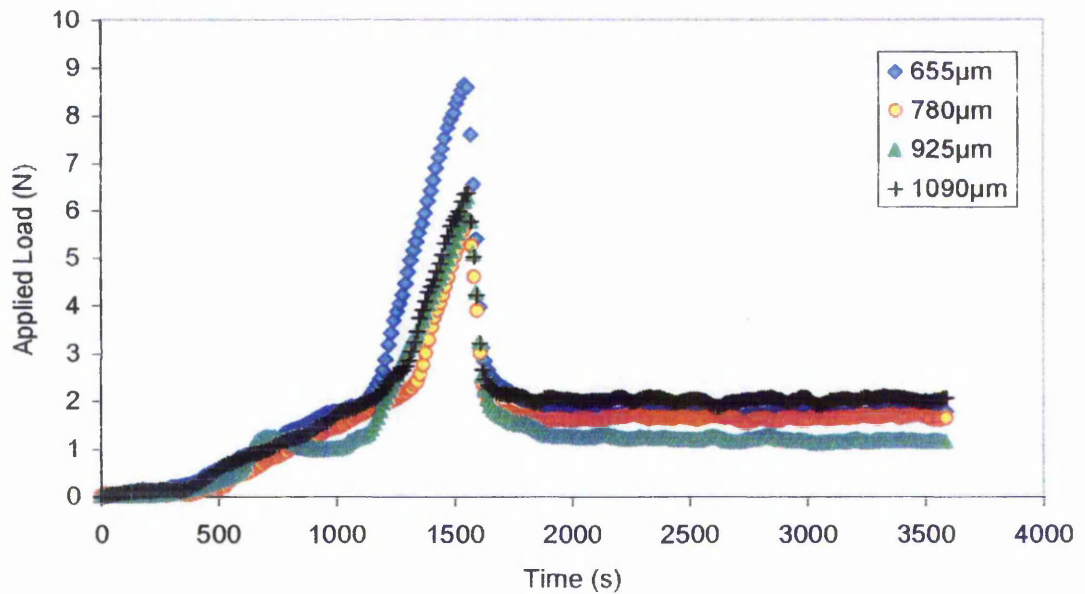


Fig 14. Applied load variation during probe penetration using granular samples of varying grain size.

In Figure 14 the loading characteristics are shown for the AE RMS curves from Figure 13. It is clear that the curves in Figures 12 and 13 follow a similar shape, indicating that the applied load has a significant effect on the AE RMS. The results also show that the load becomes reasonably constant when the probe reaches its maximum depth. The correlations of the acoustic RMS signals and the applied load are displayed in Figure 15.

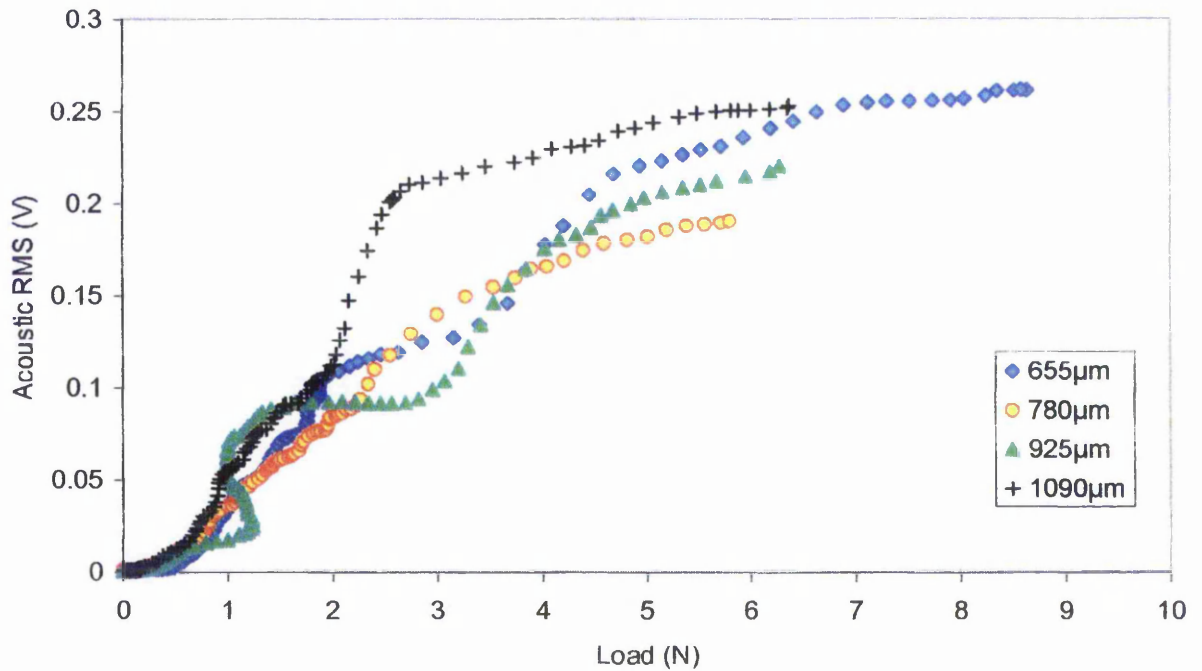


Fig 15. The acoustic RMS signal against the applied load for a continuous probing penetration to a depth of 50mm using granular samples of varying size.

The data shown in Figure 15 highlights that the AE RMS increases with applied load. However, no clear relationship exists between the acoustic RMS signals and the different particle sizes. It can be seen that the data is non linear and this may be caused by the instability of the probe as a result of the probe tip oscillating while it rotates. The accuracy of the load cell was 0.001% of the full-scale load (1000N) therefore, the load output was found to be accurate to $\pm 1\text{N}$, which is significant compared to the load range used in these experiments.

Results have shown that the AE RMS is sensitive to loading conditions. Therefore any oscillation of the probe tip could have a significant effect on the AE due to horizontal loading, especially at larger depths. It is clear at this stage that substantial improvements

to the experimental system are needed regarding the stabilisation of the probe tip, the load signal resolution and reducing the attenuation of the acoustic signals.

3.3 The Development of a New Experimental Test System

The load cell was changed to a 1kN load cell range, which could be electrically scaled to a lower range of 10N with an accuracy of $\pm 0.01\text{N}$. The load cell could not be directly attached to the existing fittings on the materials testing machine and a new attachment fitting was constructed to house the new load cell on the base of the materials testing machine.

Initial experiments highlighted two main issues that had to be considered:

- Probe stability and sensitivity
- Acoustic signal stability

The probe often rotated out of alignment, which caused fluctuations in the acoustic signal as well as the load signal. The misalignment was mainly due to the rubber vibration damper attached to the main shaft as well as the poor stability of the probe fixings along the shaft. The development of a new experimental test system required an improved method of holding the probe in a stable fixed position although the damping of the mechanical drill and the level of mechanical noise still needs to be considered. It was advantageous to improve the sensitivity of the probe as the frictional forces involved appeared to be small. Small applied loads generated smaller frictional forces resulting in a poorer acoustic signal. Therefore a distinguishable acoustic response to the frictional contact was only produced after the probe had reached a depth greater than 15mm into the granular medium.

The results obtained from the initial experiments were difficult to interpret due to the non-linear characteristics of the recorded AE signals and applied load. The anisotropic behaviour encountered with granular deformation as well as the effects of the mechanical noise generated by the drilling mechanism are some of the factors that could attribute to non-linear characteristics on the AE signal. It was presumed that improving the stability of the probe would greatly enhance the stability of the acoustic signal. The transfer box also needed to be isolated from the upper drill housing mechanism, as the vibration generated from the drill motor would also propagate vibration strain waves through the transfer box thus creating additional acoustic signals that are not associated with the granular-probe friction pair.

The schematic diagram in Figure 16 highlights the main problems associated with the existing experimental test system. The load cell will be changed as it is too large for this application. Redesigning the structure of the drilling mechanism will reduce the any vibrations from the drilling mechanism being transferred to the probe by separating the structures that hold the drill and support the probe shaft. The new structure will also help to reduce the probe oscillation by improving the probe shaft support mechanism. Eliminating the coupling joint reduces the number of physical boundaries between the probe tip and the acoustic sensor. Reflections occur at these boundaries due to the mismatch in impedance and cause the acoustic waves to attenuate more quickly. Therefore, by not having the coupling joint will reduce the losses during acoustic wave propagation thus resulting in a stronger acoustic signal.

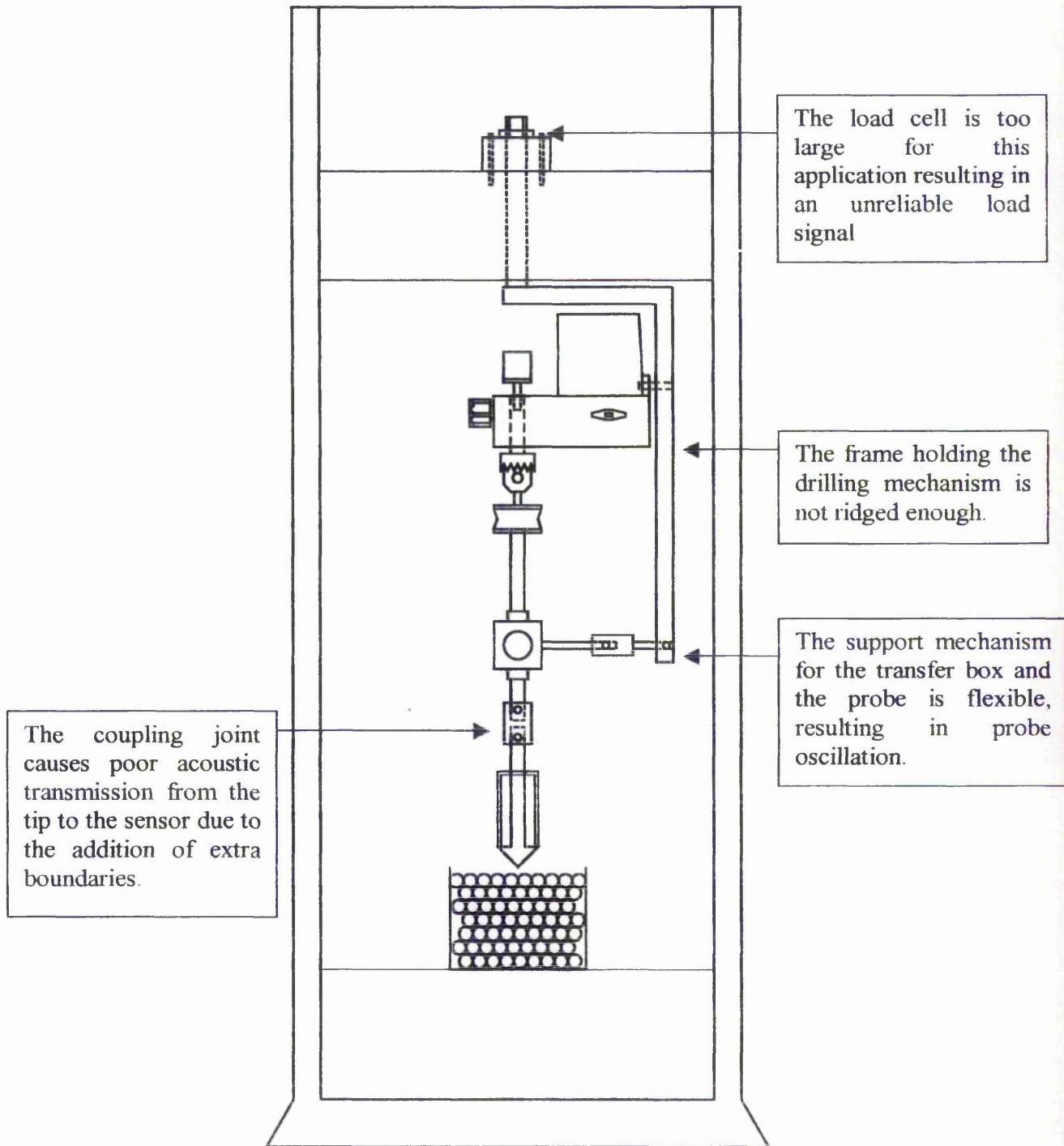


Fig 16. Diagram summarising the required improvements to the experimental system.

3.3.1 Probe Design

Since the probe was the most important component in the test system and crucial to making the technology work, a number of issues had to be considered relating to the probe design. The main aim of redesigning the probe was to improve its sensitivity to the frictional contact generated by the probe-granular interface. The coupling junction that provided probe inter-changeability (Figure 8) was considered to be the main contributor to the acoustic wave attenuation. The junction had two interfaces immediately before the transfer box, reducing amplitude of the signal generated by the friction pair. Ideally the probe should be made in one piece. The probe design is considered in more detail by Taylor [96]. Three probes with different shaped tips and different hardness coatings were constructed:

- 120°apex angle (hard chrome coated)
- 60°apex angle (Hard chrome coated)
- multi-angle tip (electroless Nickel coated)

3D CAD images of the probes are shown in Figure 17. These probes were designed to have wear resistant properties without reducing their acoustic transmission properties. It was a requirement that a uniform contact area was provided regardless of the penetration depth and that the main probe shaft was constructed in one piece. The probes incorporated a free-rotating sleeve, which remained stationary while the probe was submerged into the granular medium but still allowed the probe to rotate. Therefore, a constant granular-probe-tip contact area was provided as well as the shaft friction noise being greatly reduced by the rotating sleeve. A tapered shaft was incorporated between the probe tip and the main shaft in an attempt to improve the propagation of the friction generated stress waves from the outer perimeter of the probe tip to the smaller diameter of probe shaft.

Figure 17 to be inserted New probe designs.

3.3.2 Probe Performance Investigation

An investigation to determine and compare the sensitivity of the new probes was carried out. The new probes were initially very noisy, which was shown by an unstable and erratic level of acoustic energy being produced while the probes were rotating, even without the probe being in contact with the granular medium. The machining process for producing the probes left the shaft surface too rough and increased the friction between the probe shaft and the seals on the transfer box. Therefore, the friction between the transfer box and the rough shaft caused a lot of mechanical noise to be transferred to the acoustic sensor. The probe shaft surface was improved using lapping paper until the level of friction acoustic energy was reduced and a stable acoustic signal was produced during unloaded probe rotation. The three probes were tested and compared by monitoring the changes in the acoustic energy due to a change in the applied load. The plots of the acoustic energy against the applied load are shown in Figures 18 and 19. Results indicate that the probe with a 120° apex angle was more sensitive to frictional excitation as well as providing a larger bearing capacity than the 60° apex angle. Figure 19 highlights that the multi-angle tipped probe produced no correlation between the acoustic energy and the applied load. The data indicates that this particular probe was insensitive to the sliding friction generated between the probe and the granular medium. The insensitivity of the multi-tip probe was due to the hardness coating rather than the probe shape. In this case the coating appeared to act as an acoustic insulator, which may have been attributed to the polymer additives that improve the lubricity of the coating solution. After testing, the multi-tipped probe appeared to have a smoother surface finish indicating wear of the probe's surface. This was expected as "electroless" nickel coatings do tend to wear faster than the substrate despite their higher hardness properties. Therefore, the larger hardness value had been

compromised with a lower wear resistance contributing to its brittle and flaky nature. The random scatter of the recorded data produced by this probe might be due to the pressure impulses generated by flaking of the hardness coating.

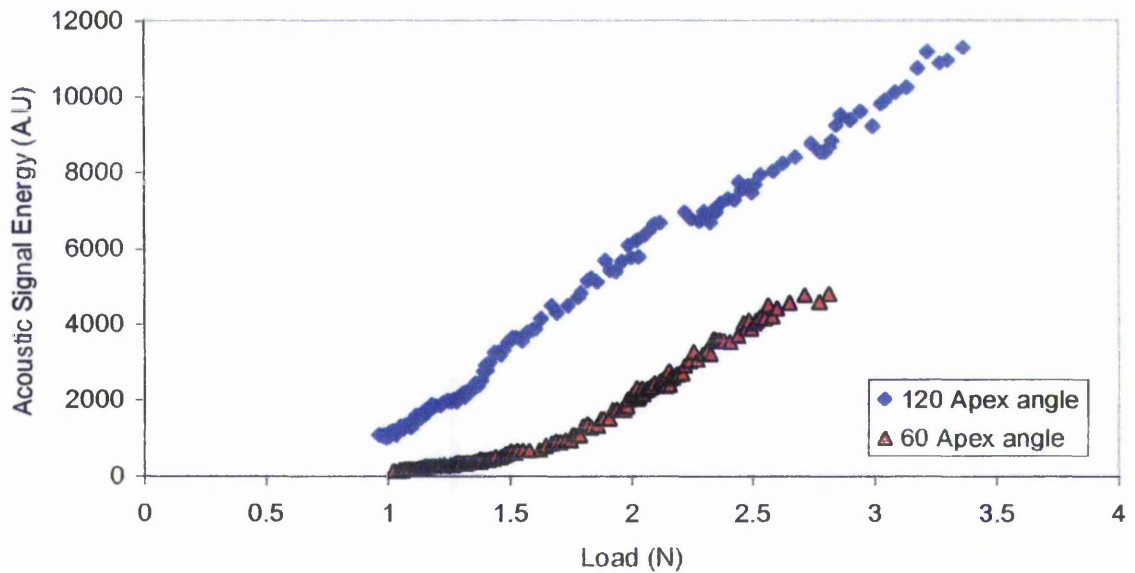


Fig 18. Two new designed probes with different apex angles. Probe velocity 8Hz (Granular particle diameter 655E-6).

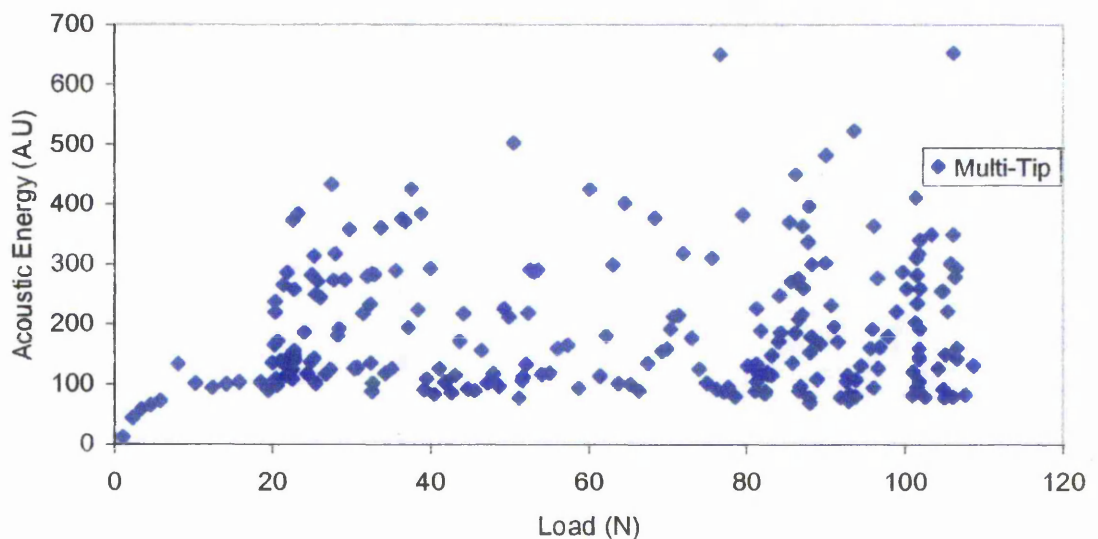


Fig 19. Variation of AE signal energy against the load using the multi-tip probe. Probe velocity 8Hz (Granular particle diameter 655E-6).

The Ra value (mean surface roughness) for each probe was recorded before and after testing to highlight the amount of wear that took place during probing. Table 1 shows the two sets of readings for the three probes tested.

Probe Type	Ra Before Testing	Ra After Testing	Roughness Change
120° Apex angle	0.33 μm	0.48 μm	+15 μm
60° Apex Angle	0.52 μm	0.67 μm	+15 μm
Multi-Tip	0.52 μm	0.32 μm	-20 μm

Table 1. Comparison of the surface roughness values before and after testing using the three new probes.

Table 1 indicates that wear of the probe tip had occurred and confirms the smoother finish that was visibly apparent with the multi-tip probe. Both the 120° and the 60° suffered a similar amount of wear despite different loading conditions used during the experimental procedure. The effect of wear must be considered when carrying out a thorough investigation of the effects the granular material test parameters have on the acoustic emission produced during sliding frictional contact.

3.3.3 Improvements of the Testing System

The experimental test system was redeveloped incorporating a new housing mechanism to stabilise the probe, a new probe and a new load cell arrangement. A schematic diagram of the new arrangement is shown in Figure 20. The housing mechanism was constructed in two parts: the drill housing and the probe housing. The drill housing was attached to the old load cell and was isolated from the probe housing system. The probe

housing system incorporated two bearings, which hold the probe in a stable vertical position. The transfer box was also attached to this mechanism using a rubber damper to reduce any noise being transferred from the frame to the acoustic transducer. The probe was constructed in three parts: the rubber vibration damper, the universal joint and the probe. The universal joint allows the rubber damper to run out of alignment without affecting the rotation of the probe. The load cell is mounted to the base of the materials testing machine and incorporated a counterbalance to compensate for the weight of the granular test sample. A rubber platform was attached to the counter balance to evenly distribute the applied load as well as reducing the oscillation of the load signal resulting from the vibrations of the granular container brought about by probe penetration and rotation. It was observed that any slight misalignment of the probe would cause a variation in the load signal due to moment forces caused by a small displacement of test sample container. The rubber bed dampened the container oscillations and reduced the effect of the moment forces.

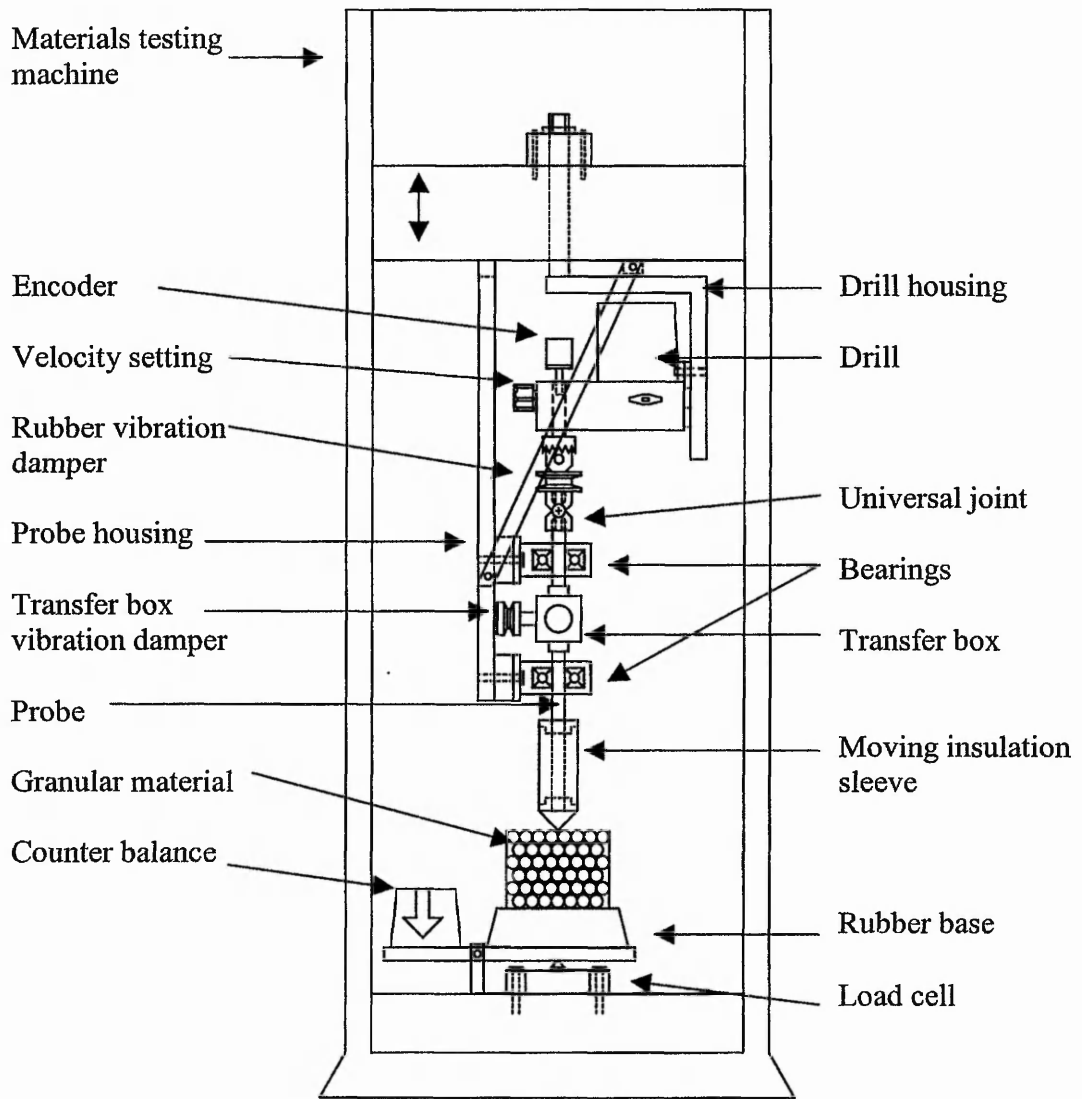


Fig 20. Schematic diagram of the improved experimental arrangement.

The rubber bed also provided a method of using different samples of sand paper (varying grade), which were used to monitor the change in the number of asperity contacts and the effect on the acoustic signal. The experimental study was considered as a method to reduce some of the uncontrollable variables associated with granular materials such as the number of asperity contacts and deformation properties. The rubber base effectively acted as a spring, providing an elastic reaction force due to the probe's vertical displacement. A probe with a flat face was required in order to maximise the surface interactions from a nominal contact area. The multi-angled tip probe was machined flat and polished to remove the electroless Nickel coating, since this coating was found to reduce the acoustic emission generated by frictional contact. The probe was tested to ensure that it produced an acoustic signal. Tests indicated that the probe was sensitive to the frictional contact between the probe and the abrasive paper and confirmed that the hardness coating restricted the sensitivity of the probe. Figure 21 shows the configuration used for experiments to investigate the changes in the abrasive paper roughness and its effect on the acoustic signal.

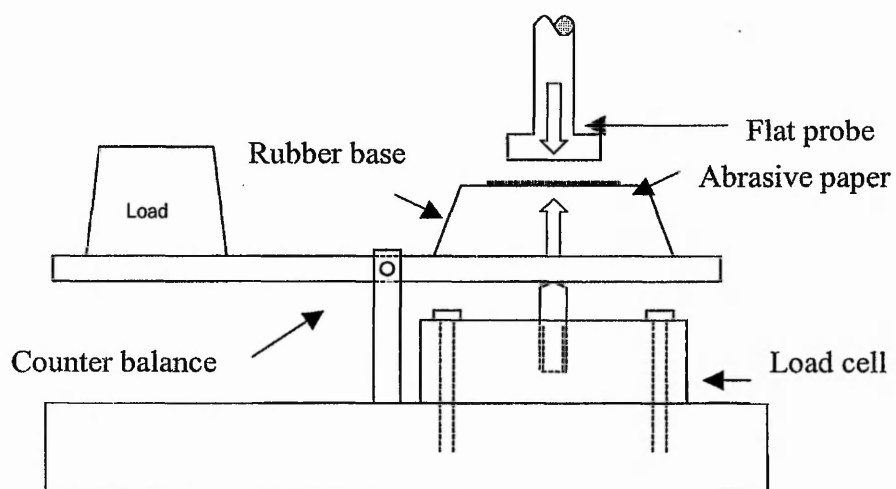


Fig 21. Experimental arrangement using abrasive paper as an alternative to granular materials.

3.3.4 Standard Methods for Studying Granular Materials

Every granular system is unique and producing repeatable experimental data is very complicated thus making it difficult to critically compare data with other sources of research. The shear strength and frictional properties of the granular materials used in this study were investigated as data from other research studies would not provide a reliable comparison. The shear strength of a granular material is not a fundamental property of soil. A granular material's shear strength is dependent upon the in-situ conditions, such as: the water content, the pore pressure, the bulk density and the confining pressure. It is not easy to compare laboratory experiments with real site conditions as laboratory results also depend on the conditions imposed during testing and reproducing comparative in-situ conditions can be difficult. Two types of shear box experiments have been used, the direct shear box and a ring shear apparatus. A brief summary will be given in the following sections although Head [97] provided an extensive description of standard apparatus used as well as typical experimental procedures.

3.3.4.1 Standard Shear Box Test

A standard shear box test provides a measure of the internal friction angle for a given sample of granular material. The granular sample is sheared in the horizontal plane, which is achieved by placing the soil in a steel box composed of two halves with the bottom half displaced horizontally relative to the upper half (Figure 22). During granular shear, the relative displacement of the sliding portion of the shear box along with the shear force is measured. The vertical displacement of the shear box can also be measured to determine the dilation properties of the granular sample and to monitor the changes in the granular density. The shear box cannot be used with wet samples, as

there is no provision for measuring the pore water pressure and so the effective normal stress cannot be determined.

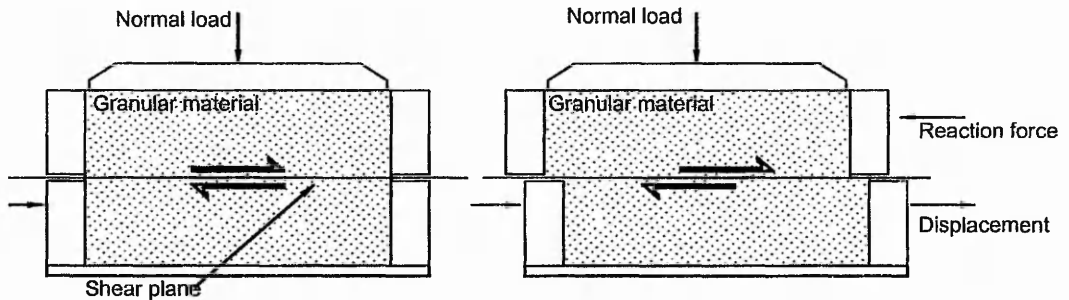


Fig 22. The principle of a shear box test.

The frictional angle is determined by completing several tests on a granular sample under different loads (usually three). Each load corresponds to a specific value of the normal stress, with the granular sample's surface area remaining constant. For each test a stress/displacement curve is plotted and the peak shear stress can be found (Figure 23).

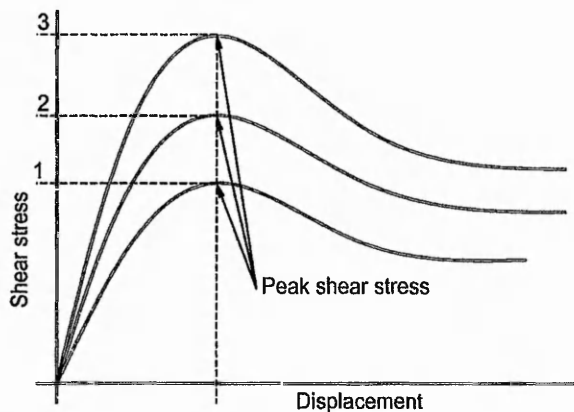


Fig 23. Illustration of the relationship between the shear stress and displacement in a shear box test for three different applied loads.

Using the peak stress values from individual stress/displacement curves the peak stresses can be plotted against the normal stresses. The relationship in most cases approximates to a straight line (Figure 24). The gradient of the straight line is used to determine the friction angle or the shearing resistance of the soil while the intercept of the y-axis is referred to as the apparent cohesion. The relationship between the shearing resistance, τ_f , and the normal stress, σ_n , for granular materials is given by the Coulomb relationship:

$$\tau_f = c + \sigma_n \tan \phi \quad (25)$$

Where, c , is the apparent cohesion and ϕ is the friction angle. This relationship only holds true for dry samples of granular material, as the effect of pore pressure will affect the shearing resistance of the soil. The effect of pore water is accounted for by using the effective stress, which is equal to the normal stress minus the pore water pressure. However, as stated earlier the pore water pressure cannot be measured using a standard shear box test. Therefore, the shearing resistance can still be measured but not the effective normal stress.

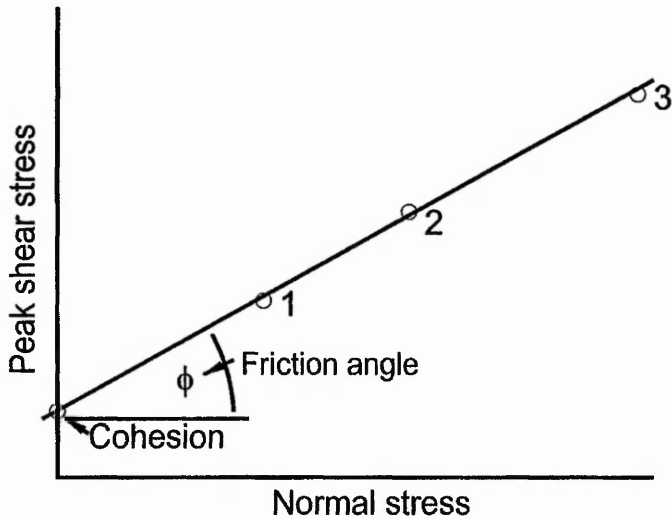


Fig 24. An Illustration of the functional relationship between the peak shear stress and the normal stress using results from shear box tests (Coulomb envelop relationship).

The aim of using the shear box was to determine the frictional characteristics of materials due to particle-particle friction for different particle sizes and saturation levels. The particle-particle friction was compared to the acoustic signals generated by the probing system using granular systems of similar conditions. Although the granular samples were placed in different containers, similar bulk densities were used as well as similar saturation levels. It was stated earlier that the standard shear box is not really suitable for wet sands due the unknown pore pressures occurring during shear; this might also be true for the probing system for similar reasons. However, the shear box tests provided indication of the effects that water content has on the friction angle and whether the change in the friction angle could be correlated with any changes in the acoustic signals.

3.3.4.2 Ring Shear Test

The residual shear corresponds to the stable shear resistance that occurs after the peak shear resistance is achieved (see Figure 23) and the ring shear apparatus is often used to measure the residual shear strength of a granular material. The residual shear arises due to frictional resistance associated with the sliding of solid bodies, while the granular peak shear stress arises due to the static limiting friction of solid bodies. The apparatus incorporates a ring shaped specimen box, which holds the granular materials (the ring shaped box is also made in two parts like the standard shear box as shown in Figure 25a). The top portion of the ring shear has been replaced with a steel ring to produce a steel-granular sliding interface, which in part replicates the probe-granular interface used in our AE rotating probe experiments. The bottom section of the ring shear rotates at a constant velocity while the top section is held in a stable position by two load rings, which compress in proportion to increasing shear force (see Figure 25b). The compression of the load rings are monitored by two linear transducers and recorded using a suitable data logger. Results are recorded for a set period of time and the normal load was increased throughout the test. The residual shear resistance is calculated for each loading condition and the Coulomb envelope method (equation 25) was used to determine the friction angle. This experimental arrangement was used to measure the frictional characteristics of the different granular samples under various loading conditions using a sand-steel sliding interface.

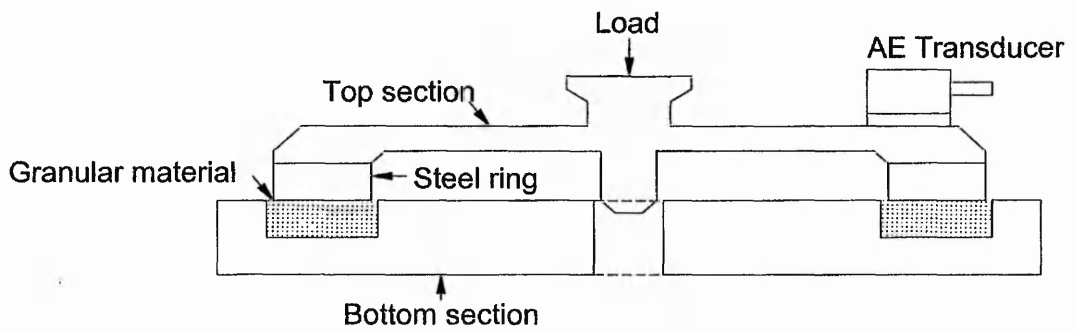


Fig 25a

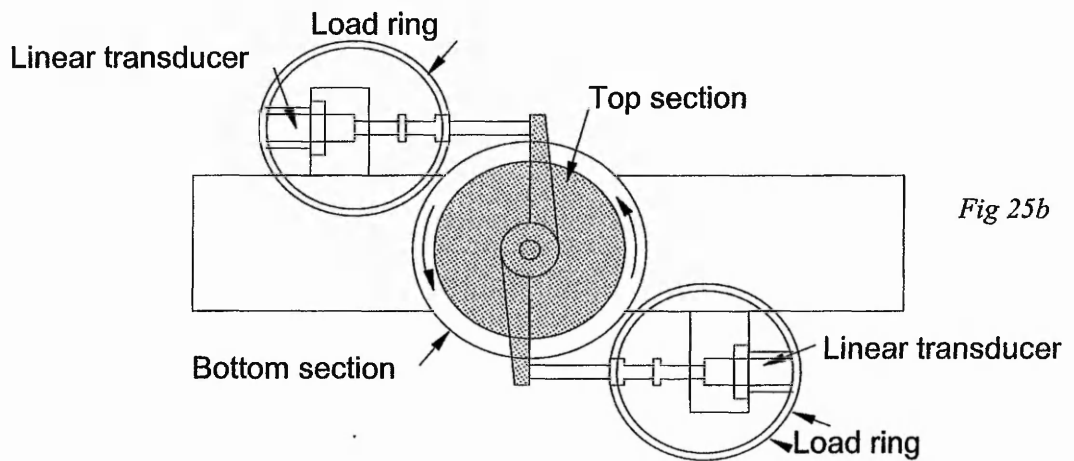


Fig 25b

Fig 25. A ring shear apparatus, (a) displays a cross section of the ring sample box, (b) displays a top view of the ring shear.

The steel rings used in the ring shear apparatus allow an acoustic transducer to be attached to it using a suitable coupling adhesive. The acoustic system described in Section 2.1.5 was used in these experiments and the AE transducer was attached to the top steel ring. The frictional resistances measured by the ring shear tests were compared with acoustic signals generated by the ring shear to investigate possible functional relationships that may exist.

3.4 AE and the Mechanical Parameters for Monitoring Friction

For AE monitoring of friction the acoustic signal is generated at the interface between the probe and a granular material. The mechanical and acoustic parameters involved in the contact between the probe and the granular grains need to be identified. Attention is focused on the friction pair (the interaction between the probe tip and the granular medium) and the main parameters are considered to be; the applied load, angular velocity of the probe, the acoustic signal parameters and the material properties of the friction pair.

There are four acoustic parameters that can be readily investigated, the acoustic RMS, the acoustic count rate, the AE event count and the acoustic energy. Due to the continuous nature of the acoustic signal it is difficult to separate different AE events and therefore, the event count was rejected as a suitable parameter. The acoustic RMS requires a sample of the raw acoustic signal and can be data intensive, which involves larger computational processing time. The count rate and acoustic energy are common parameters that have been used in condition monitoring by other researchers [66,67,70]. Models that relate the parameters of frictional contact to the acoustic energy and the count rate have also been considered for solid interactions by Sarychev et al [73] and Baranov et al [74].

4.0 Theoretical Consideration

For the AE monitoring of friction considered in this study the acoustic signal is generated at the interface between the probe tip and a granular material. The friction generated acoustics involved with a granular-solid interaction differs from other research, which mainly considers solid-solid friction pairs. In this section the AE generated by a solid-solid interaction is discussed, especially focusing on the source of the acoustic emission and how the frictional contact relates to an acoustic parameter. Further discussion will involve the physical contact between a solid-granular friction pair and describe how this interaction can be related to an acoustic parameter.

4.1 The Source of the Acoustic Emission

The source of acoustic emission results from the release of strain energy generated by surface asperity deformation at the real area of contact. When considering sliding friction, the adhesion between contacting asperities are continuously formed and destroyed resulting in stick-slip behaviour. Asperity deformation creates an elastic energy potential that is suddenly released when the asperity bonds are destroyed and is considered to be the main source of the acoustic emission generated by the friction pair.

4.2 Relating the Acoustic Parameters to the Friction Pair

Work by Diei [72] investigated the AE generated by tool wear in face milling using the root-mean-square AE parameter. Diei's work showed that the AE_{RMS} increases as a linear function of the increasing load, with a power law relationship between the sliding velocity and AE_{RMS} . Diei proposed an equation relating the AE_{RMS} to the parameters of the friction pair:

$$AE_{RMS} = (k\eta\tau A_a \nu)^{\frac{m}{2}} \quad (26)$$

Where k is a constant depending on the AE measuring system, m is a function of the material properties of the contacting pair, τ is the shear strength of the interfacial material, A_a is the apparent area of contact, η is a function of both the surface roughness and the elastic properties of the friction pair (this parameter defines the actual area of contact $A_r = \eta A_a$) and ν is the relative surface sliding speed.

The sphere and flat surface experiments conducted by Tabor [48] produced an equation, which described the frictional force F_f due to sliding:

$$F_f = \tau A_r \quad (27)$$

Where τ is the interfacial shear strength and A_r is the real area of contact.

Therefore substituting (27) into (26) provides the following relationship:

$$AE_{RMS} = (kF_f \nu)^{\frac{m}{2}} \quad (28)$$

Equation 28 shows that the AE_{RMS} is a function of the frictional force and the sliding velocity. Tabor [48] stated that the frictional force is a function of the real area of contact, which is proportional to the applied load. Therefore, changes in both the applied load and the sliding velocity will have a direct effect on the AE_{RMS} . However, Newton's law states that the frictional force increases proportionally with the applied load, which means Equation 28 also suggests that a power law exists between the AE_{RMS} and the applied load.

Equation 28 can be developed further by incorporating the frictional force relationship between a solid and granular interface as proposed by Adams et al [53]. Adams described the frictional contact at walls for spherical particles. The frictional force F_f for spherical particles (Equation 12) is substituted into equation 28 and the proposed relationship between the AE_{RMS} and a granular material is given by:

$$AE_{RMS} = \left(kv \left(\pi \tau \left(\frac{AF^2 D^2}{s^2} \right)^{\frac{1}{3}} + F \right) \right)^{\frac{m}{2}} \quad (29)$$

Where F is the total applied force, A is the nominal area, D is the contact modulus and s is the spacing parameter.

An equation has been proposed relating the AE_{RMS} to a solid-granular friction pair. The frictional force parameter that related to the solid-solid interaction was replaced by the same parameter for a solid-granular interface, which assumed the granular particles were completely spherical. Paikowsky, et al [55] however, stated the importance of the grain shape and its contribution to the interfacial friction and therefore, the validity of Equations 28 in respect to the frictional interaction considered in this study would require further investigation.

Research carried out by Sarychev and Shchavelin [73] described a general rule relating the acoustic count rate parameter to the sliding velocity.

$$\dot{N} = A + Bv^x \quad (30)$$

Where A and B are constants and $x \geq 1$.

Although a different acoustic parameter has been used compared to the work conducted by Diei, a power law is still suggested between the acoustic parameter and the sliding velocity. Sarychev and Shchavelin also proposed a similar rule for the relationship between the acoustic count rate and the applied force F :

$$\dot{N} = A + BF^x \quad (31)$$

However, in this case A and B are still constants, but $x \leq 1$.

The rules described by Equations 30 and 31 only provide a general description of the effect that sliding velocity and the applied load will have on the acoustic count rate and do not consider the parameters involved in producing the AE. However, Baranov et al [74] derived a theoretical model relating the parameters of the frictional contact for solid-solid interactions to the count rate parameter (Equation 21). The model is based on the assumption that the count rate is directly proportional to the number of contacts formed per unit time. The basis for this assumption relates to the behaviour of asperity interactions during sliding friction. Asperity interactions yield a stick slip mechanism whereby the stick phase is a result of asperity bonding while the slip phase corresponds to the release of strain energy. The sudden change in strain energy produces a pressure pulse at the point of contact resulting in elastic wave propagation through the friction pair materials. Therefore, the number acoustic pulses generated can be considered to be related to the number of asperity contact spots formed and destroyed. The assumption used by Baranov considers the number of contact spots formed during sliding and every contact spot formed must be broken for sliding to continue. Akay [68] noticed that corrugated (rough) surfaces produced impulsive contact forces at the corrugation

frequency, which related the number of asperity interactions to the number of pressure pulses generated by the friction pair. Whereas Briscoe et al [70] mentioned that the stick slip frequency increased with increasing sliding velocity and that a change sliding velocity would proportionally affect the number of asperity interactions per unit time.

In this study a similar assumption will be made (the count rate is proportional to the number of contact points formed per unit time) although a mathematical approach to determining the number of contacts for a granular-solid interaction will not be derived. The number of contacts formed within the apparent area between the friction pair will simply be represented as a single parameter N_c and an equation for the count rate \dot{N}_{AE} is given by:

$$\dot{N}_{AE} = kN_c v \quad (32)$$

Where k is constant of proportionality and v is the sliding velocity.

Due to the small diameter of the granular particles it is assumed that the granular particles in contact with the probe will only form a single contact spot. Therefore, the number of contacts between the probe and the granular material will represent the number of granular grains in contact with the probe. Therefore using the acoustics count rate parameter could provide a direct method of determining the number of grains in contact with the probe tip.

Baranov et al [74] also derived an equation for the acoustic energy (Equation 20) based on the assumption that the amount of acoustic energy developed is proportional to the total potential energy generated by asperity deformation. In this study the asperity

interaction is the contact between the granular particle and the probe tip. Therefore the contact between the probe tip and the particle is represented as a sphere in contact with a flat surface. The relationship between the contact of two spherical elastic bodies and the elastic potential energy is given in Equation 6. In Equation 33, a sphere in contact with a flat surface is considered and the elastic energy e_e is given by:

$$e_e = \left(\frac{2h^2}{5D} \sqrt{R} \right) + c \quad (33)$$

Where R represents the granular particle radius.

The contact involves a spherical body in contact with a flat surface, pressed together by an applied force. Deformation will occur symmetrically around the original point of contact and produce a small contact area over a proportion of their surfaces. Producing this contact area has also produced a linear displacement, h , which is the distance between the undeformed outer surfaces of the solid bodies, assuming no deformation has occurred and both bodies move into each other. The displacement, h , of a sphere in contact with a flat surface, is given by:

$$h = F_c^{\frac{2}{3}} \left(D^2 \left(\frac{1}{R} \right) \right)^{\frac{1}{3}} \quad (34)$$

Substituting (34) into (33) gives:

$$e_e = \frac{2}{5} \left(\frac{F_c^5 D^2}{R} \right)^{\frac{1}{3}} + c \quad (35)$$

The relationship between the amplitude of the acoustic signal, A , to the elastic potential energy generated as a result of asperity interaction was stated by Baranov et al [74]:

$$A \approx \left(\frac{\varepsilon}{\tau} \right)^{\frac{1}{2}} \quad (36)$$

Where, ε is the acoustic emission pulse-energy and, τ is the radiation time of the AE pulse. Assuming the acoustic emission pulse-energy is proportional to the potential energy generated by the elastic deformation of the contacting asperities, (35) is substituted into (36) to provide the following relationship describing the amplitudes of the acoustic signal A for a single particle contact:

$$A \propto \left(\frac{2}{5\tau} \right)^{\frac{1}{2}} \left(\frac{F_c^5 D^2}{R} \right)^{\frac{1}{6}} \quad (37)$$

The radiation time, τ of the AE pulse and is given by [74]:

$$\tau = \frac{a}{\nu} \quad (38)$$

Where ν is the sliding velocity, a is the radius of the contact spot formed by the asperity tip. The radius, a of the contact spot is given by Hertzian contact laws and considering a sphere in contact with a flat surface the following relationship results:

$$a = F_c^{\frac{1}{3}} (DR)^{\frac{1}{3}} \quad (39)$$

Substituting equations (38) and (39) into (37) gives:

$$A \propto \left(\frac{8F_c^4 \nu^3 D}{125R^2} \right)^{\frac{1}{6}} \quad (40)$$

Therefore, using the assumption stated by Baranov et al and Hertzian contact laws, an expression is derived involving a sphere in contact with a flat surface. However the

relationship only considers the acoustic emission generated by the elastic deformation and does not account for the acoustic emission generated by wear. It also assumes the granular grains are spherical, which in practice is not generally true. The relationship derived in Equation 40 highlights that the acoustic amplitude is directly affected by changes in the applied load and sliding velocity as well as being dependent on the material properties i.e. particle radius and elastic properties of contacting asperities.

The theory considered in this section seeks to relate the physical contact between the granular grains and the probe tip with an acoustic parameter. The count rate relationship is based on the assumption that the count rate is directly proportional to the number of contacts formed per unit time. An assumption is made that each grain in contact with the probe only produces a single contact and therefore, it may be possible to determine the number of grains in contact with the probe due to geometrical constraints. The acoustic energy relationship is based on the assumption that the acoustic energy is proportional to the potential energy generated during elastic deformation. Although the acoustic energy relationship only considers elastic asperity deformation it still provides a good insight to the typical parameters that may affect the generated acoustic emission.

The relationships considered in this chapter have highlighted three possible parameters that could be used to investigate the material properties of the friction pair. The number of asperity interactions is an important contact parameter as it determines the number of acoustic sources occurring between the friction pair. The count rate parameter is assumed to be directly proportional to the number of contact points formed per unit time and therefore provides a direct method of determining the number of asperity contacts.

However, the assumption that led to the relationship between the count rate and the number of asperity contacts will need to be validated.

Both the AE_{RMS} and the acoustic energy can be related to the physical contact between the probe tip and the granular medium. However, this project requires an acoustic parameter that can be processed continuously and quickly in order to provide a system capable of real-time soil characterisation. The AE_{RMS} signals are to be determined using the Viewdac software, which requires a true sample of the acoustic waveform. Sampling the acoustic waveform is expected to be data intensive and will involve large processing times. The acoustic energy parameter however, is a standard parameter on the signal processing unit. The count rate and acoustic energy are parameters that have been used in condition monitoring by other researchers [66, 67, 72].

4.3 Summary Comments

Investigating the count rate and the acoustic energy may provide a method of determining the number of particle-probe contacts and the total energy associated with those contacts. Therefore the average energy for a single contact can be investigated leading to a further analysis involving mechanical contact between the probe and a singular granular particle. However, the acoustic parameters must be investigated to validate their relationships with the physical contact between the probe and the granular material before an investigation of the actual contact can be made.

5.0 Presentation of Results

The theoretical consideration in the previous chapter developed three equations that related the frictional contact to an acoustic parameter. The three parameters being considered are: the AE_{RMS} (Equation 29), the count rate (Equation 32) and the acoustic energy (Equation 40). The two general equations for the count rate (Equations 30 & 31) involving the applied load and the sliding velocity were also considered. This chapter details a series of investigations, which have been carried out to develop an understanding of what parameters affect the acoustic emission generated from solid-granular friction pairs as well as providing data, which could be used to validate the equations developed in the theoretical consideration.

The aim of this project is to develop a novel method of characterising ground structures using the AE generated from a typical drilling process. Therefore, the focus of this investigation is to develop a method for determining the properties of the granular material using the acoustic signal generated by the frictional contact between the probe tip and the granular material. The AE_{RMS} will not be considered in the investigations as a real time characterisation process is preferred and the large amount of data required to analyse the AE_{RMS} does not permit rapid data acquisition.

The theoretical relationships developed between the frictional contact and the acoustic parameters are dependent on the applied load and the sliding velocity, the effects of these two parameters on the acoustic parameters need to be established. This will allow a further investigation involving different granular materials and their characterisation. Results obtained from this investigation will be compared to the relationships presented

in the previous chapter (Equations: 29, 31, 32 and 40) in order to validate their relevance to the friction pair considered in this project.

Initial tests suggested that abrasive paper could be used as a suitable method of changing the number of surface asperities in contact with the probe tip during sliding friction and it was used to investigate the relationship between the number of asperity contacts and the count rate (Equation 32). The use of abrasive paper with different grades allowed the count rate parameter to be investigated over a larger range of applied loads and provided a detailed study of the effects of different loading conditions on the count rate.

A novel method of processing the acoustic signal was developed to focus on a particular characteristic of the count rate parameter, which was identified during the experimental investigation. Focusing on this particular characteristic of the count rate allowed the particle size to be identified. The ability of characterising the particle size using different soil densities and water content was also addressed.

The count rate and the acoustic energy parameters were used to investigate the average contact force at a single particle contact. Therefore, information relating to the material properties of the friction pair as described by Equation 40 could be investigated.

Standard soil testing techniques were carried out to investigate the shear properties of the soil and its effect on the acoustic parameters. Both the peak shear and the residual shear parameters were considered as well as the AE generated during these tests in order to provide acoustic data directly related to the shear box test results.

5.1 Investigation of the Count Rate and the Acoustic Energy

The count rate and the acoustic energy parameters were determined by applying a threshold to the raw amplified acoustic signal supplied by the transducer. The threshold was adjusted to eliminate any acoustic counts generated by the mechanical operation of the probing system. The effects of the applied load and sliding velocity on the acoustic parameters were investigated.

The probe was set to rotate at a constant velocity and moved vertically until it was just above the upper surface of the granular sample. The threshold was adjusted so that no counts were registered while the probe was not in contact with the granular sample (Threshold set at 0.015V). The vertical feed rate of the probe was set at a constant speed while the data acquisition sequence was started simultaneously with the probe penetration. The probe's angular velocity was controlled using the speed setting dial on the drilling system, which was adjusted throughout the test and maintained to within limits of +/- 0.1 Hz. The applied load depends on the resistance force provided by the granular material and during constant penetration the load increased with penetration depth. Tests were repeated using different probe rotational speeds in order to identify the effects of sliding velocity on the acoustic signals.

The results in Figure 26 highlight the typical effects of the applied load on the acoustic parameters. To help describe the results the data has been divided into three sections: 1, 2 and 3. Section 1 corresponds to the initial penetration of the probe. The probe initially started its penetration just above the top surface of the granular material and for the first 30mm of penetration the probe tip is not in complete contact with the granular sample. The change in the acoustic signal generated is very small and the amplitude is too low to

be detected by the threshold that was applied to the acoustic signal. In Section 2 there is full contact between the probe and the granular material, which is shown by a rapid increase in the count rate and acoustic energy. The results in section 2 suggest that a power law relationship exists between the applied load and the acoustic parameters. Within section 3 there is an appreciable reduction in the rate of increase of the count rate and acoustic energy due to the applied load. The change in the curve suggests that two expressions are needed to describe the relationship between the applied load and the acoustic parameters. The general shape characteristic of the complete data set resembles an S-shaped curve. It is interesting to note that the variations of the count rate parameter and the acoustic energy parameter have very similar shape characteristics and it could be argued that only one of these parameters would need to be recorded. However further investigations are required to validate this argument.

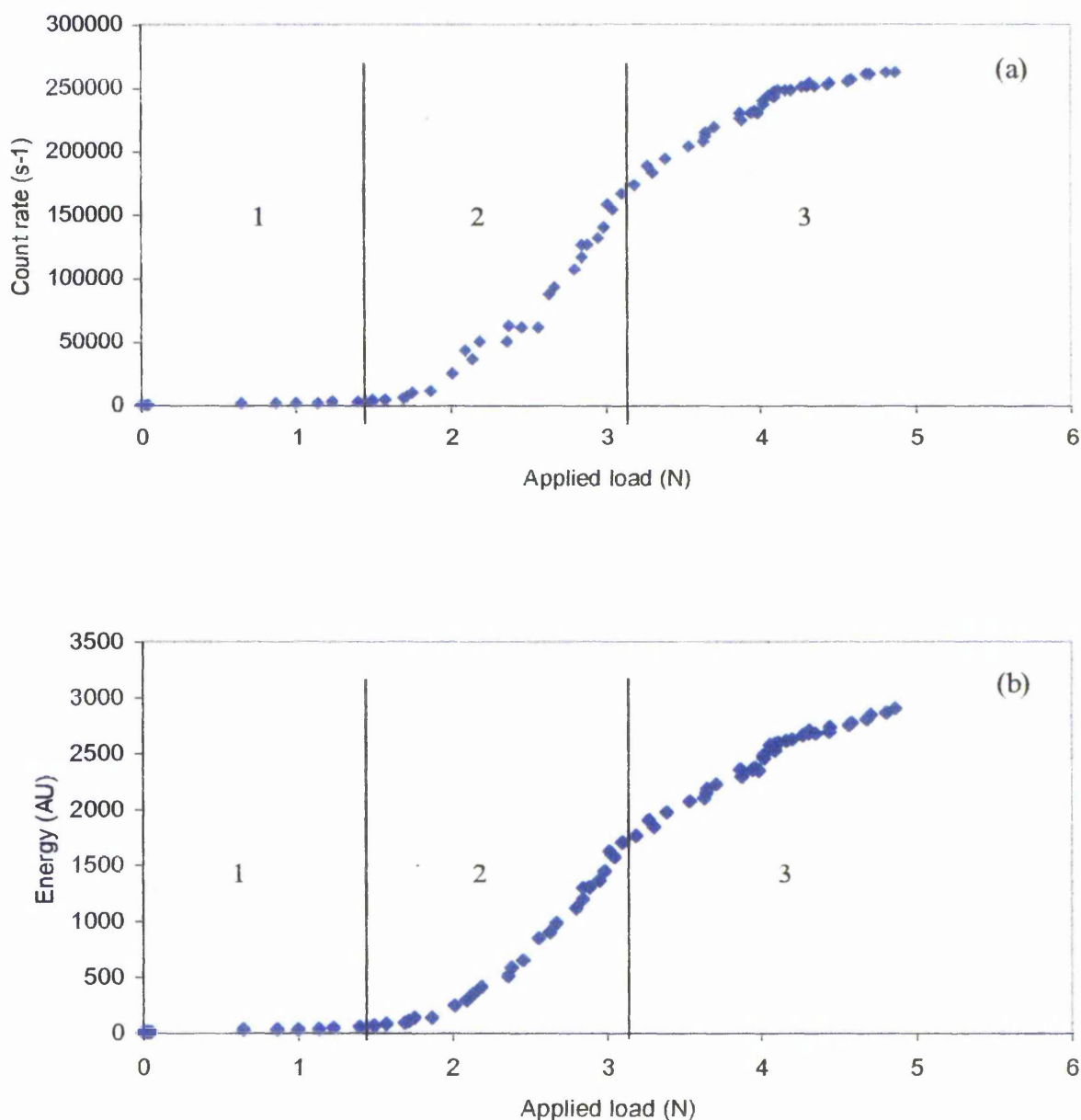


Fig 26. The change in the acoustic signals due to an increase in the applied vertical load using Leighton Buzzard sand ($655\mu\text{m}$ average particle diameter) and a rotational sliding velocity of 7Hz , a) the count rate, b) the acoustic energy.

The results indicate the main change in the acoustic parameters occurred when the probe tip was in full contact with the granular material (sections 2-3). Investigating the acoustic signals for complete probe-tip-granular contact required optimising the testing

procedure so that the data acquisition sequence began when the probe was at an initial depth of 30mm into the granular sample. Once the probe reached the required depth of 30mm the data acquisition sequence started and data was recorded for a further probe penetration depth of 50mm. Saturation of the acoustic signal was avoided by increasing the applied threshold from 0.015V to 0.02V. The results in Figure 27 display the change in the count rate due to an increase in load caused by probe penetration for four different rotational velocities. Unlike the previous results (Figure 26) where an S-Shape curve was obtained, increasing the threshold and commencing the monitoring process at an initial probe depth of 30mm has reduced the amount of data available in sections 1 and 3. Therefore, the results shown in Figure 27 mainly consist of data within section 2. The results suggest a power law relationship between the applied load and the count rate, of the form $y = kx^n$. A power law curve has been fitted to each set of the data to provide an estimation of the index value. The results indicate that the index value of all four curves is approximately 2. As a first estimate the count rate increases approximately to the square of the applied load. The data in Figure 26a displayed an S-shape curve and the line separating section 2 and 3 indicated a change in the relationship between the count rate and the applied load. In Figure 27 the change in the power law is also evident and is shown by the data not fitting the power law curve at larger applied loads. The power law equations also highlight the significant effect that the sliding velocity has on the count rate, which is shown by the variation in the multiplying constant. An increase in the sliding velocity produces a significant increase in the multiplying constant. A faster sliding velocity will therefore produce a larger count rate at a given applied load.

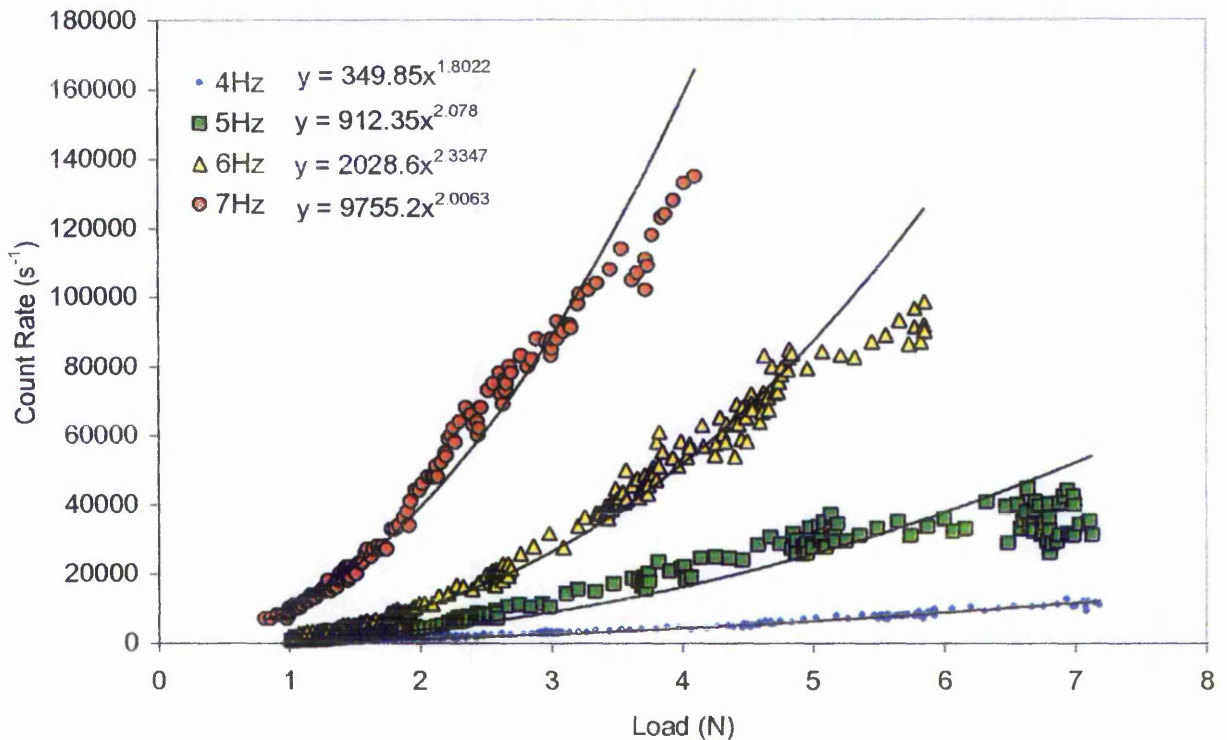


Fig 27. The count rate against the vertically applied load for four different rotational velocities. Data considers full probe particle contact from an initial depth of 30mm.

The change in the acoustic energy due to increasing applied load is shown in Figure 28 using four different rotational velocities. Power law curves have been fitted to the data and an estimation of the index value of the power law relationship is provided. The data obtained for the acoustic energy is also very similar to the data shown in Figure 27, which considered the count rate. The results show that the acoustic energy also increases approximately to the square of the applied load. The similarities between the count rate and acoustic energy indicate that a relationship may exist between them.

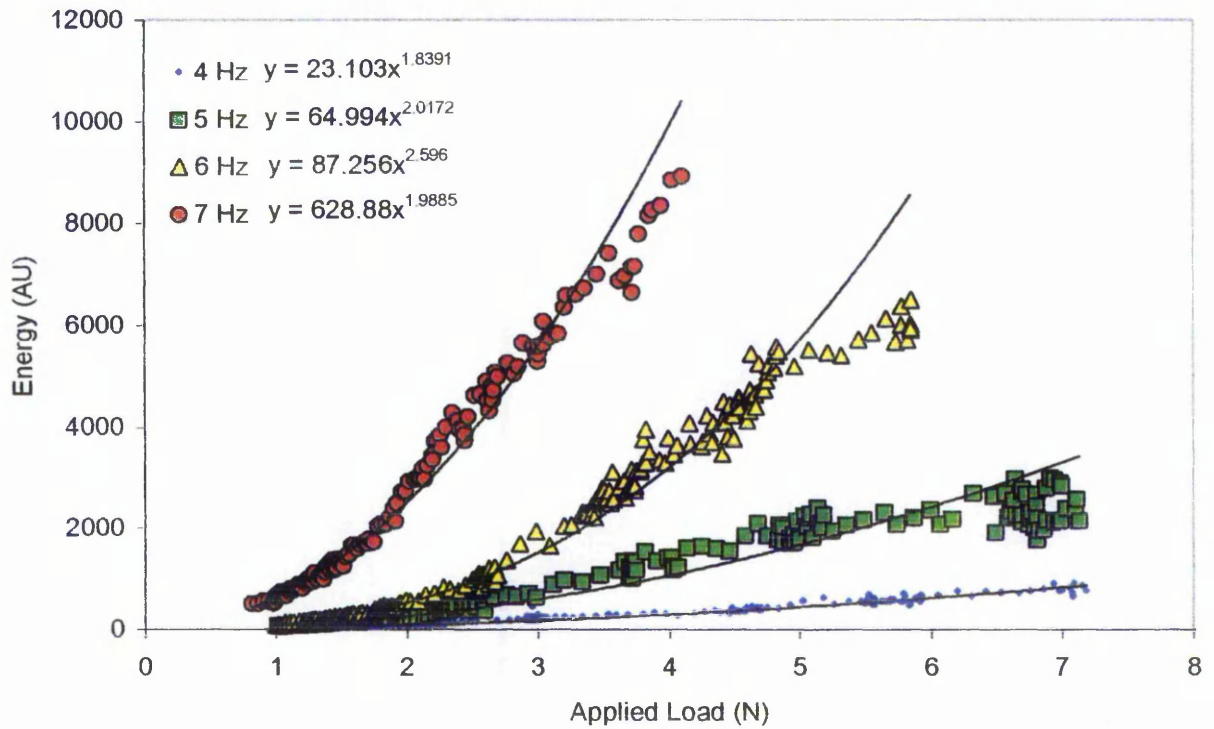


Fig 28. Acoustic energy against vertically applied load for four rotational velocities using Leighton Buzzard sand ($655\mu\text{m}$ average particle diameter).

The relationship between the count rate and the acoustic energy has been investigated by correlating the count rate data (Figure 27) with the acoustic energy data (Figure 28) for four rotational velocities. Figure 29 shows that a linear relationship exists between the acoustic energy and the count rate. It can be seen that all the data collapses on to a straight line, which may be represented by the equation $y = 0.0648x - 53.595$. This suggests that the relationship between the count rate and the acoustic energy is independent of the applied load and the sliding velocity. Consequently it can be concluded that changes in the applied load and sliding velocity produced proportional effects on both the acoustic energy and the count rate. Therefore at any instant the acoustic energy can be calculated from count rate or vice versa using a predetermined empirical function.

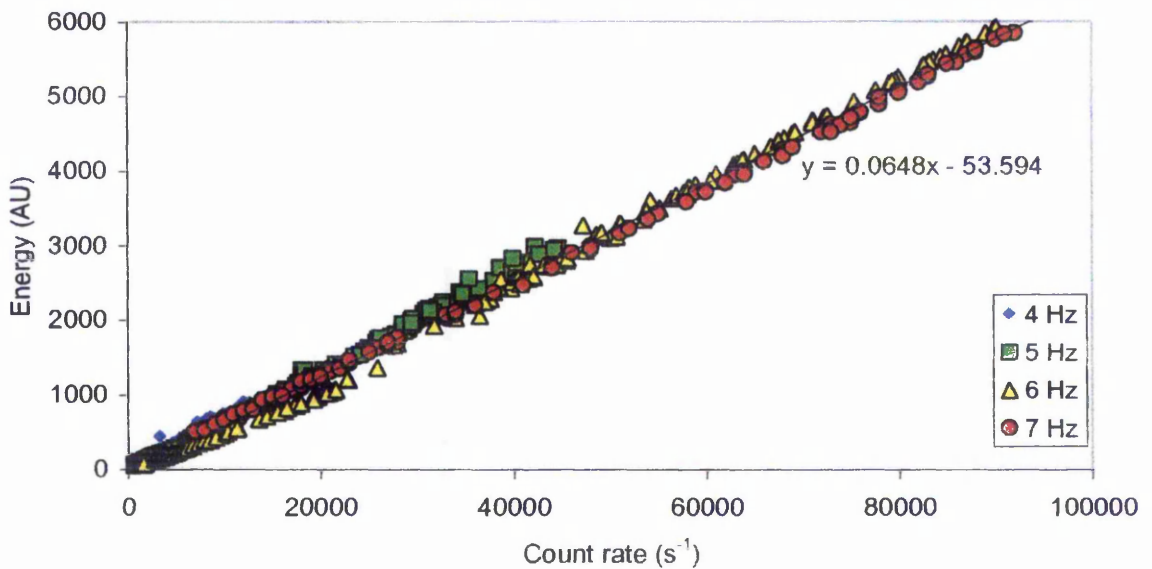


Fig 29. Acoustic energy against count rate for four different rotational velocities using Leighton Buzzard sand ($655\mu\text{m}$ average particle diameter).

In the theoretical consideration (Chapter 4), two assumptions were stated by Baranov et al [74], which related the count rate and the acoustic energy to the physical contact between the friction pair. One assumption stated that the count rate is directly proportional to the number of contact spots formed per unit time. The other assumption stated that the acoustic energy was proportional to the potential elastic energy generated as a result of the elastic deformation of contacting asperities. The results displayed in Figure 29 may be considered as the variation of the total elastic energy against the total number of contact spots formed during sliding friction and the gradient of the line may be taken as a measure of the average elastic energy for a single contact spot. A linear gradient indicates that the energy at a single contact spot remains constant. Therefore, to maintain a constant energy at a single contact, the increase in the applied force or sliding velocity must be counterbalanced by an increase in the number of contact spots

formed. The actual number of contacts between the probe tip and the granular medium is unknown, although using granular samples of different particle sizes should provide a method of changing the number of contact spots formed as a result of geometrical constraints. It would be expected that larger particle sizes will produce fewer contacts on the probe's surface and smaller particles will produce more contacts.

The next step is to investigate the acoustic energy against the count rate with respect to a change in the particle size. Figure 30 shows the acoustic energy plotted against the count rate for different particle sizes. The results highlight that changing the particle size does affect the gradient, which indicates that the average elastic energy at a single contact spot is affected. Therefore, it can be concluded that the relationship between the count rate and the acoustic energy also depends on the grain size of the granular medium. However, the change in the gradient as a result of increasing particle size does not show a clear pattern. Average particles sizes between 655-925 μm average particle diameter, showed an increase in the gradient with increasing with particle size, but the 1090 μm average particle diameter showed a reduction in the gradient. Larger particle sizes, especially those that are not spherical, which may have flatter surfaces, could produce more than one contact spot during a particle-probe interaction. Therefore, granular particles producing more than one contact spot could be represented as a granular material having smaller spherical particles, which would also produce more particle-probe contacts. Furthermore the 1090 μm granular sample did not produce a strong acoustic signal, which may account for the change in the gradient.

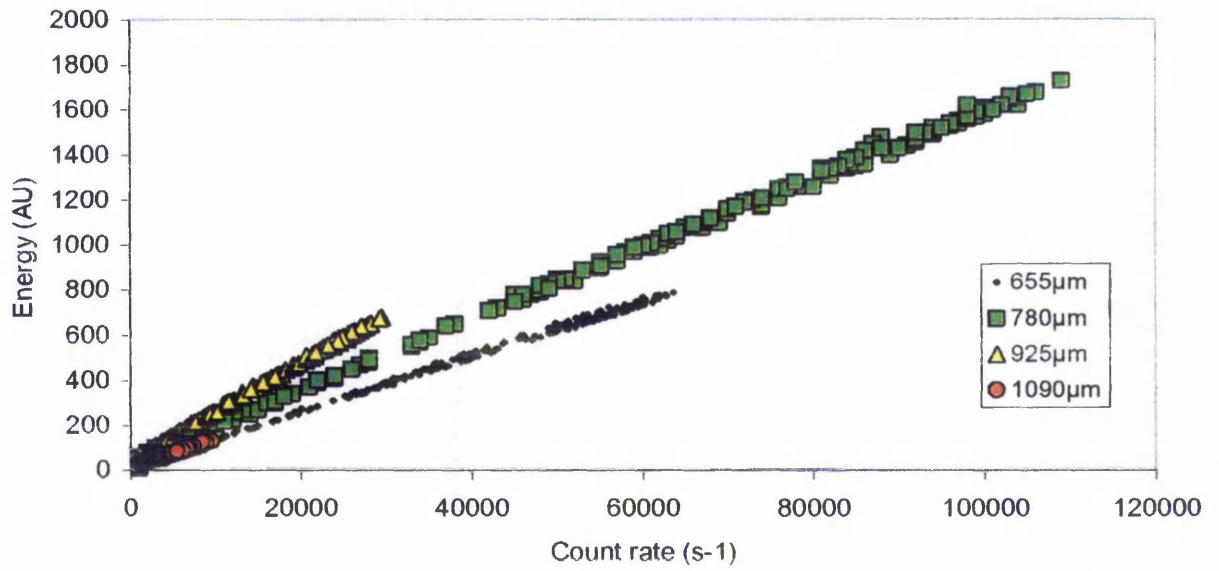


Fig 30. Acoustic energy against count rate, for four different grain sizes. Leighton Buzzard sand samples, rotational velocity set at 6.5Hz

5.2 Abrasive Paper: The Controlled Granular Medium

In the previous section a relationship between the acoustic energy and the count rate was highlighted, which was both independent of the applied load and sliding velocity but was dependent on the grain size of the granular material. It was postulated that an increase in the applied load and sliding velocity was directly counterbalanced by an increase in the number of probe granular contacts based on the assumption that the count rate was related to the number of contact sports formed per unit time. An investigation was carried out to determine whether an increase in the number of asperity contacts produced an increase in the count rate. Graded abrasive paper was used to represent a controlled medium, where different grades of abrasive roughness created a controlled change in the number of probe-asperity contacts. The experimental arrangement has been described in Section 3.3.3. Three grades of abrasive paper have been used, P1200, P800 and P400, where a smaller P number represents a coarser surface roughness with P400 representing a smaller density of particle-probe contacts. The rubber base in the experimental arrangement allows the applied load to be controlled by adjusting the vertical displacement of the probe. The investigation focused on the effect of an increase in the applied load and sliding velocity on the acoustic parameters. Another advantage of this experimental setup was that a larger range of applied loads could also be explored.

5.2.1 Abrasive Paper: Effects of the Applied Load

The effects of the applied load were investigated using four different rotational velocities and three grades of sand paper. The feed rate was adjusted to 0.1mm/min and the reaction force of the rubber base provided the applied load, which changed

proportionally with the vertical displacement of the probe. The abrasive paper was cut to size and fixed to the rubber base using a double-sided tape.

Figure 31 shows the effects of the applied vertical force on the count rate using four different angular sliding velocities and the P1200 abrasive paper (smoothest surface roughness). The data for 10Hz may be divided into the three different sections for ease of analysis. The first section considers the data, where the amplitude of the signal is smaller than the applied threshold, which results in a negligible change in the count rate due to an increase in the applied load. Within this section the acoustic signal is smaller than the system noise and no counts are registered. The data in section 2 shows a rapid increase in the count rate and suggests a power law relationship between the count rate and the applied load. The data in the third section shows that the rate of increase of the count rate reduces. The overall shape of the data resembles an S-curve, which is similar to the results shown in Figure 26a. A similar behaviour can be seen for 9Hz. At lower angular velocities of 7Hz and 8 Hz, the results can only be divided into two parts as the third section is not apparent. However, if larger loads were explored it is postulated that a third section will occur around 300000 counts similar to the results obtained for the 9Hz and the 10 Hz experiments. The results also show that an increase in the sliding velocity produces a change in the threshold, which is indicated by the line separating sections 1 and 2. The threshold for the 7Hz data occurs at 55N (approximately), while the threshold for the fastest sliding velocity occurs at 21N (approximately). The largest change in the count rate occurs within part 2. Therefore, a faster sliding velocity means that a smaller range of applied loads can be used, which is a very important feature for the development of an in-situ testing machine for industrial applications.

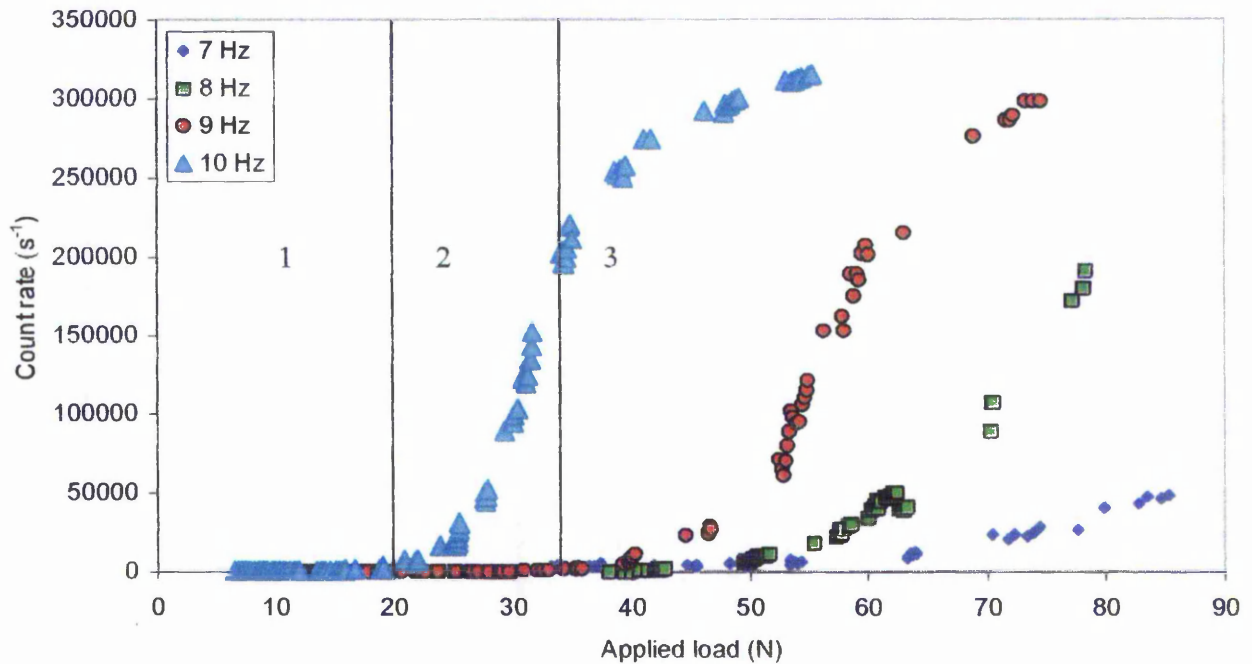


Fig 31. Count rate against applied vertical load using P1200 abrasive paper for four angular velocities.

Sarychev et al [73] suggested a general rule involving a power law relationship between the count rate and the applied load with the index value less than one (Equation 30). The 10 Hz count rate data from Figure 31 has been re-referenced from a count rate value of 25000 and the change in the count rate due to increasing load is presented in Figure 32. Two power law curves have been fitted to the data, which highlights the change in the relationship between the count rate and the applied load. The applied power law curves highlight the change in the data, which divided sections 2 and 3. The index of the power law is greater than 1 for section 2 but is less than 1 for the section 3. It appears that the, the general rule suggested by Sarychev (Equation 31) only applies to the data indicated by section 3 in Figure 31.

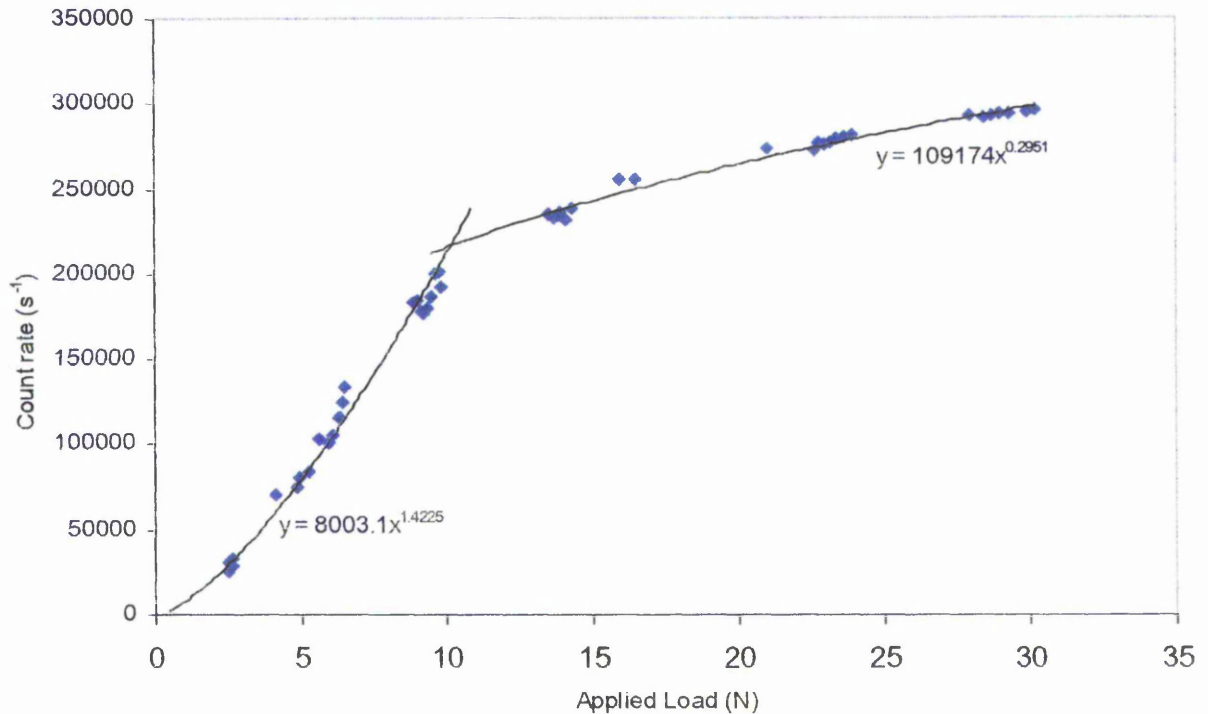


Fig 32. Count rate against applied vertical load using P1200 abrasive paper for an angular velocity of 10Hz.

The investigation is repeated for the P800 abrasive paper for 4 angular velocities (Figure 33) and the results show that the data can be divided into three parts. However, unlike the results for P1200 the data produced for the different sliding velocities are close to each other in section 2 and a single relationship between the count rate and the applied load can be determined in section 3. The order of separation between the different sliding velocities within section 2 is different to those presented in Figure 31. For the smoothest surface roughness (P1200, Figure 31) the rapid change in the count rate occurred at a lower applied load for the faster sliding speed, but in Figure 33 (a rougher surface, P800) the results show that a slower sliding velocity produced the larger increase in the count rate at lower applied loads. Also for the P800 abrasive paper the range of threshold values, which separates part 1 and part 2 is between 5-7N for the

four angular velocities investigated. In section 3 all the data collapses on to a common line, which indicates that the count rate within this section is independent of the sliding velocity.

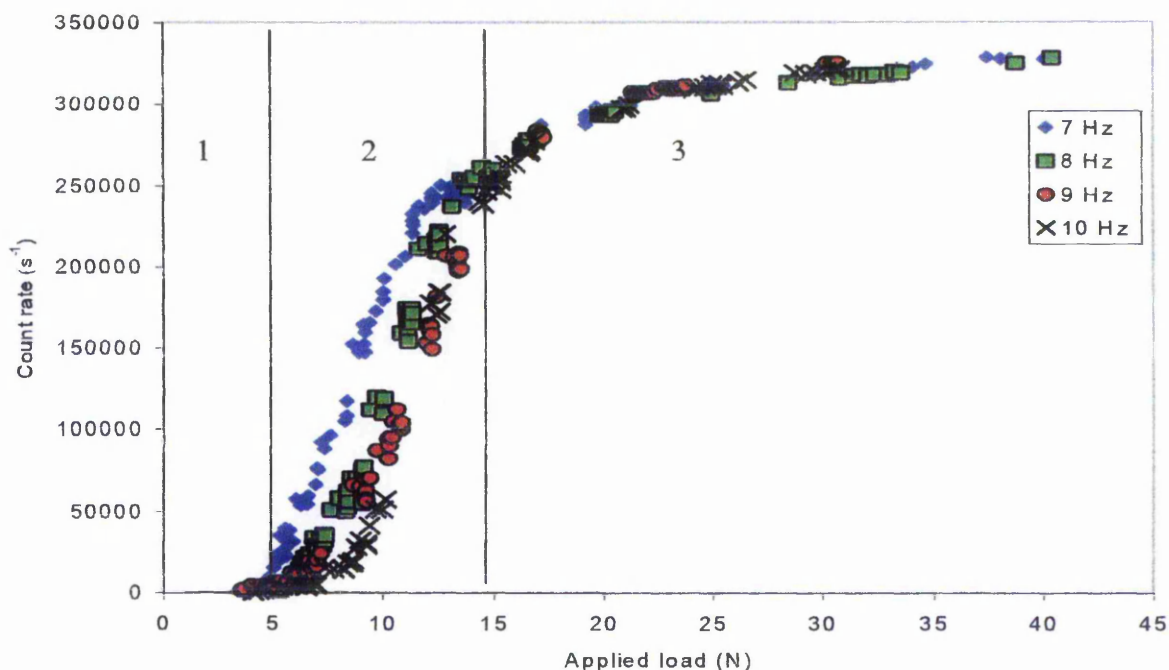


Fig 33. Count rate against applied vertical load using P800 abrasive paper for four different angular velocities.

Figure 34 shows the results for the P400 abrasive paper (roughest). Only two sliding velocities have been presented due to the fact that the frictional force between the probe and the abrasive paper caused the drill to stall at faster sliding velocities. The data clearly shows the S-shape curve that has been seen in the previous results. The threshold line has shifted to 18-20N approximately depending on the angular velocity. The results also suggest two general power law relationships for each set of data. As in the case for P1200 (Figure 32), the first power law relationship relates to the data in section 2 and has an index value greater than 1. The power law relationship in section 3 has an index

value less than 1. Also the data in section 3 for the two sliding velocities collapsed on to a single curve as in P800.

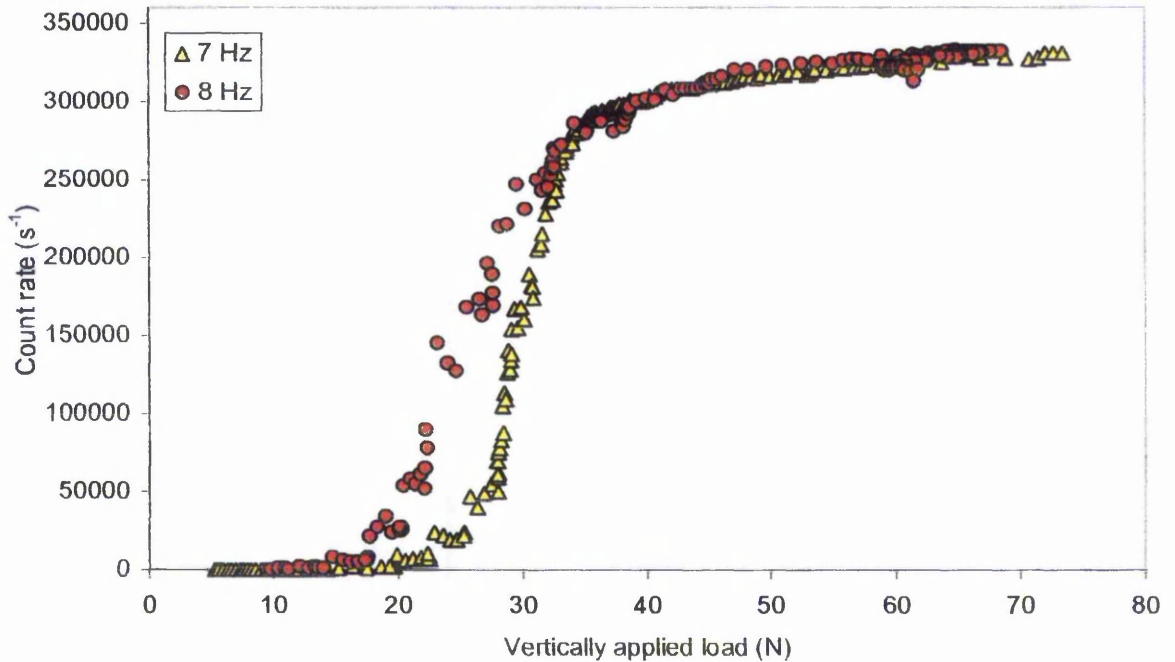


Fig 34. Count rate against applied vertical load using P400 abrasive paper for two different angular velocities

Previous experiments (Figure 29) highlighted a strong correlation between the acoustic energy and the count rate, where the effect of the angular velocity was considered for a given granular size. Further investigations were carried out to determine if a linear relationship also exists between the acoustic energy and the count rate using different grades of abrasive paper. In Figure 35 the acoustic energy has been plotted against the count rate using 3 grades of abrasive paper and 4 sliding velocities. Although the plot is very congested it does provide an excellent example showing that linear relationship only exists between the count rate and the acoustic energy within a certain range. To help explain the results the data has been separated into 2 sections for convenience. The

transition from section 1 from section 2 is shown by the large change in the gradient. The results in section 1 show a linear relationship between the acoustic energy and the count rate, similar to those presented in Figures 29 and 30. The change in the relationship between the acoustic energy and the count rate occurs at a count rate value of approximately 260000. However, in section 2 the relationship resembles an exponential rise. The change in the relationship between the acoustic energy and the count rate occurs when the count rate approaches a steady state but the acoustic energy continues to increase. Therefore, the increase in the acoustic energy does not increase in proportion to the count rate resulting in the change from a linear relationship to a non-linear relationship.

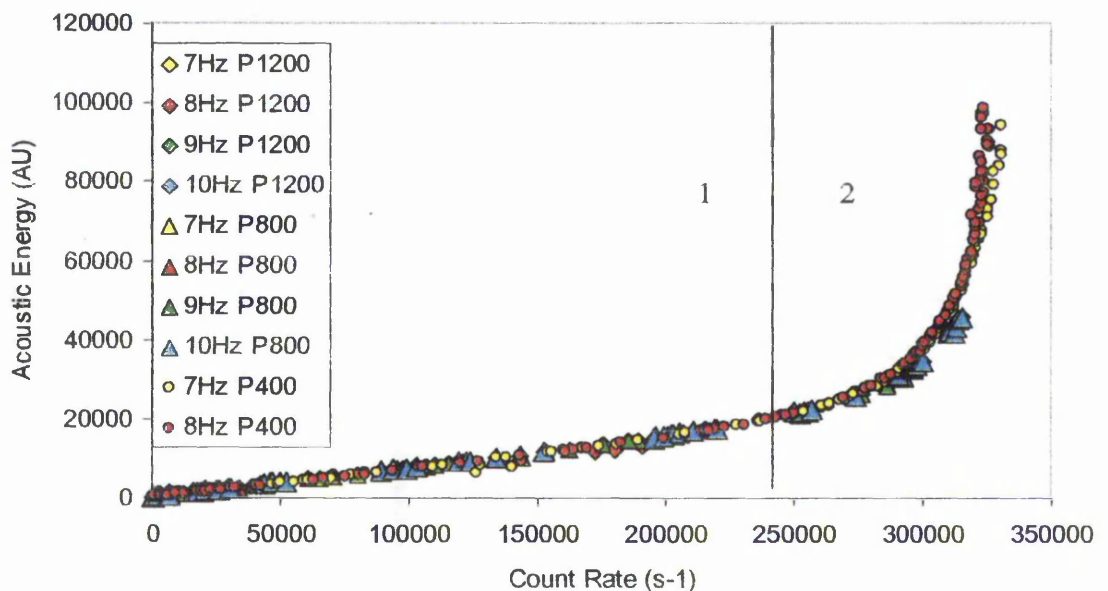


Fig 35. Acoustic energy against count rate using three grades of abrasive paper and 4 sliding velocities.

The count rate represents the number of oscillations that exceeds a set threshold per unit time and the gradient of the linear relationship between the acoustic energy and the count rate relates to the average energy per oscillation. The linear relationship has been

shown to be independent of both the applied load and sliding velocity. This observation is only applicable to the linear section of the data presented in Figure 35. The count rate appears to approach a steady state, which means that the frequency of oscillations produced by the friction pair as a result of increasing load approaches a constant value. Therefore the increase in the count rate is no longer proportional to the increase in the acoustic energy. When the count rate reaches a steady state the increase in the acoustic energy is predominantly affected by an increase in the oscillation amplitude and not by an increase in the number of oscillations detected.

5.2.2 Abrasive Paper: Effects of the Sliding Velocity

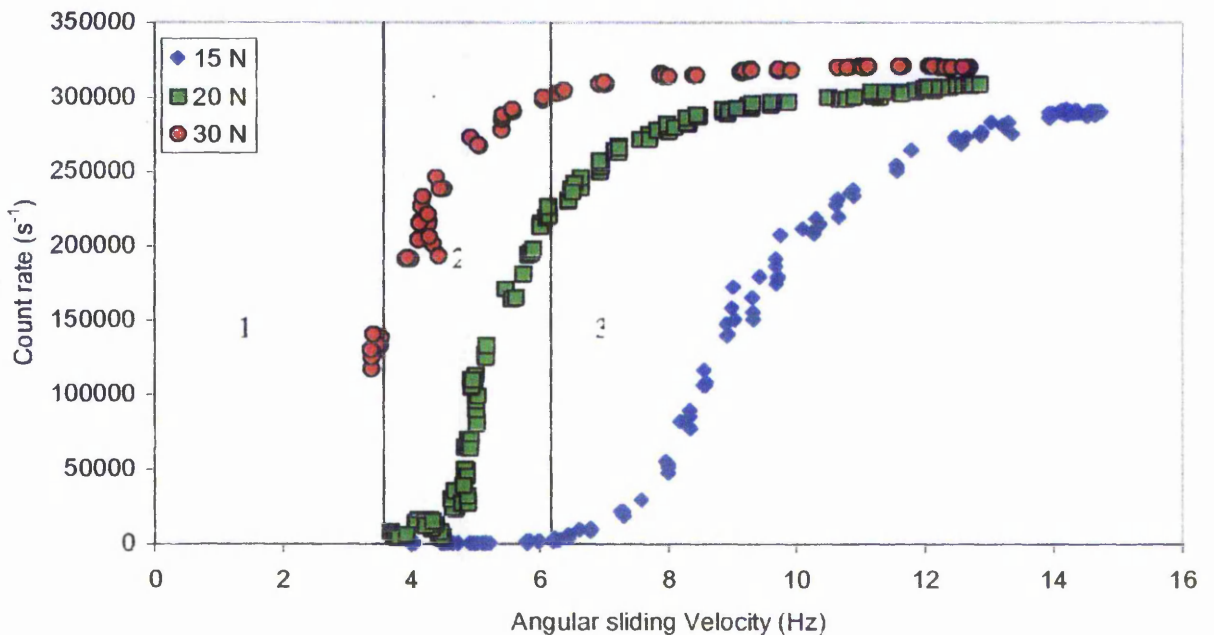
The investigation in this section is focused on the effect of the sliding velocity on the acoustic signal. The results obtained are used to identify any functional relationships between the sliding velocity and the acoustic signals as well as validating the theoretical relationships discussed in the previous chapter.

The experimental arrangement allowed the vertical displacement of the probe to be adjusted to produce a constant vertically applied load while the angular velocity of the probe was steadily increased to 15Hz.

Figure 36 shows the count rate plotted against the sliding velocity at 3 levels of applied load 15N, 20N and 30N. To aid the analysis the 20N data has been divided into three sections to indicate three significant changes in the curve. The results show that the threshold indicated by the line separating sections 1 and 2 increases as the applied load decreases. The threshold for the 30N data could not be obtained due to fact that the probing system stalled at lower sliding velocities however, the results do suggest that

the threshold is a function of both the angular velocity and the applied load. There is also a clear indication that the count rate approaches a steady state at higher sliding velocities. However, in this case the count rate at steady state does not tend towards the same value. A larger applied load produces a higher count rate at steady state. Therefore, the value that the count rate approaches may not be a point of signal saturation and may have some relevance to the properties of the friction pair. The results also indicate that larger applied loads produce a higher count rate at a given angular velocity. The general effect of the sliding velocity on the count rate produced similar characteristics to the effect of the applied load. However, in this case considering data within section 2 the index value of the power law was approximately 10 ± 1 .

Fig 36. Count rate against angular sliding velocity using P400 abrasive paper for three



constant vertically applied loads.

In the theoretical consideration (Chapter 4) the count rate was assumed to be proportional to the number of asperity contacts formed per unit time. It is also true for

two elastic bodies in contact that the number of asperity interactions increases with increasing applied load. Therefore the increase in the count rate due to the increase in the applied load may also be related to an increase in the number of contact spots formed per unit time.

A plot of the acoustic energy against the count rate is shown in Figure 37 for increasing angular velocity at three constant applied loads. Up to a count rate value of approximately 270000 the results show a linear correlation between the acoustic energy and the count rate. After a count rate value of 270000 the count rate approaches a steady state, but acoustic energy continues to increase.

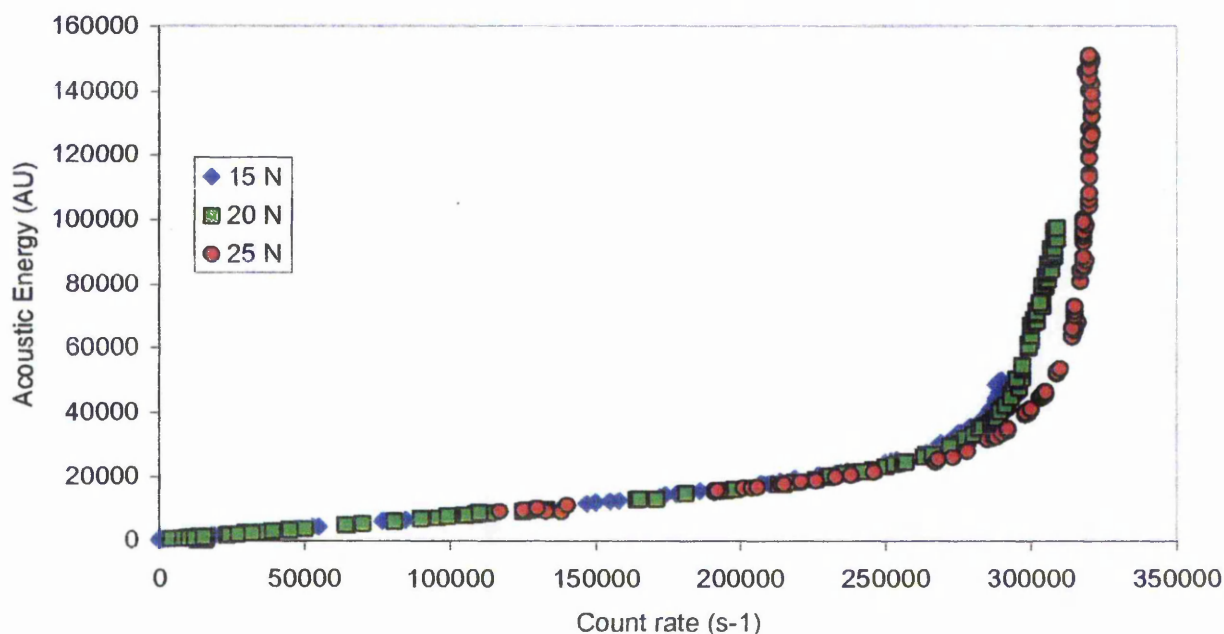


Fig 37. Acoustic energy against count rate using P400 abrasive paper for three constant vertically applied loads.

The results have shown that the changes in the sliding velocity also produce an S-shape curve similar to the investigations involving the effects of the applied load on the count rate. The data within sections 1 and 2 produce a linear relationship between the acoustic

energy and the count rate that is independent of the applied load, sliding velocity and in this investigation the abrasive roughness. Therefore within this linear range both parameters are affected by the frictional interaction in the same way. It is only when the count rate approaches a steady state in Figure 37 that the two acoustic parameters behave independently.

After each experiment it was observed that the abrasive paper had become worn very quickly producing a much smoother surface roughness. Even after a single test it was difficult to distinguish between the different abrasive grades. It was therefore concluded that comparing different grades of abrasive paper to represent a controlled change in the number of contacting asperities was not appropriate. The large amount of wear may have affected the repeatability of the results, especially within region 2 where it was very difficult to obtain consistency between results generated from similar experiments. However, the experiments did allow a large range of applied loads and sliding velocities to be investigated, which highlighted that the count rate approached a steady state.

5.3 The Steady State Count Rate and the Acoustic Energy

Previous results have shown that the count rate within section 2 produced a power law relationship and the count rate assumes a steady state value within section 3. In this section the steady state value of the count rate is investigated. In order to obtain more acoustic data within this region the raw acoustic signal was amplified by a further 20dB. The applied threshold to the acoustic signal was increased to a new level just above the amplified mechanical noise. The threshold was adjusted to eliminate any counts being registered while the probe was not in contact with the granular sample (In this instance the threshold was set at 0.025v). The probe was maintained at a set rotational velocity and was moved vertically until it is just above the upper surface of the granular sample. The vertical feed rate of the probe was set to a constant speed and maintained throughout the test. Due to the fact that the abrasive paper became worn very quickly it was no longer used in this study and was replaced with graded samples of Leighton Buzzard sand.

The results in Figure 38 show the effects of the applied load on both the count rate and the acoustic energy. The energy signal has been scaled by 50:1 to fit on the same graph as the count rate. The data has been divided into two regions a vertical line at 1.3N. In region 1 there is a threshold at 0.4N where there are only a few counts generated above the system noise. At loads above 0.4N there is a steady increase in the count rate and the acoustic energy up to 1.3N. In region 2 the count rate approaches a steady state value of approximately 280,000, but the acoustic energy continues to increase almost linearly with the applied load up to the maximum measured load of 5N.

A visual inspection of the granular particles during the compression process suggested that densification occurred initially at the point of contact and then within the lower sub-layers of the material. No further densification of the particles occurred at the point of the applied force, due to the fact that such densification would have required actual grain deformation. Consequently, the count rate would stabilise for any further increase in the applied load, as no further particle-probe contacts could be formed. This suggests that there is very little change in the number of particle-probe contacts during loading. For that reason, the number of particles in contact with the probe may be related to a function of the average particle size. It is postulated that the increase in the count rate within region 1 is not due to an increase in the number particle-probe contacts, but is due to an increase in the amplitude of the characteristic signal generated by the friction pair.

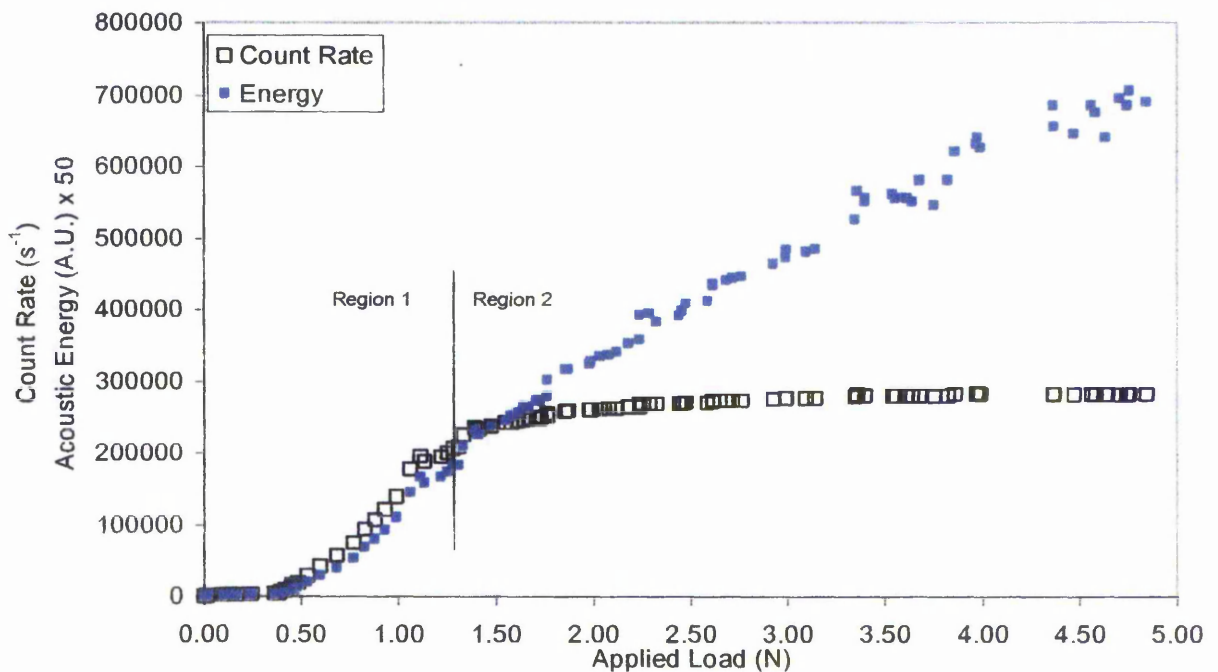


Fig 38. Acoustic energy and count rate against vertically applied load for a single penetration into the test sample of 50mm at 5mm/min feed rate. Leighton Buzzard sand particle size 850-1000 μ m.

Figure 39 displays the count rate and the acoustic energy against the angular velocity. The results have been divided into two regions by a line at an angular velocity of 6Hz, which identifies where the count rate starts to approach a steady state value. It can be seen that there is still a small increase in the count rate due to an increase in the sliding velocity in region 2, but the acoustic energy continues to increase rapidly with increasing sliding velocity. For sliding velocities greater than 8Hz the acoustic energy appears to saturate resulting in no further data. Comparing the results presented in Figures 38 and 39 there is little or no change in the characteristic count rate resulting from an increase in the applied load, although there is a small dependence on the sliding velocity. The increase in the count rate due to the sliding velocity is probably attributable to more particle-probe contacts occurring per unit time as the velocity increases.

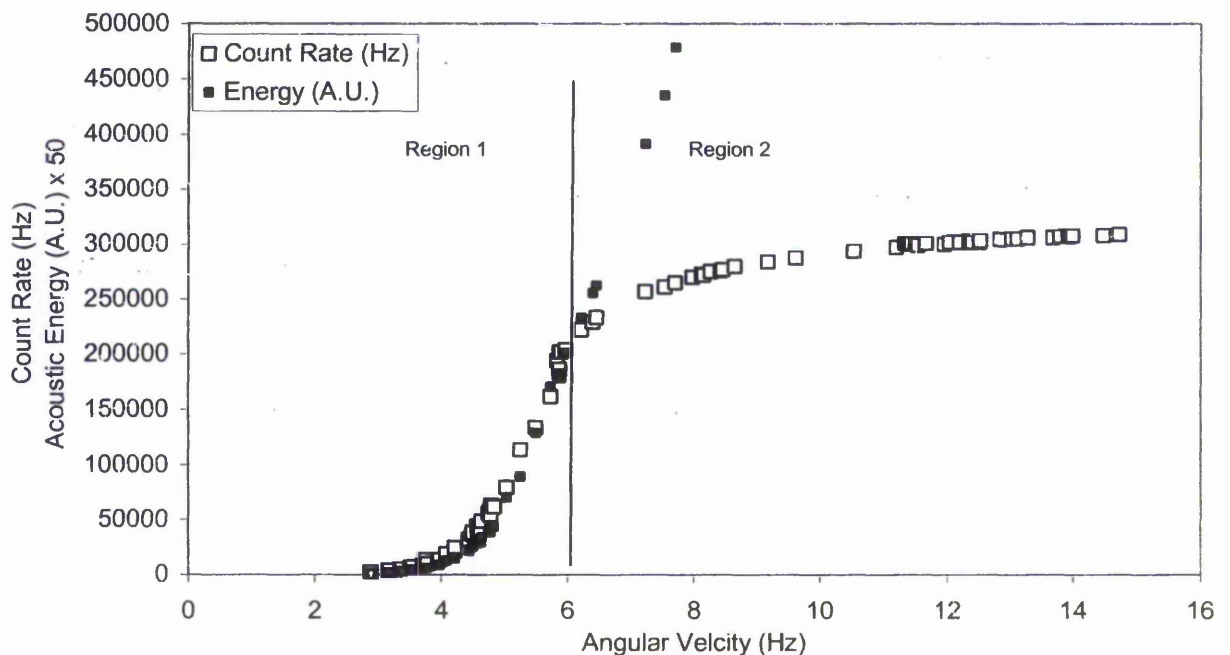


Fig 39. Acoustic energy and count rate against vertically applied load for a single penetration into the test sample of 50mm at 5mm/min feed rate. Leighton Buzzard sand particle size 850-1000 μ m.

Results have shown that in region 2, the characteristic count rate does not change due to an increase in the applied load but a small increase in the count rate occurs due to sliding velocity. This observation may be explained as follows. If the number of particle-probe contacts does not change significantly with increasing load (as particle deformation would be required for further deformation to occur) the count rate is not expected to increase. Earlier it was stated in the theoretical consideration that the count rate is proportional to the number of contacts formed per unit time. Consequently any increase in the count rate due to an increase in the sliding velocity would imply that more particle-probe contacts are formed per unit time.

5.4 Development of a Novel Signal Processing Technique

The previous results have indicated that the count rate approached a steady state value and the acoustic energy increased almost linearly with the applied load. Obtaining a larger range of data where the count rate settles at a steady state is impractical due to the fact that large applied loads or sliding velocities would be required. This section describes a novel method of processing the acoustic data, which allows more data to be monitored within region 2 without the need for larger applied loads or sliding velocities. The “novel thresholding technique” was developed to improve the results produced by the sharp sand especially for samples with a small average particle diameter as they did not generate strong acoustic signals. For practical reasons, it is important to be able to undertake material characterisation at smaller applied loads as some soils can have a low bearing capacity as well as allowing the size of the equipment to be reduced.

A typical method of determining the count rate and acoustic energy using a narrow bandwidth system utilises a threshold that is adjusted to a level just above the signal

noise, thus eliminating any noise components of the detected signal being above the threshold. Results in the previous sections have suggested that the friction pair will generate its own characteristic count rate, but in order for the signal to be investigated every oscillation will have to be large enough in amplitude to cross the applied threshold. In this investigation the raw acoustic signal is studied to determine its characteristics when the probe is pushed into the granular material.

A typical example of the acoustic signal produced by the probe-granular friction pair is shown in Figure 40. The signal oscillates about zero and a small amount of noise is superimposed on a lower frequency signal with larger amplitude. For demonstration purposes two thresholds are displayed, T1 (at 0.15) and T2 (at 0.01). It is obvious that more signal peaks are recorded using a threshold set at T2, but this allows the system noise to generate peaks above the threshold, which will directly influence the count rate and acoustic energy. Therefore, knowledge of the impact of the system noise on the acoustic signal generated by the friction pair is important.

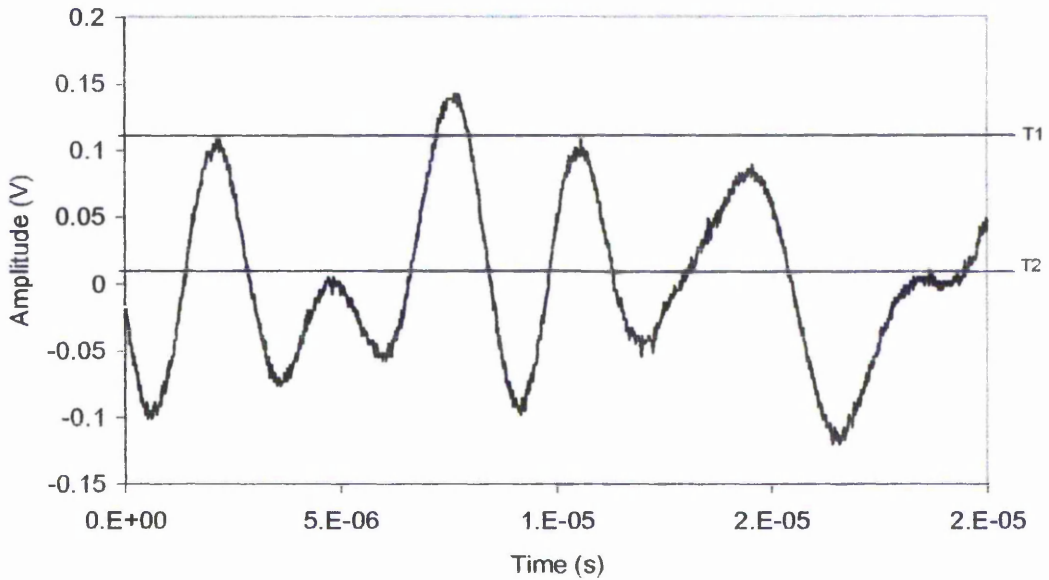


Fig 40: An example of the signal generated by the probe-granular interaction for a time period of $20\mu\text{s}$ sampling at 1.5GHz using a $250\text{-}500\text{ kHz}$ band pass filter.

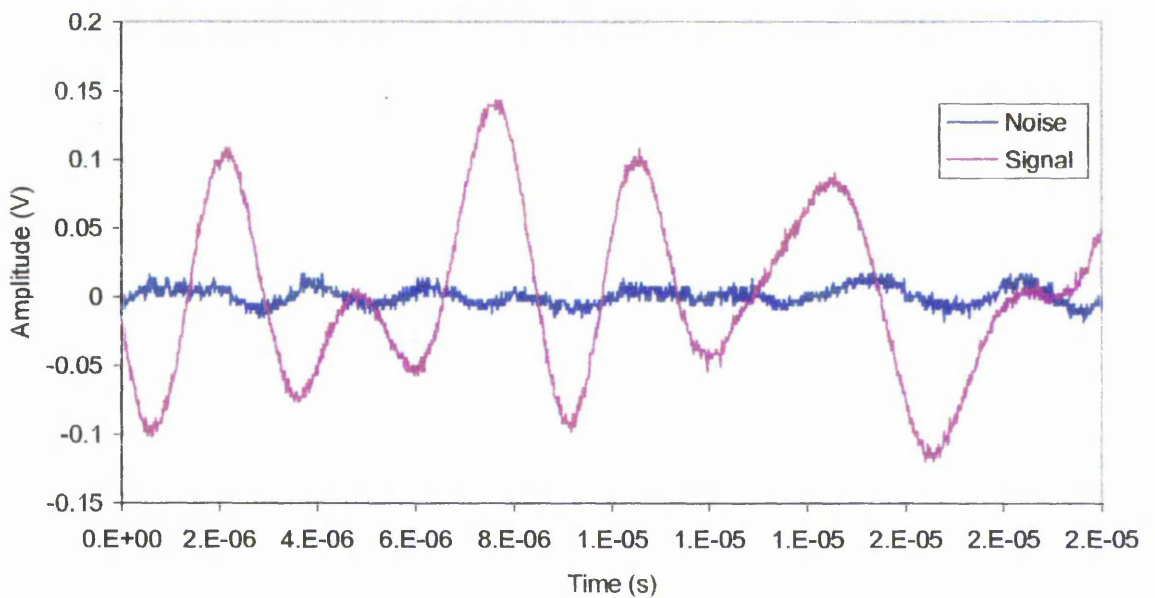


Fig 41. An example of an un-submerged probe's acoustic signal (noise) and a submerged probe's acoustic signal (signal). Data shown for a time period of $20\mu\text{s}$ sampling at 1.5GHz using a $250\text{-}500\text{ kHz}$ band pass filter.

The results in Figure 41 show a comparison between the system noise and the acoustic signal generated by the friction pair. The system noise signal comprises of low amplitude high frequency electronic noise, while the signal generated by the drilling system has a lower frequency with larger amplitude. The signal generated by the friction pair is a combination of these two signals, which has a lower frequency, larger amplitude and appears to have the high frequency electronic noise superimposed on it. The high frequency system noise only has a small effect on the count rate at the point where the friction generated signal exceeds the threshold as the system noise is displaced by the signal generated by the drilling system. These results clarify that the threshold can be set to its lowest level due to the fact that the system noise is superimposed on the drilling system signal, which prevents the system noise from registering a significant amount of counts. However, the system noise has an effect on the acoustic energy, although this is usually small owing to the small amplitude of the system noise compared to the amplitude of the friction generated signal.

The system noise generated by the drilling machine could be increased by changing the probe's angular velocity. The effect of the system noise on the acoustic signal generated by the friction pair has been investigated. Figure 42 provides a comparison between of the count rate for a submerged probe with that of an un-submerged probe with increasing sliding velocity. The data for the un-submerged probe represents the system noise, which decreases with increasing angular velocity. The reduction in the count rate suggests that the amplitude of the mechanical system noise is becoming larger and therefore the number of counts generated by high frequency electrical noise reduces. The count rate produced by the submerged probe is dominated by high frequency electrical noise at lower sliding velocities, due to the smaller amplitude of the friction

generated signal. Increasing the sliding velocity causes an increase in the amplitude of the friction generated signal, resulting in a reduction of the count rate (as the effects of system noise are greatly reduced by superposition). It can be concluded that, once the characteristic signal generated by the friction pair is established, the changes in the system noise resulting from an increase in the sliding velocity have a negligible effect on the count rate.

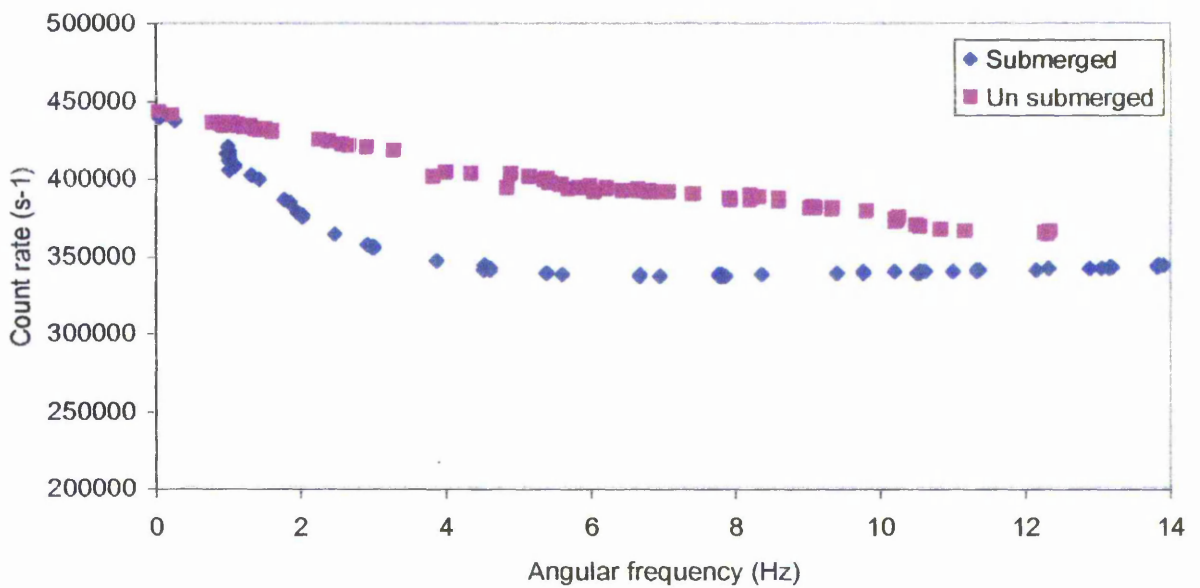


Fig 42. The effects of varying angular velocity on the count rate for a submerged probe (friction generated signal) and an un-submerged probe (system noise).

Results have shown it is acceptable to reduce the applied threshold to a minimum value of 10mV, which allows more data to be obtained in the region where the count rate approaches a steady state value. The steady state count rate is termed the characteristic count rate representing the characteristic frequency generated by a particular granular-solid friction pair.

5.5 Characteristic Count Rate Investigation

A novel processing technique has been developed to produce more data in the region where the count rate approaches a steady state value, which is termed the characteristic count rate. In this section the effects of the particulate material parameters on the characteristic count rate is investigated. The particulate parameters under investigation were the particle size, particle type and the level of saturation.

5.5.1 Effects of Particle Size and Type

Two types of granular material have been investigated, Leighton Buzzard sand and Shape sand. The threshold was set at its lowest setting of 0.01v and the count rates were recorded for each type of granular material over a range of particle sizes. Figure 43 shows the change in the count rate due to an increase in the applied load for five Leighton Buzzard sand samples. In all cases the count rate initially starts at a high value as it is affected by system noise. As the load increases the count rate reduces rapidly until it approaches a steady state value at a relatively smaller applied load using the lower threshold voltage. An important feature of these results is that the characteristic count rate is a function of the particle size. Smaller particulates produce a larger characteristic count rate and vice versa. This observation may be explained by the fact that increasing the particle size reduces the number of probe-particle contacts generated between the granular material and the probe tip, thus reducing the characteristic count rate.

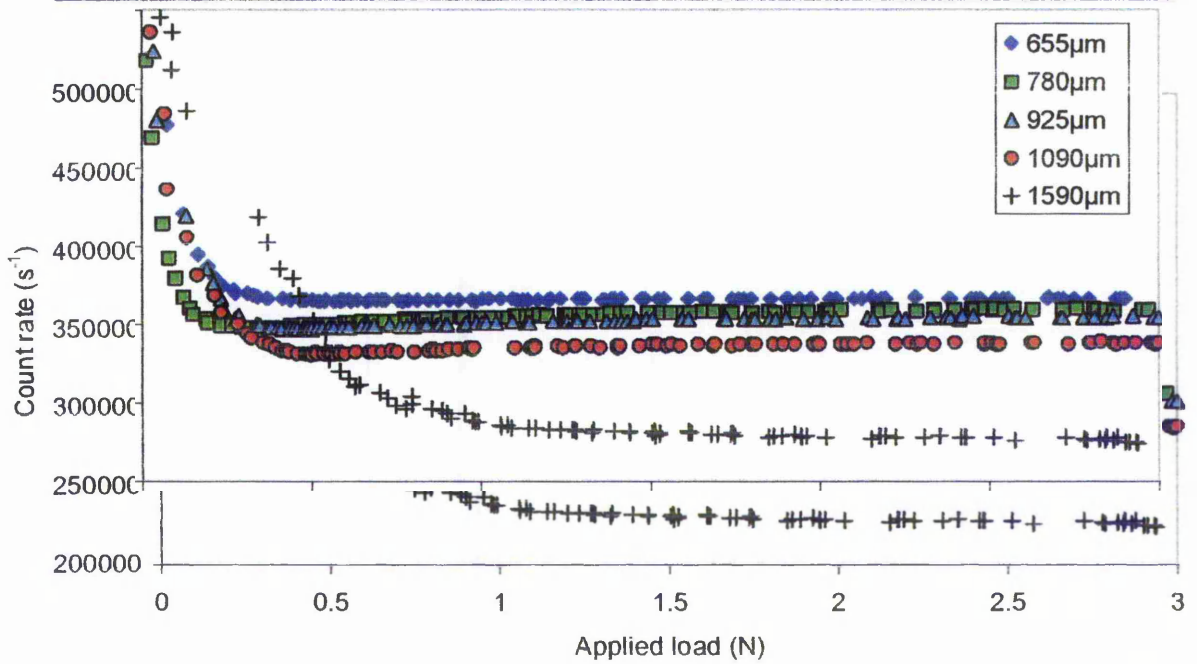


Fig 43. Count rate against applied load for the Leighton Buzzard sand samples at an angular sliding velocity of 8Hz.

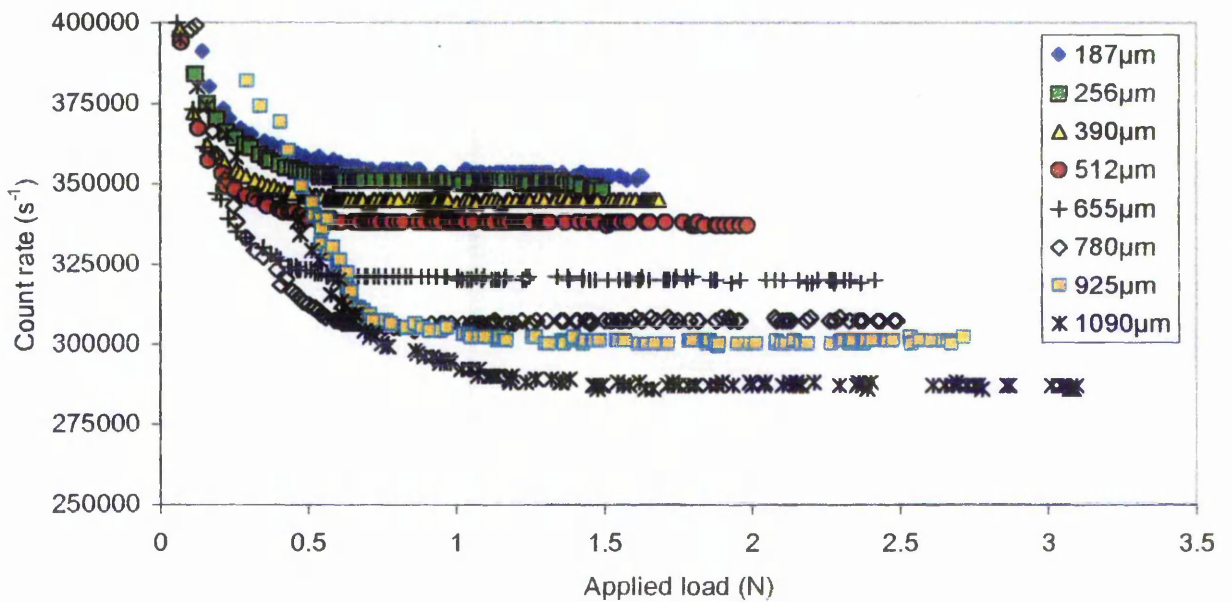


Fig 44 Count Rate against applied load for the Sharp sand samples at an angular sliding velocity of 8Hz.

The experiments were repeated for eight sharp sand samples and the results are shown in Figure 44. Compared to the Leighton Buzzard sand the acoustic signal generated by the sharp sand was generally lower in amplitude (which is discussed in section 5.6) and resulted in the characteristic count rate developing at larger applied loads. A similar behaviour of data distribution to Figure 43 is observed showing that the characteristic count rate reduces as the average particle diameter increases. Having confirmed the assumption that the count rate is proportional to the number of contacts formed per unit time, it can be postulated that the count rate will only be affected by the particulate size, shape and packing density. Other parameters such as the material type are unlikely to have an appreciable effect on the packing density and hence the effect on number of particle-probe contacts is relatively small. Nevertheless, the material type does have an effect on the particle-probe contact area because of different elastic properties.

Figure 45 shows the variation of the average characteristic count rate against the average particle diameter for both the Leighton Buzzard and Sharp sand samples. Results highlight the reduction in characteristic count rate due to an increase in particle size. The trend is approximately linear, although some deviation would be attributable to the natural variability in the grain shape. The experiment was repeated for other Leighton Buzzard sand samples and Sharp sand samples with the same average grain size and it can be concluded that the characteristic count rate is a function of the particle size, which can influence the number of particle-probe contacts. The results lend support to the assumption that the count rate is proportional to the number of contacts formed per unit time.

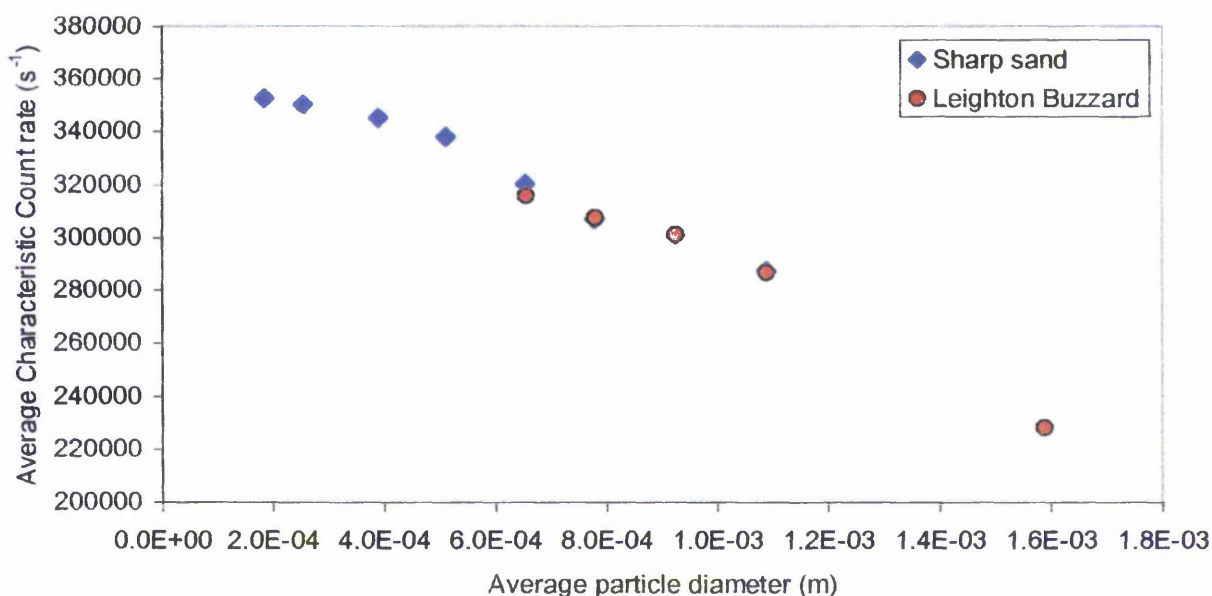


Fig 45. Average characteristic count rate against average particle size for the sharp sand and Leighton Buzzard sand samples.

In addition to the particle size it is predicted that changes in the particulate density will also have an effect on the characteristic count rate due to the fact the density will influence the number of contacts formed between the probe tip and the granular material. A series of experiments have been carried out to investigate the effect of bulk density on the characteristic count rate by comparing loose and compacted sand samples. The compacted samples were prepared using a 1kg mass and built up in layers of similar granular mass to create a uniform density throughout the granular material. The loose samples were prepared by carefully pouring the sand into a container. Figure 46 shows a comparison between the dense and loose granular samples and their effects on the characteristic count rate. The graph shows a reduction in the count rate, as in the previous case the load increases until the characteristic count rate for a particular sample has been reached. The results confirm earlier observations that smaller particle sizes produce a higher characteristic count rate. The compacted sand samples (dense granular

samples) show a slightly higher characteristic count rate level than the loose sand samples, but the difference is too small to have any influence on the characterisation of the particle size.

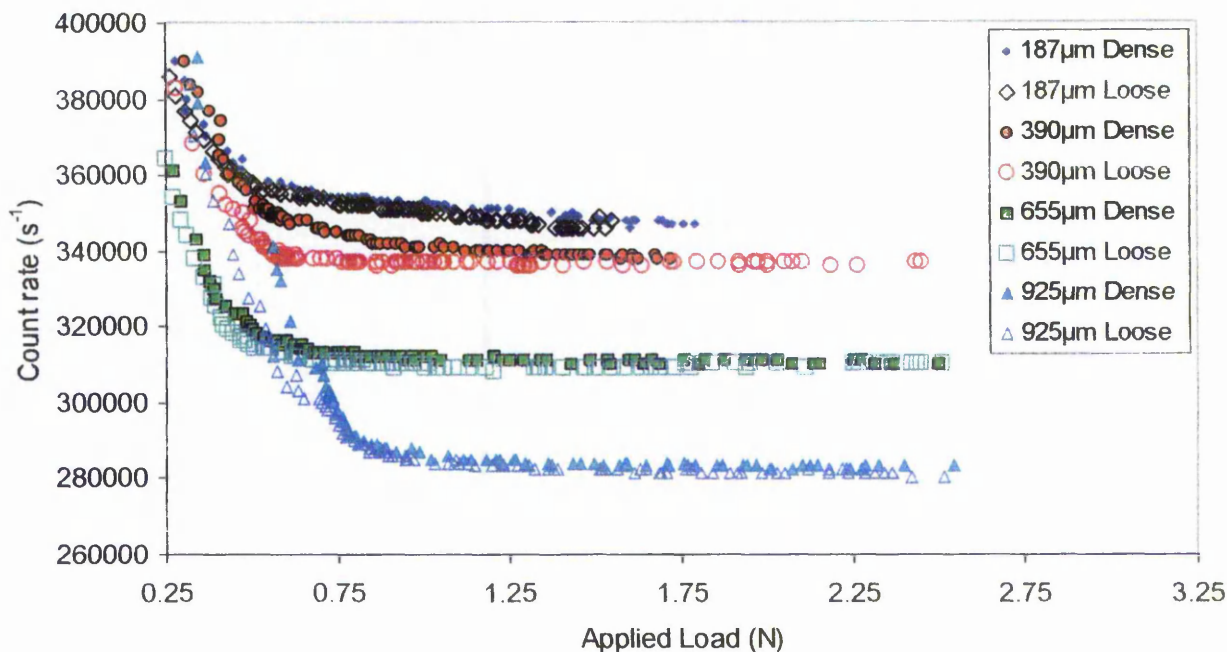


Fig 46. Count rate against vertically applied load using compacted and loose granular samples at an angular sliding velocity of 8Hz.

5.5.2 Effects of Particulate Water Content

In practice soils are not completely dry and the water content within the granular material may affect the material properties. In this section the effects of different water contents of the granular material have been investigated. A series of tests were undertaken and the water content was varied between 0-20%. The water content is defined as the ratio between the mass of the water and the mass of the dry granular sample. Each test used a fresh sample of sand and water to reduce the effects of water evaporation that would occur over a period of time. The granular samples were compacted in controlled layers to form a uniform density throughout the granular

medium. The container holding the granular sample was solid and did not allow drainage during testing. Similar testing conditions were provided for all experiments. Figure 47 shows the characteristic count rates against the water content for four different particle sizes. The data appears to show that the water content has a minor effect on the characteristic count rate but the results are inconclusive. While every effort has been made to reduce the variability in the density of each granular sample during preparation the dependency of the characteristic count rate on the particle size is still evident. The cohesive behaviour of the wet granular material made it difficult to achieve a high degree of consistency in the densities when preparing each granular sample and the deviation in the characteristic count rate may be attributable to this variability in the density for a given water content.

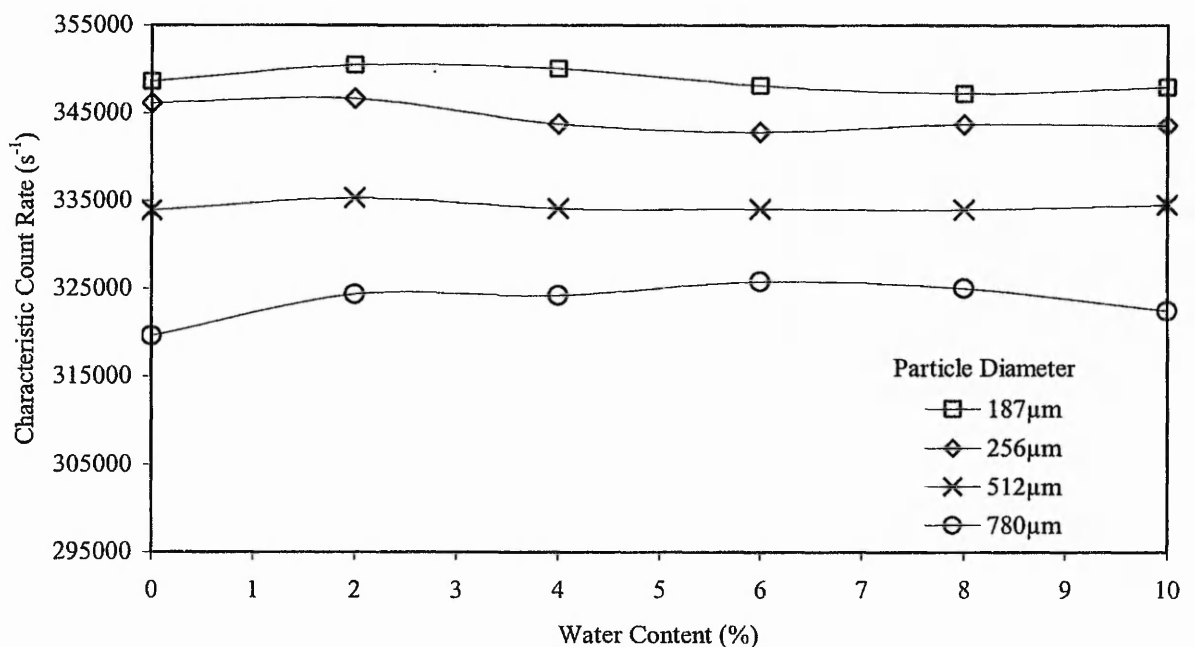


Fig 47. Count rate against water content for different particle sizes of sharp sand.

5.5.3 Using Different AE Systems

The previous results have shown that the characteristic count rate increases as the average particle size reduces, regardless of the material type and the ratio of water content. However, different acoustic arrangements may respond differently to changes in the monitored friction pair and therefore different acoustic settings need to be considered. In this section different acoustic emission (AE) band pass configurations have been investigated to determine whether it is possible to characterise the particle size using the acoustic signal. Due to the limitation imposed by the maximum sampling frequency of 1MHz, lower frequency bandwidths have been considered as well using a different sensor types with different resonant frequency ranges.

A narrow bandwidth system with a lower frequency range was used to investigate the effects of the particle size on the characteristic count rate. A low frequency piezoelectric resonant sensor (frequency range 125-250 kHz) was used with a suitable band pass filter. The threshold was set to its lowest setting possible (0.01v). Figure 48 shows the count rate against the applied load using the low frequency band pass arrangement. The results agree with earlier investigations (Figure 43) in that an increase in the particle size reduces the characteristic count rate, but the characteristic count rate is a lot lower. The reduction in the characteristic count rate is due to the lower frequency components of the AE signal, which are more dominant owing to their larger amplitude, thus displacing the higher frequency components, which are superimposed on it. The frequency components above 250 kHz have been filtered out, which account for the reduction in the count rate at the initial stages where there is no contact between the probe and the granular material. The increase in the amplitude of the AE signal allowed

the characterisation of larger particulates at smaller applied loads, which had been using a higher band-pass system (250-500 kHz).

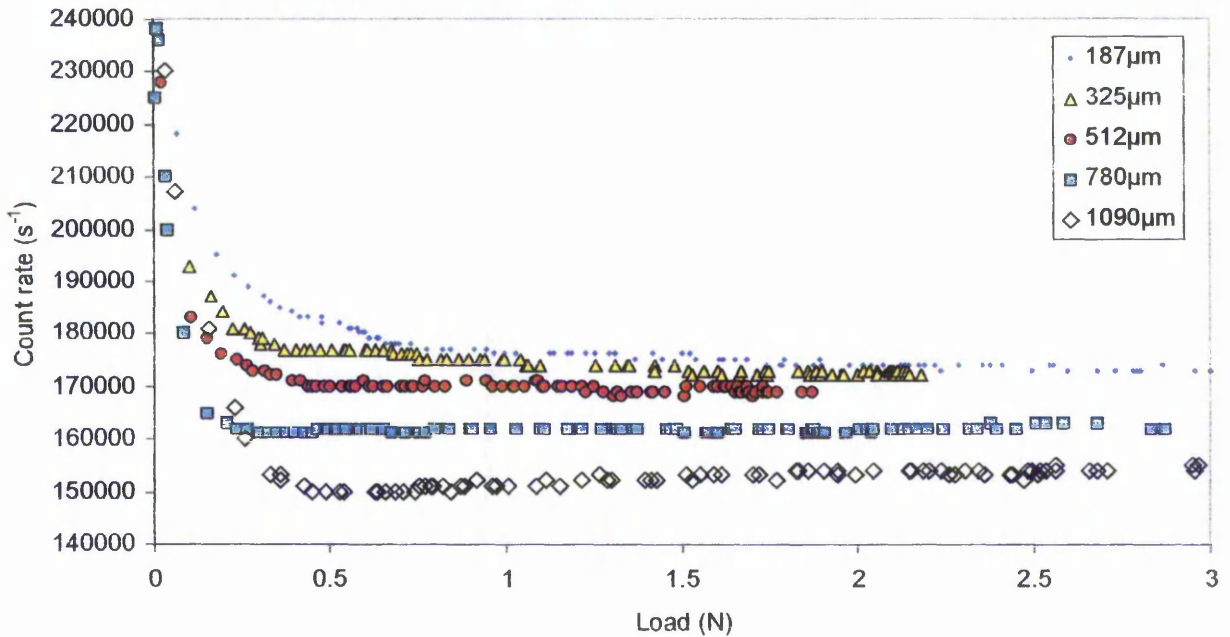


Fig 48. Count Rate against vertically applied load using a lower frequency narrow band-pass system (125-250 kHz) for sharp sand granular samples.

Figure 49 shows a comparison of the average characteristic count rate against the particle size for two band-pass systems. The higher band-pass filter (250-500 kHz) provides a larger separation between finer particulate materials, but the low band-pass system (125-250 kHz) provides a more gradual change in the characteristic count rate. The low band-pass system is also better suited to granular materials, which do not produce a strong acoustic signal, as lower frequencies were generally associated with larger amplitude. The main drawback is that the lower frequency band-pass filter reduces the resolution between the characteristic count rates generated by different particle sizes.

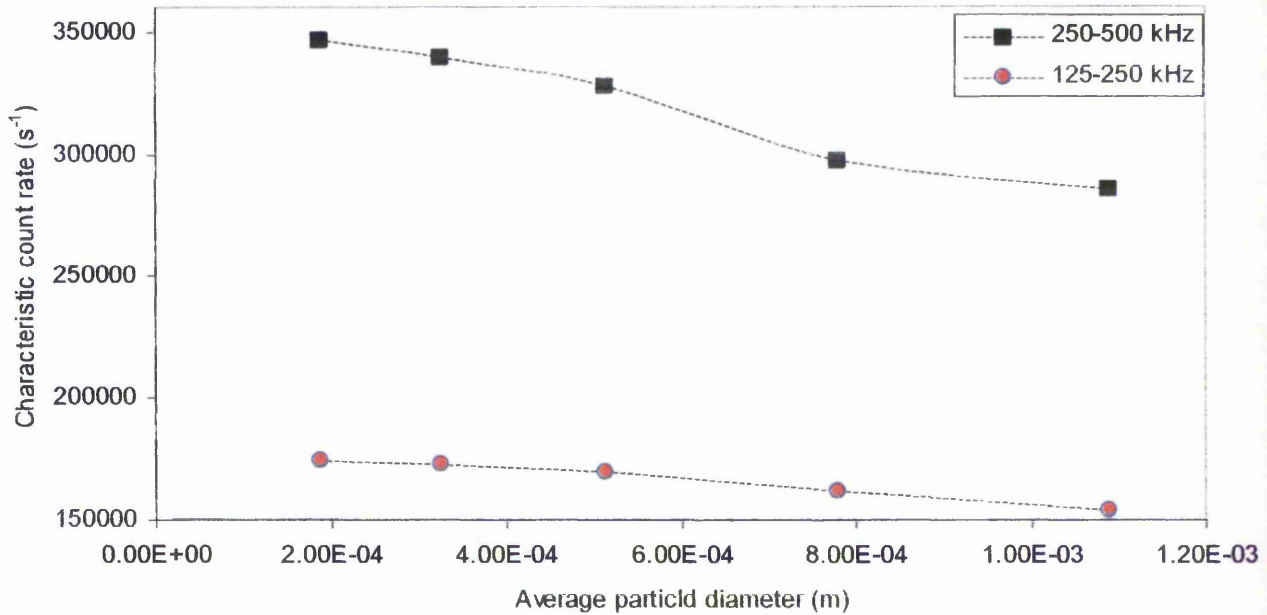


Fig 49. Average characteristic count rate against average particle diameter using sharp sand of graded particle size for two band-pass frequency ranges.

Further investigations were focused on optimising the acoustic system by adjusting the band pass filter. Optimising the AE system should improve the quality of the results by increasing the resolution between the signals generated by different particle sizes as well as producing larger signal amplitude. The results in Figure 50 show the effects of decreasing the lower band-pass frequency for the AC375L transducer (rated frequency range 250-500 kHz). A lower band pass frequency reduces the characteristic count rate as a result of the lower frequencies with larger amplitude. The high frequency components of smaller amplitude are superimposed on the lower frequency signals and as a result the high frequency pulses are not detected by the thresholding system. Reducing the lower band-pass frequency improves the resolution and the signal amplitude, as indicated by the 117-500 kHz-frequency range. Lowering the lower band-pass frequency too much in the case of the 50-500 kHz frequency range will cause a

reduction in the resolution, but there will be a further increase in the signal amplitude. It can be concluded that changing the band-pass filter does not affect the system's ability to characterise the particle size.

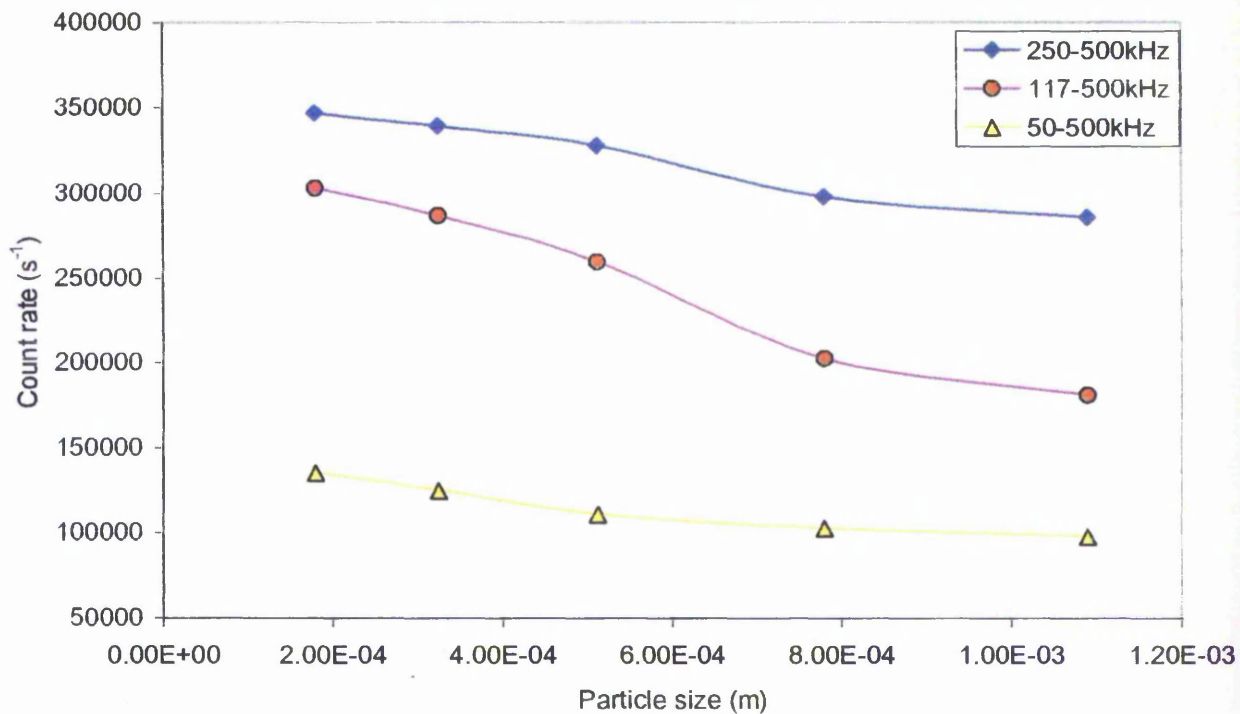


Fig 50. Characteristic count rate against particle size for three band-pass filter settings, using sharp sand samples.

Figure 51 provides evidence of the higher frequency signals being superimposed on the lower frequency signals. Samples of the monitored waveform were taken using the Lecroy oscilloscope sampling at 1.5GHz for two band-pass filter settings. The results show an increase in the signal amplitude when the lower frequency band-pass filter is used. The lower frequency band-pass signal appears to have the higher frequency components, which are monitored using the higher band pass filter super imposed on it. Consequently the number of high frequency components detected by the threshold

(threshold indicated by the black line) is reduced. The higher frequency oscillations occur above the threshold and are not detected.

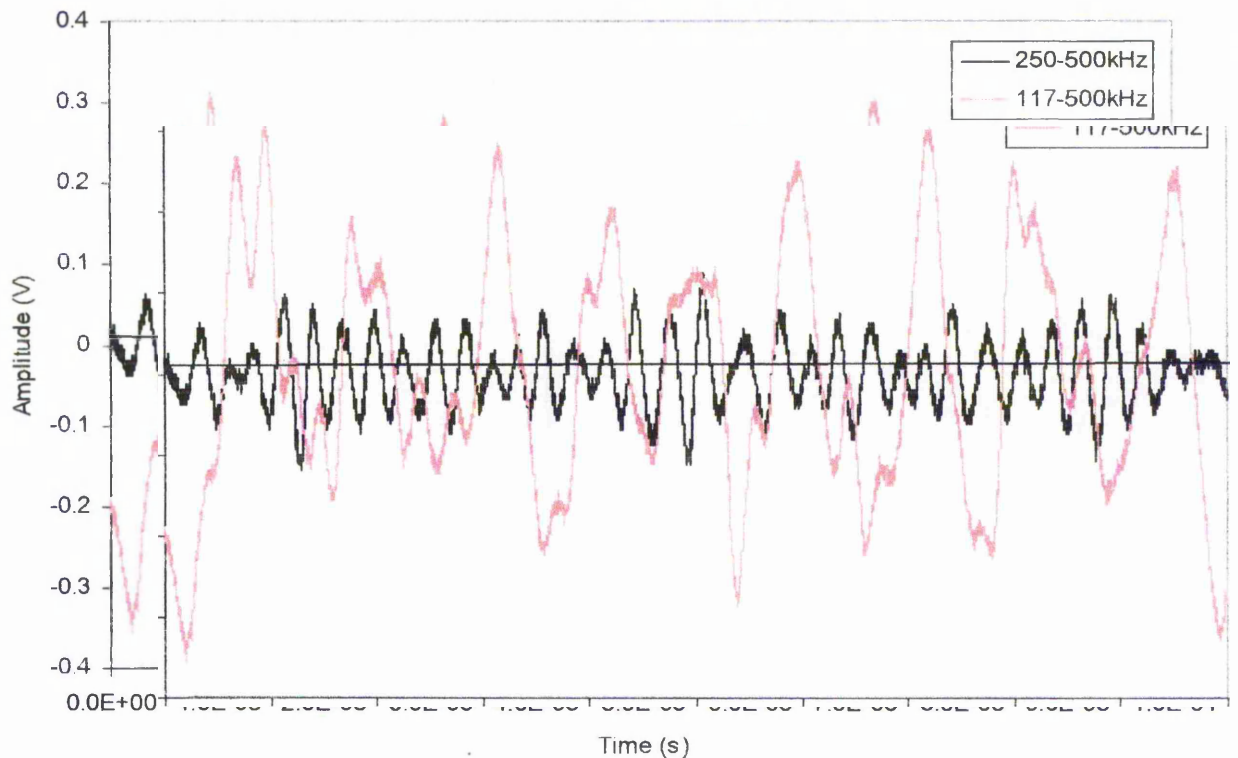


Fig 51. The variation of signal amplitude for two band-pass filter settings.

A Digital Wave B225 broadband transducer (frequency range 50-500 kHz) was used to determine if the broadband sensor with a wide range band-pass filter improved the acoustic signal generated by the friction pair. Figure 52 shows the count rate against the vertically applied load using the broadband transducer. It can be seen that an increase in the particle size produces a reduction in the characteristic count rate, this confirming the earlier observation. However, using a broader bandwidth acoustic system means that the signal is dominated by lower frequency components, leading to a smaller separation between the characteristic count rates generated by different particle sizes. The broadband transducer was found to be less sensitive to the friction generated acoustic

signal and larger applied load was needed before the characteristic count rate was reached.

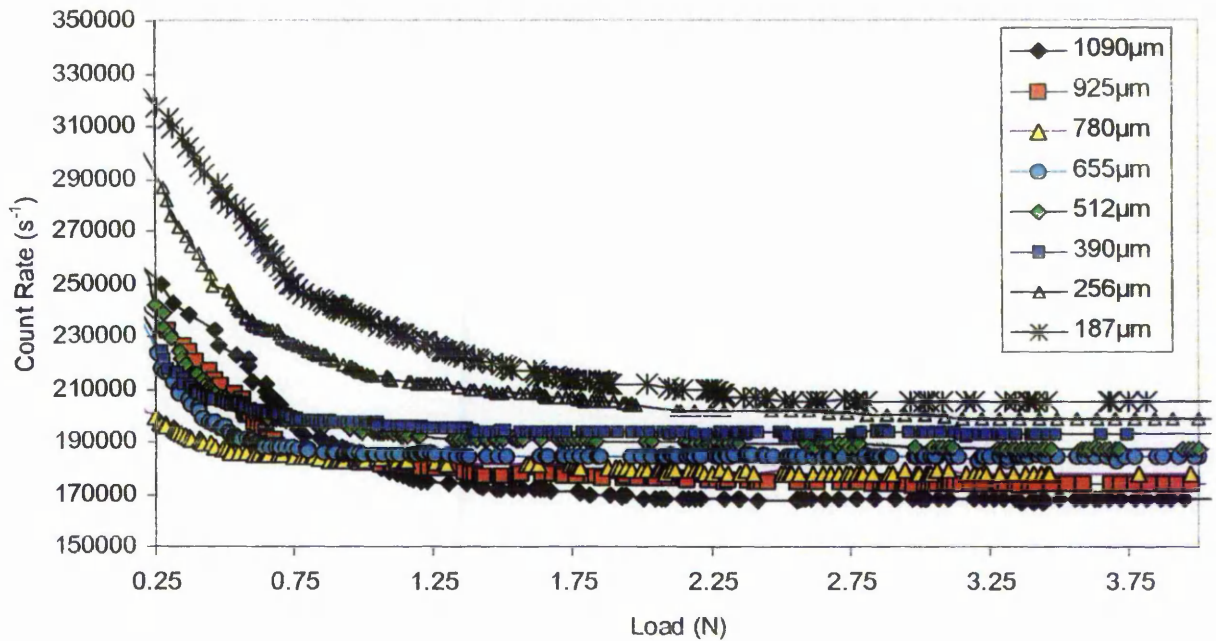


Fig 52. Count rate against vertically applied load using the broadband BN225 transducer and sharp sand granular samples.

Figure 53 shows the variation of the characteristic count rate plotted for different particle sizes using the broadband BN225 transducer. It can be seen that the characteristic count rate decreases almost linearly with increasing particle size and the separation between the characteristic count rates produced by different particle sizes is sufficiently distinctive to allow a reliable method for classifying the particle size based on knowledge of the characteristic count rate.

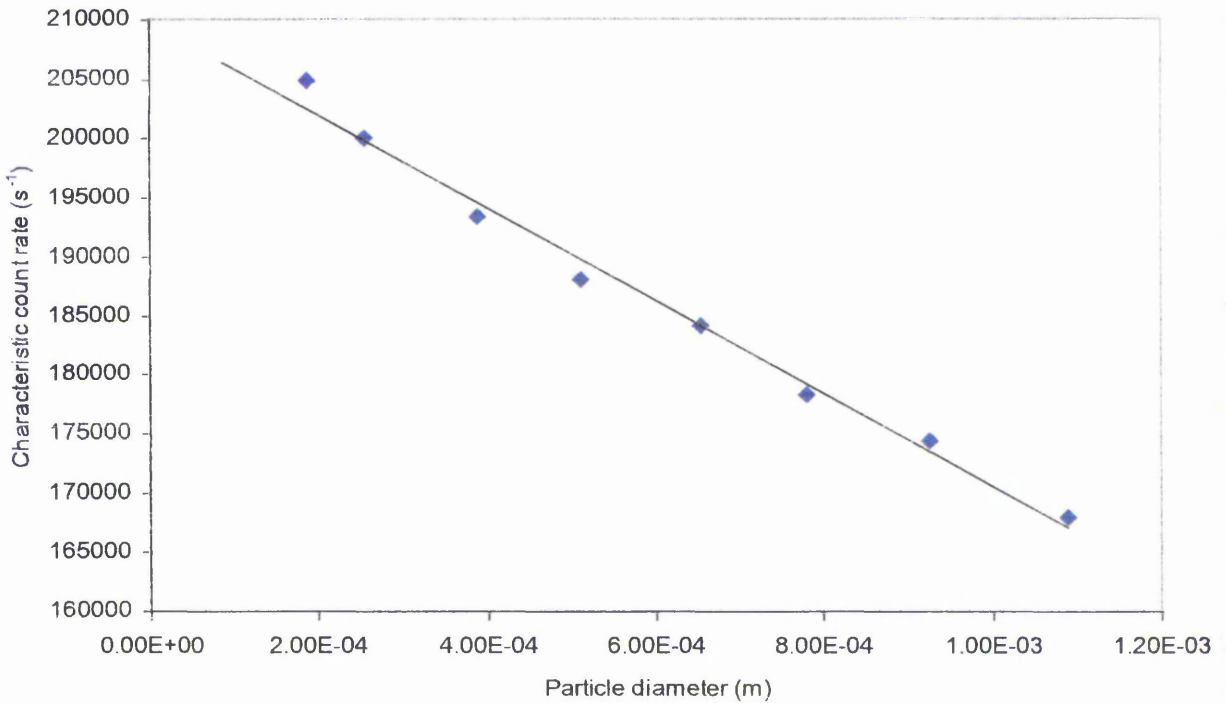


Fig 53. Average characteristic count rate against average particle size, using the broadband BN225 transducer, and sharp sand granular samples.

It is important to note that a change in the acoustic arrangement can affect the values of the characteristic count rate as well as the gradient of the linear relationship between the characteristic count rate and the particle size. However, all acoustic arrangements considered have shown the ability to characterise the particle size. The amplitude of the different characteristic count rates can be improved by reducing the low frequency threshold of the band-pass filter. However, lowering the low pass threshold to much can reduce the separation between the characteristic signals generated by each particle size.

5.6 Investigation of the Acoustic Energy

It has been shown that the characteristic count rate is related to the number of contacts formed between the probe tip and particulate material. The change in the acoustic energy while the count rate has a steady state value is mainly due to an increase in the amplitude of the characteristic signal and it may provide further information relating to the material properties of the friction pair. This section investigates the effects of the particle size, water content and granular density on the acoustic energy within the same data range as the characteristic count rate.

5.6.1 The Effect of the Particle Size

The change in the acoustic energy due to an increase in the applied load for different size particulate materials has been investigated. Figure 54 shows the change in the acoustic energy due to an increase in the applied load using Leighton Buzzard sand samples. Equation 40 suggests that a power law relationship exists between the acoustic amplitude and the applied load and power law curves have been fitted to the data. The applied power law curves do fit fairly closely to the data and the results show that the exponents vary between 1.1 and 1.47. Also the constant of proportionality generally decreases as the particle size increases, although this was not the case for the smallest grain size. The presented results show that the variation of acoustic energy for a given particle size could also be represented by a linear relationship and this will be discussed at a later stage in this thesis.

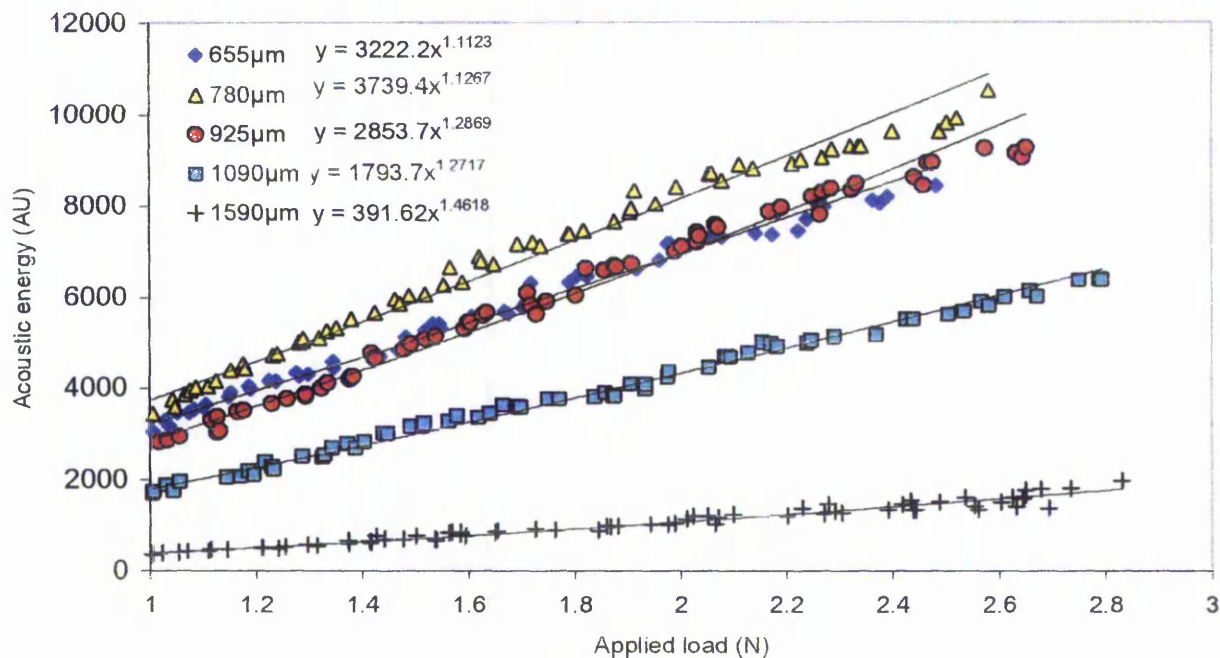


Fig 54. Acoustic energy against applied vertical load using Leighton buzzard sand samples a 375 transducer and a 250-500kHz band pass filter.

The experiment was repeated for Sharp sand samples and the results are shown in Figure 55. Power law curves were also fitted to the data, although the equations have not been shown to avoid the congestion on the figure but are shown later in Table 2. The equations relating to the applied power law curves for the sharp sand sample samples had exponent values between 1.13 and 1.61, which is slightly larger than the results obtained using the Leighton Buzzard sand. Also there did not appear to be an obvious relationship between the constant of proportionality of the power law and the particle size. The results show that a high level of acoustic energy is produced by the granular material with an average particle diameter of 390µm and a further increase in the particle size reduces the acoustic energy.

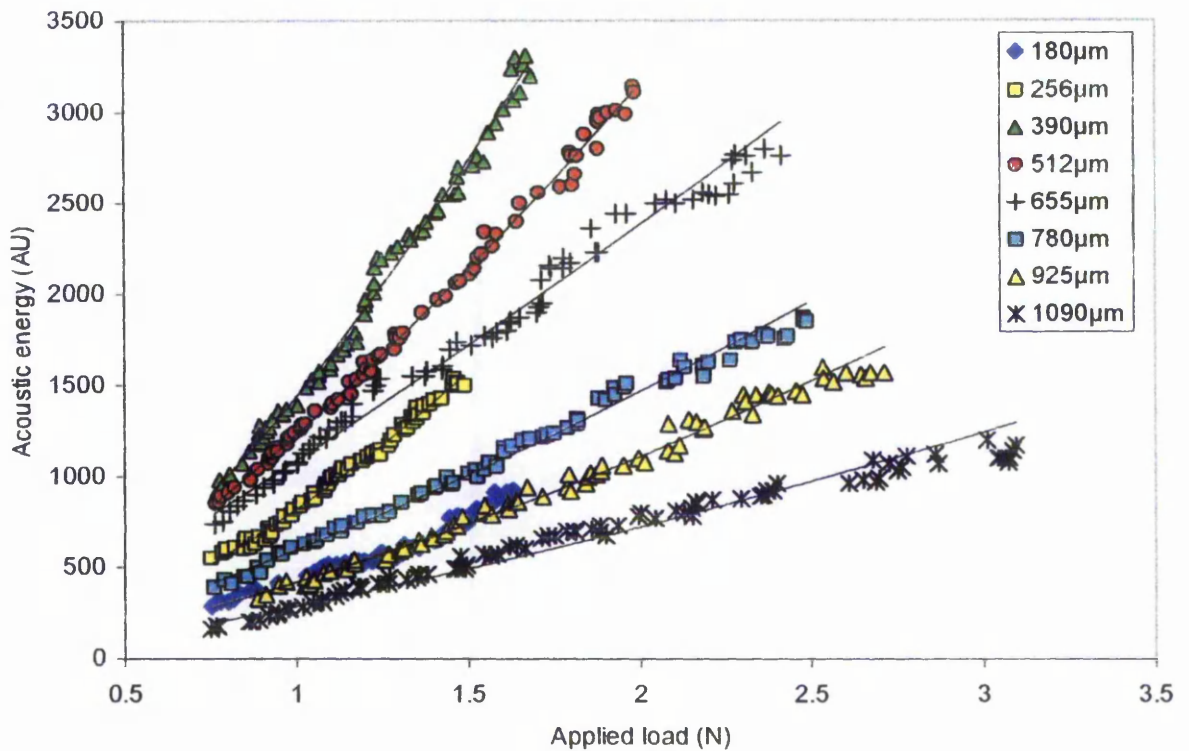


Fig 55. Acoustic energy against applied vertical load for sharp sand granular samples a 375 transducer and a 250-500 kHz band pass filter.

It was observed that the relationship between the acoustic energy and the applied load could easily be considered linear for the range of applied loads used in this investigation. Both linear lines and power law curves were fitted to the data and the equations for each fitted line or curve are displayed in Table 2. For each trend line fitted the average deviation of the actual data from the trend line was calculated and rounded up to the nearest acoustic energy increment (The smallest increment of the acoustic energy was 10 AU). The R^2 value (Correlation coefficient) is also shown and provides a measure of the reliability of the applied trend line, whereby a value closer to 1 indicates better reliability.

Leighton Buzzard	Power Law	Linear	Power Law		Linear	
			+/- (AU)	R ²	+/- (AU)	R ²
655µm	$y = 3222.2x^{1.1123}$	$y = 3702.2x - 462.99$	140	0.9895	130	0.9899
780µm	$y = 3739.4x^{1.1267}$	$y = 4317.5x - 509.79$	220	0.9848	190	0.9849
925µm	$y = 3853.7x^{1.2869}$	$y = 4163.6x - 1346.7$	220	0.987	180	0.9887
1090µm	$y = 1793.7x^{1.2717}$	$y = 2626.8x - 888.43$	110	0.9918	80	0.9951
1590µm	$y = 391.62x^{1.4618}$	$y = 755.62x - 406.56$	70	0.9758	70	0.9601
:						
Sharp Sand	Power Law	Linear	Power Law		Linear	
			+/- (AU)	R ²	+/- (AU)	R ²
180µm	$y = 420x^{1.4163}$	$y = 677.04x - 262.48$	30	0.9647	40	0.9412
256µm	$y = 820.54x^{1.6074}$	$y = 1417.3x - 586.18$	20	0.9906	30	0.9908
390µm	$y = 1433.7x^{1.5897}$	$y = 2549.8x - 1096.1$	50	0.9929	70	0.989
512µm	$y = 1231x^{1.1325}$	$y = 1869.4x - 638.7$	30	0.9977	50	0.995
655µm	$y = 1087x^{1.1325}$	$y = 1261.1x - 158.49$	70	0.9866	60	0.9867
780µm	$y = 597.76x^{1.2972}$	$y = 862.66x - 261$	40	0.9926	30	0.9946
925µm	$y = 417.04x^{1.4153}$	$y = 731.88x - 355.61$	30	0.9919	40	0.99
1090µm	$y = 287.23x^{1.3345}$	$y = 428.31x - 123.55$	50	0.9747	40	0.983

Table 2. A comparison of the power law and linear relationships, showing the mean average error and the R² values for each trend line.

The data in Table 2 shows that there is very little difference between applying a power law relationship or a linear relationship. The average +/- deviation for both the power law and the linear relationships are very similar, which is also the case for the correlation coefficients. It can be seen that it is acceptable to use a linear relationship between the acoustic energy, but if a larger range applied loads are used this may not be the case. However, considering range of applied loads used in this investigation a linear relationship describes the data just as effectively as the power law relationship.

For a single asperity contact Equation 40 (Chapter 4) suggests that the acoustic amplitude is a function of the contact force, the sliding velocity, the elastic properties of the material and the particle radius. In the present investigation the sliding velocity and the material properties are fixed and the two parameters that are allowed to vary are the contact force and the particle radius. An increase in the particle size would reduce the acoustic amplitude, but would also increase the contact force at a given total applied load due to fewer particle-probe contacts. The gradients of the linear relationships between the acoustic energy and the applied load for different particle sizes, (listed in Table 2) are shown in Figure 56. The results highlight the non-linear change in the gradient due to an increase in the particle size. Both samples of granular material exhibit a peak gradient at a certain grain size, although they do not occur at the same point. The results also highlight the large energy difference between the types of granular material and it can be seen that the Leighton buzzard sand generated a signal of larger amplitude.

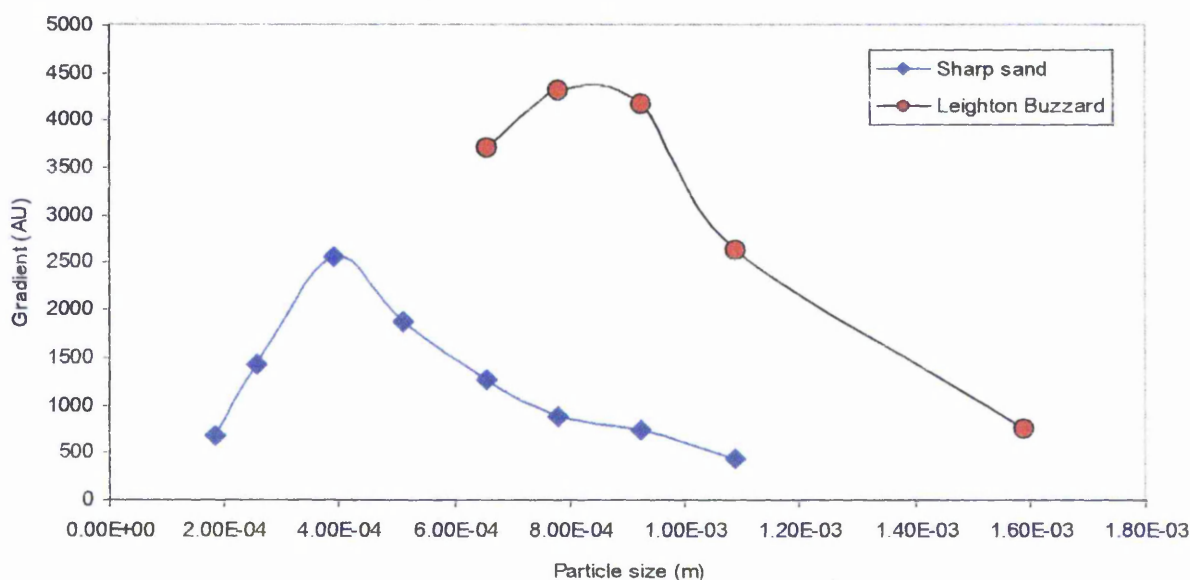


Fig 56. The change of acoustic energy due the applied load against average particle diameter for two types of granular material.

It should be noted that the recorded acoustic energy relates to the total acoustic energy produced by the frictional contact, which is a function of all the individual energies generated at each asperity interaction. Equation 40 only considers a single asperity interaction and the force at a single asperity contact needs to be determined. Therefore, knowledge of the number of particle-probe contacts is required to provide an estimate of the average contact force.

5.6.2 The Average Energy Per Oscillation

In this section the interaction at a single particle-probe contact is considered in order to investigate the validity of Equation 40 for the frictional interaction used in this study. The acoustic energy is a function of the number of oscillations as well as their amplitude and previous investigations have shown that different particle sizes produce a different frequency of oscillations. The total acoustic energy is affected by the number oscillations above the threshold and is consequently influenced by the count rate. Therefore the average energy for a single oscillation is considered, which focuses on the change in the acoustic energy due to an increase in amplitude and reduces the change in the acoustic energy caused by a change in the count rate. The average acoustic energy for a single oscillation is determined by dividing the total acoustic energy by the count rate and will be referred to as the oscillation energy. The average number of contacts is determined using the assumption of a cubic packing arrangement described in Equation 11 the cubic packing arrangement assumes that all neighbouring particles are in contact and the spacing parameter is equal to 1. Therefore, the number of contacts generated between the probe and the particulate medium is a function of the nominal probe tip surface area divided by the average grain diameter squared. Figure 57 shows the average energy per oscillation against the average contact force using sharp sand

granular samples. Linear trend lines have been fitted to the data to and it was noticed that the smallest particle size produces the steepest gradient, which decreases with increasing particle size. Therefore, at a given contact force the average energy per oscillation increases as the particle size decreases. The results show there is an uneven change in the gradient and the largest change occurs between particle sizes 655 μm and 780 μm .

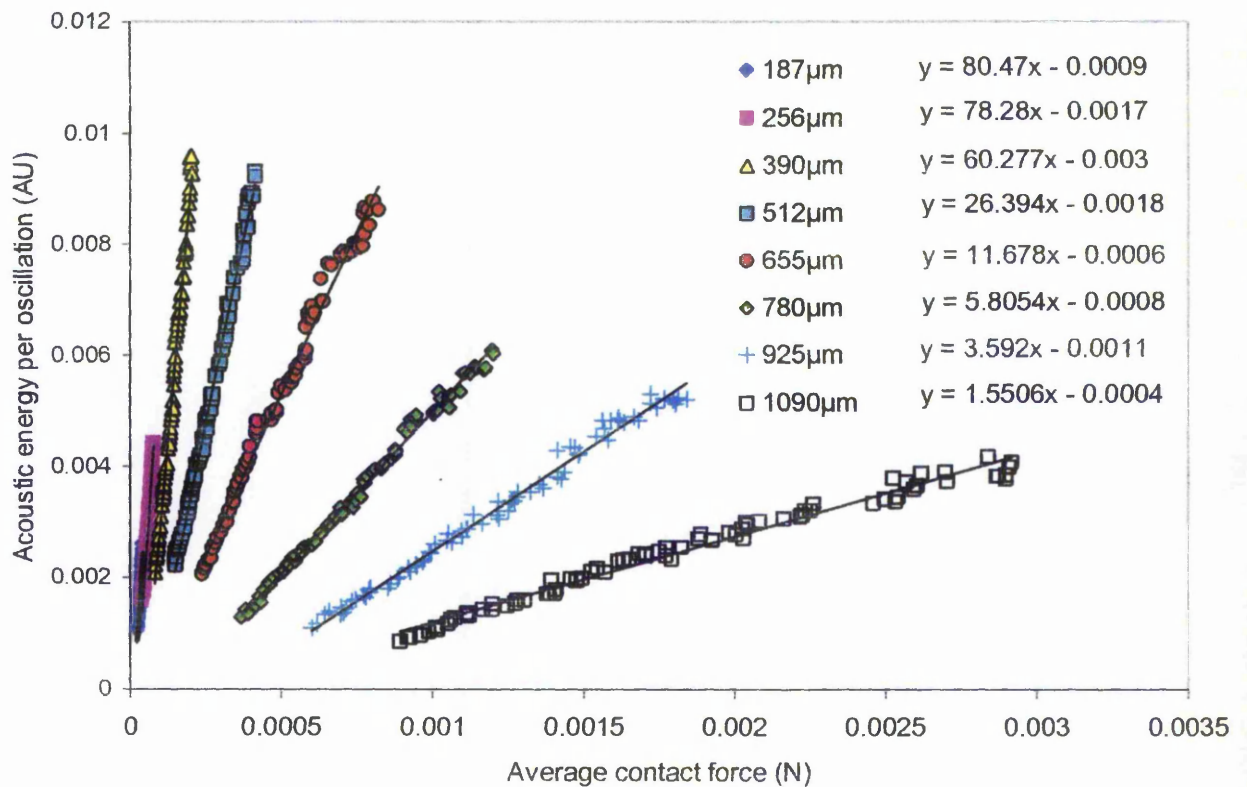


Fig 57. Average oscillation energy against average particle contact force for sharp sand granular samples (375 transducer, frequency range 250-500kHz).

The experiments have been repeated using Leighton Buzzard sand samples and the results are shown in Figure 58. The results exhibit a similar behaviour to that of the sharp sand samples, where an increase in the particle size reduces the gradient.

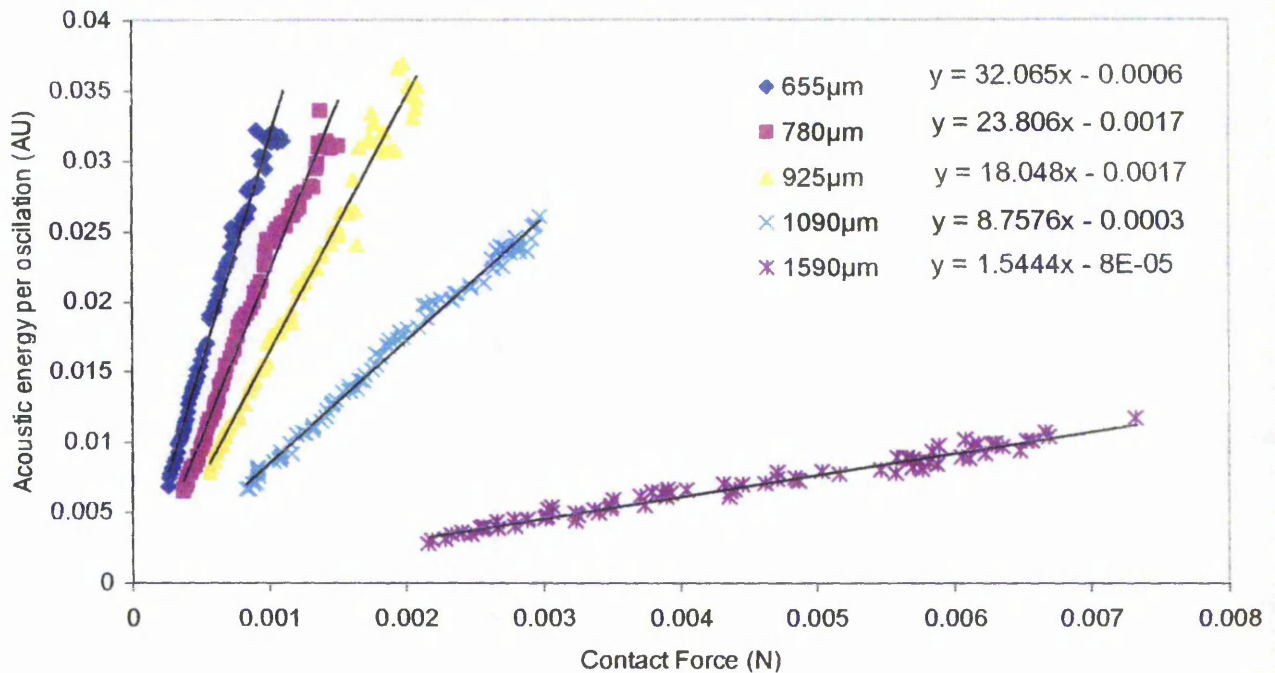


Fig 58. Average oscillation energy against the average particle contact force, using Leighton Buzzard granular samples (375 transducer, frequency range 250-500kHz).

The gradients produced for both sharp sand samples and Leighton buzzard sand samples are plotted against the particle size in Figure 59. The gradient is termed the contact energy function as it represents the change in the oscillation energy due to a change in the contact force. The results show a reduction in the contact energy function due to an increase in the particle size and there is an offset between the contact energy functions for the two granular materials. The trends are not linear and there is no agreement with the power law suggested in Equation 40.

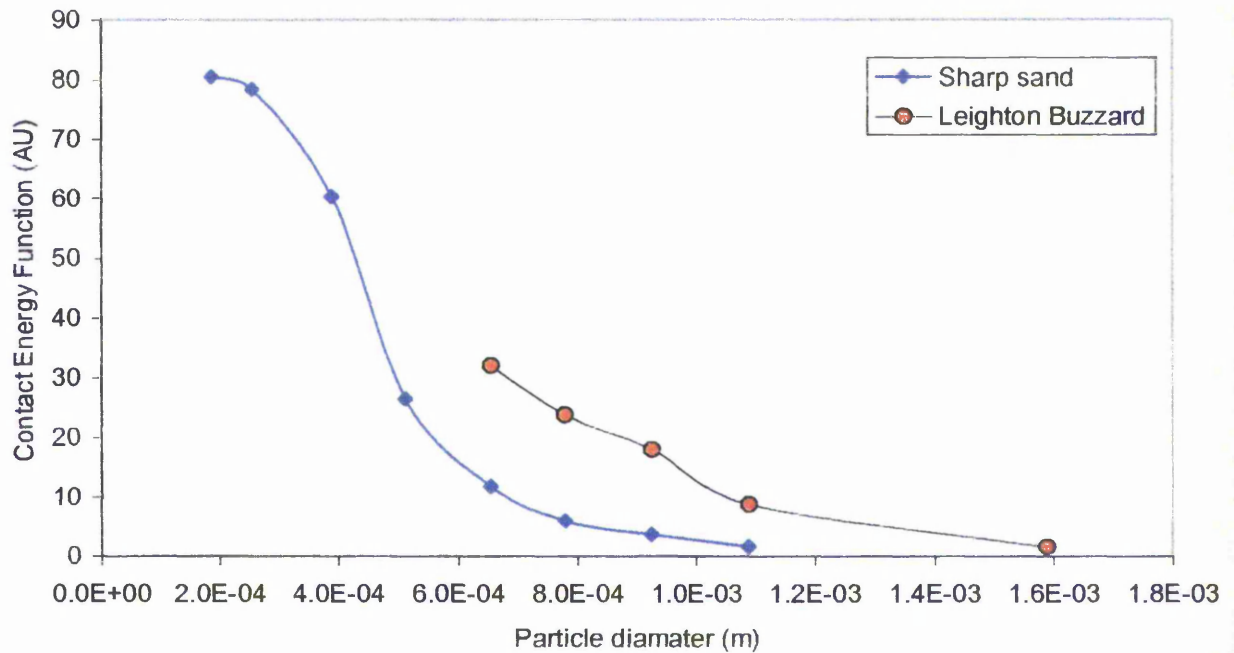


Fig 59. The contact energy functions against the average particle diameter, for both sharp sand samples and Leighton Buzzard sand samples.

5.6.3 The Effects of Density on the Acoustic Energy

In practical soil structures there is a lot of variability in the soil density, which may affect the level of acoustic energy that can be generated. Figure 60 shows the variation of the acoustic energy against the applied load for both compacted and loose sharp sand samples. It can be seen that loose sands with a lower packing density produce a larger acoustic energy signal at a given load. This is because the reduction in the number of contacts formed between the probe tip and the particulate material has led to an increase in the total acoustic energy.

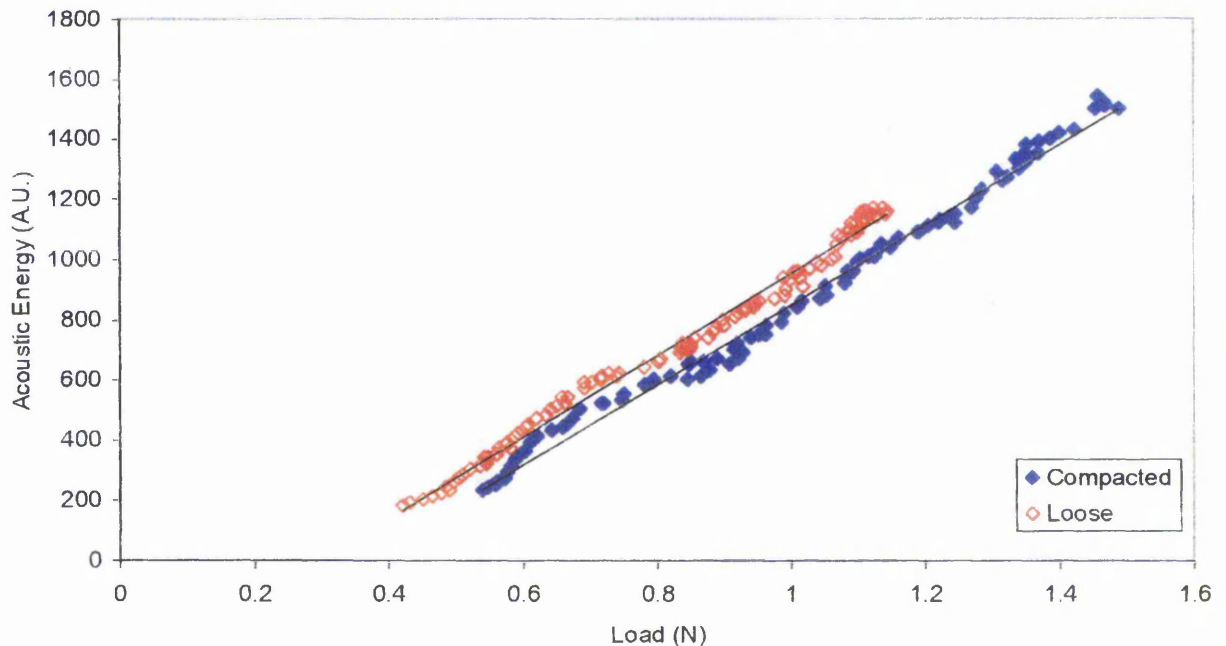


Fig 60. Acoustic energy against applied load, for sharp sand with an average particle size of $256\mu\text{m}$.

With a known average particle size and assuming a cubic packing relationship, the average contact force can be determined from Equation 11. However, using the known average grain size diameter of the sample does not take into account the change in the packing density, which can affect the number of particle-probe contacts and hence the value of the count rate.

An empirical function relating the characteristic count rate to the average particle size has been determined using the data from compacted and loose particulate samples (Figure 61). The empirical function allows a change in density to be represented by an equivalent change in particle size, which is calculated from the change in the count rate.

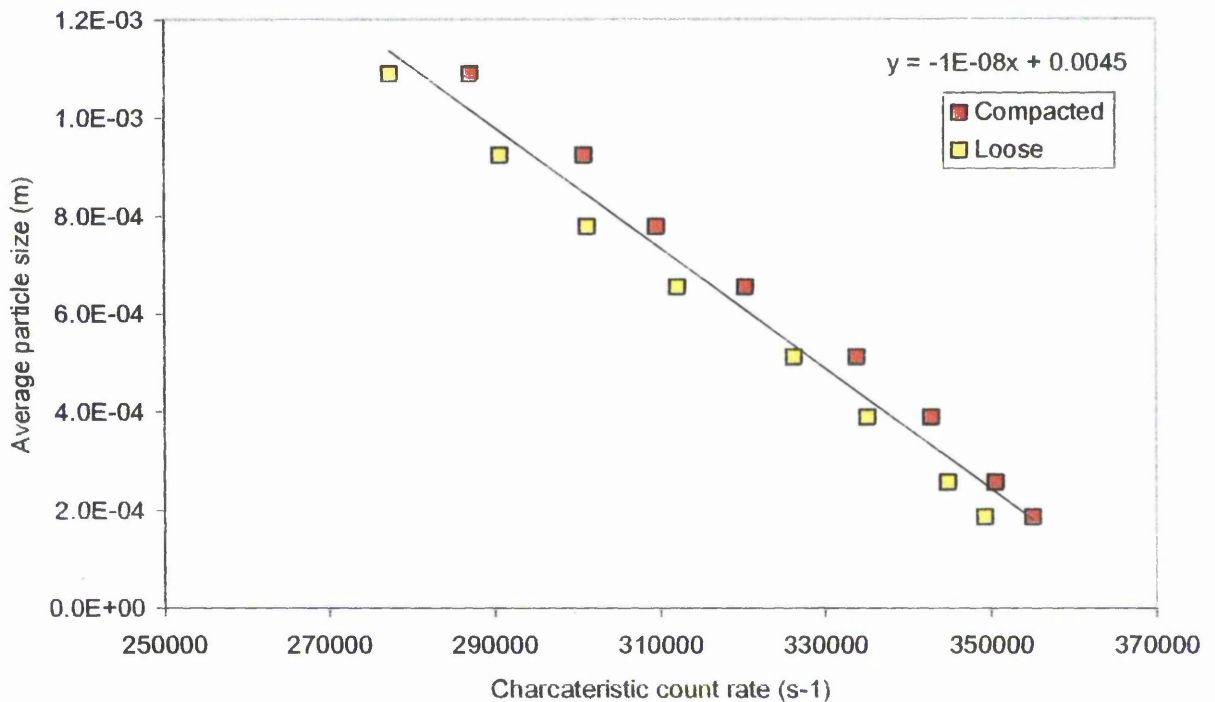


Fig 61. Average particle size against the characteristic count rate for compacted and loose granular samples of sharp sand.

The results in Figure 62 show the variation of the average oscillation energy against the average particle contact force for both compacted and loose sharp sand samples. The average oscillation energy is consistently higher for compacted samples as there are more particle-probe contacts under the same average contact force. A higher oscillation energy implies that a larger total elastic potential energy is released from asperity deformation. Therefore, the results suggest that fewer particle-probe contacts produce a reduction in the contact energy function (gradient of the average acoustic energy per oscillation against the average particle contact force).

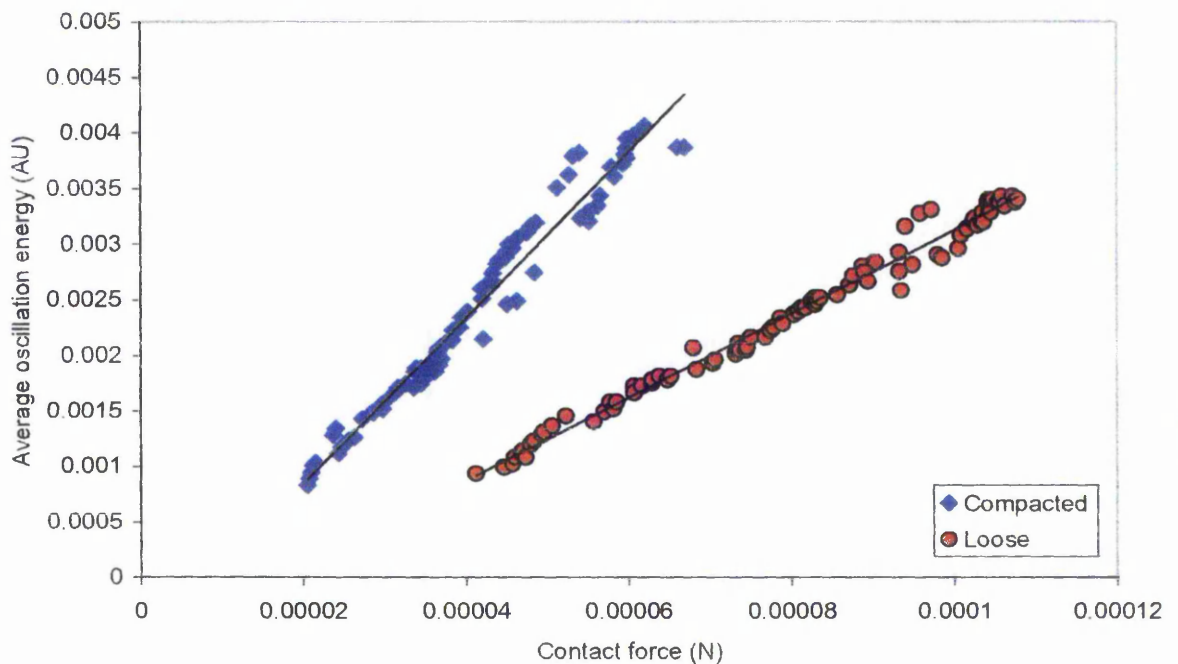


Fig 62. Average oscillation energy against estimated average contact force, for sharp sand samples with an average particle size of 256 μ m.

5.6.4 The Effects of Water Content on the Acoustic Energy

A previous investigation (Section 5.5.2) has shown that the water content of a granular sample had a negligible effect on the characteristic count rate. It was observed during the experiment that there was a significant drop in the signal amplitude, which would have an effect on the acoustic energy. An empirical relationship is determined between the characteristic count rate and the particle size using granular samples with different levels of water content (Figure 63). The spread within the characteristic count rate does become slightly larger and it is postulated that this may be due to a larger variance of the granular density caused by the addition of water, but the results are inconclusive. However, the separation in characteristic count rate due to different particle sizes is still evident. A linear relationship between the count rate and the average particle diameter was assumed to determine an estimate of the average contact force.

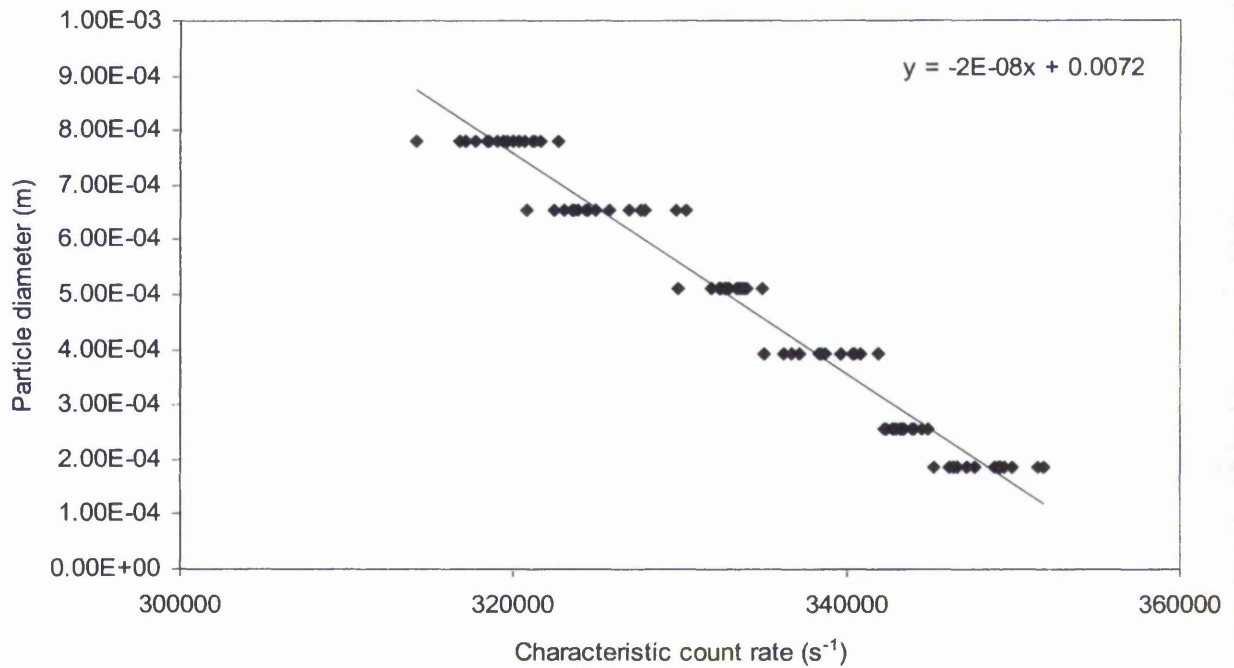


Fig 63. Average particle diameter against the average characteristic count rate using samples of sharp sand with different levels of water content.

Figure 64 shows the variation of the average oscillation energy against the average contact force for different levels of water content. The addition of water to the sample has caused a reduction in the average oscillation energy for a given contact as well as a reduction in the gradient of the data. This may be explained by the fact that increasing the water content reduces the frictional forces between the particle-probe contacts, which has a direct influence on the amplitude of the friction-generated signal.

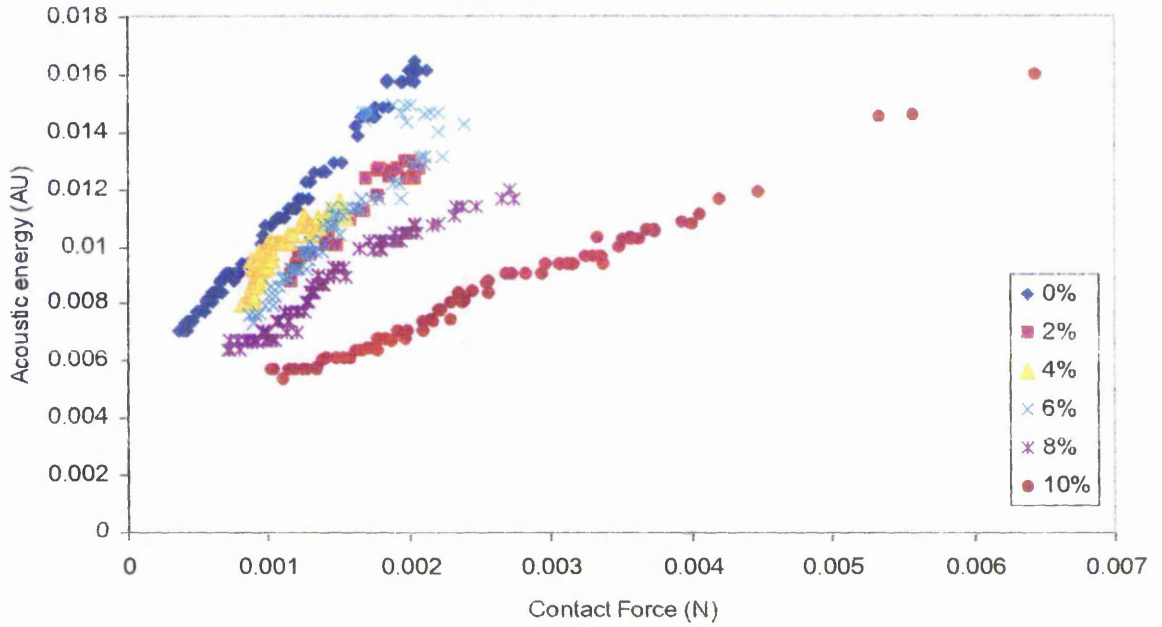


Fig 64. Average acoustic energy per oscillation against average estimated contact force, for sharp sand samples having different levels of water content with an average particle diameter of 655 μ m.

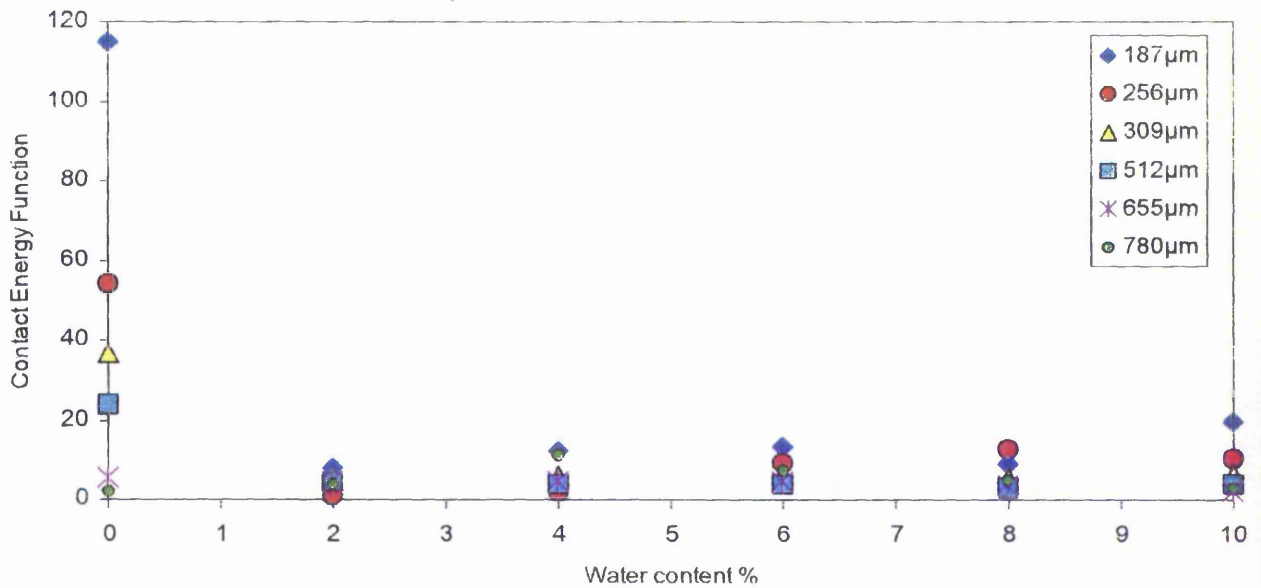


Fig 65. The contact energy function against the water content using a range of different sized granular samples.

The results in Figure 65 show the contact energy function against the water content for a range of particle sizes. A large difference can be seen in the contact energy function for the dry granular samples. However, the addition of water to the samples severely affects the contact energy function, to the extent that differentiating between grain sizes is no longer possible. The addition of water would act as a lubricant between the particle-probe contacts, accounting for the reduction in the acoustic amplitude. It is also difficult to determine whether there is a functional relationship between the contact energy function and the water content. It should be noted that, when monitoring actual soil structures, the presence of water in the soil may not affect the count rate but it can have a significant effect on the acoustic energy parameter.

The results have shown that the acoustic energy is sensitive to the applied load, the sliding velocity, the particle size, the density and the water content. However, a wet granular sample severely affects the acoustic energy and distinguishing the difference between the acoustic signals generated by each granular sample becomes difficult. It is considered that the fluid in the granular sample may act as a lubricant. Therefore, it is important to determine whether the shear force between the probe and the granular material can be affected by the water content.

5.7 Standard Shear Box Investigation

A fundamental property of granular materials is the shear strength the presence of water in the granular sample often acts as an unintended lubricant. The results produced from this investigation will be compared with the oscillation energy function provided by the probing system for similar levels of water content. Two samples of sharp sand with average particle diameters of $256\mu\text{m}$ and $512\mu\text{m}$ were used in a standard shear box test. The basic principals of the shear box have been explained in Section 3.3.4. Figure 66 shows an example of the shear-stress displacement curves and the inset chart shows the variation of the peak shear stress against the normal stress, from which the friction angle can be determined.

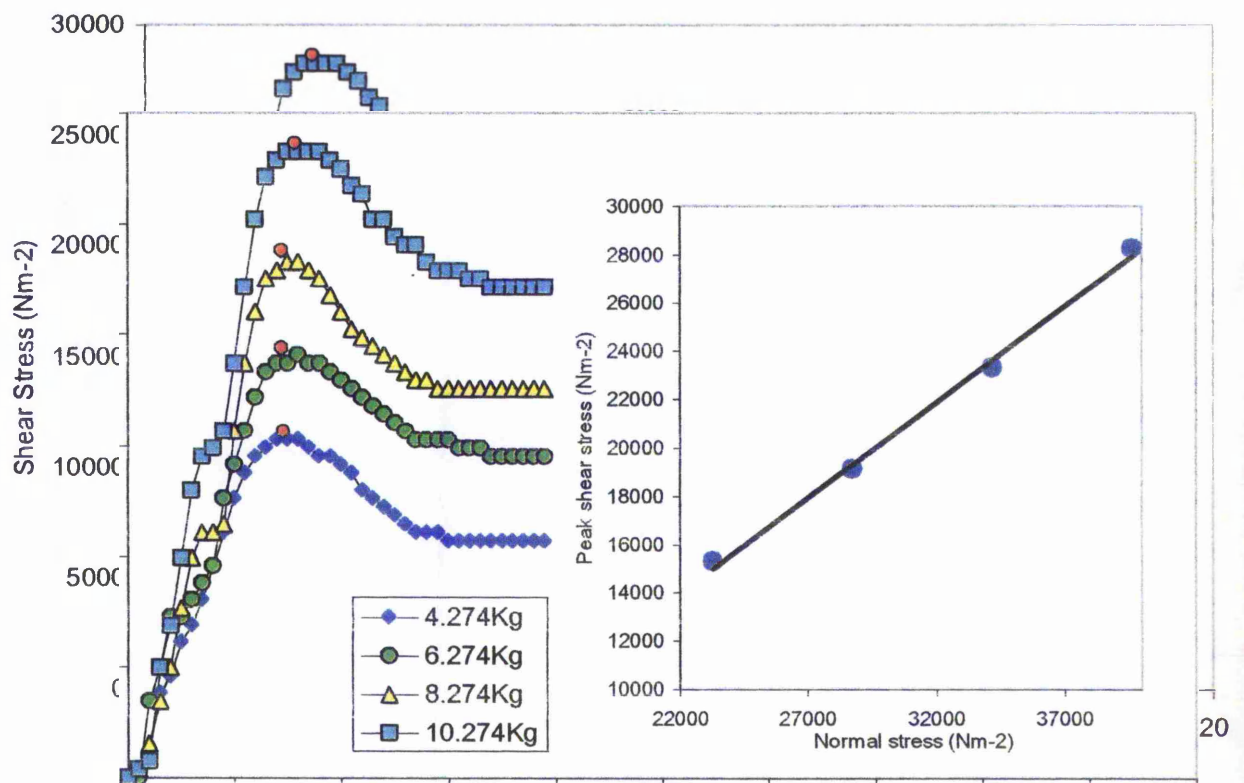


Fig 66. Shear stress against the linear displacement using a standard shear box, for a $256\mu\text{m}$ particulate sample having 12% water content.

The friction angles were determined for different levels of water content using two sizes of particulate material. A sample of sand with the same average particle diameter was measured out and a controlled amount of water was added to the sample. The particulate sample was mixed thoroughly to provide an even consistency of wetness and the material was placed into the shear box in layers to maintain a uniform density throughout. The applied load was increased to provide four peak stresses for determining the friction angle. The water content was increased until the granular material was fully saturated. The same sand samples were also tested with the probing system and the contact acoustic energy functions were monitored for a range of water contents. Figure 67 shows the variation of the friction angle and of the contact energy function against the water content. The results do not suggest any functional relationship between the two parameters (the water content and the friction angle). Furthermore there does not appear to be any similarities between the contact energy function and the friction angle. Dry sand produces a large contact energy function, which is reduced considerably with the addition of water. However, there is not a significant change in the friction angle between the dry and wet samples.

The standard shear box test measures the internal friction angle of the granular material to be determined based on the knowledge of the peak shear strength, which is larger than the residual shear strength, a parameter usually associated with the study of continuous sliding interfaces. Therefore, an investigation using a ring shear apparatus is considered appropriate as it involves both a continuous sliding interaction and a solid-granular interface.

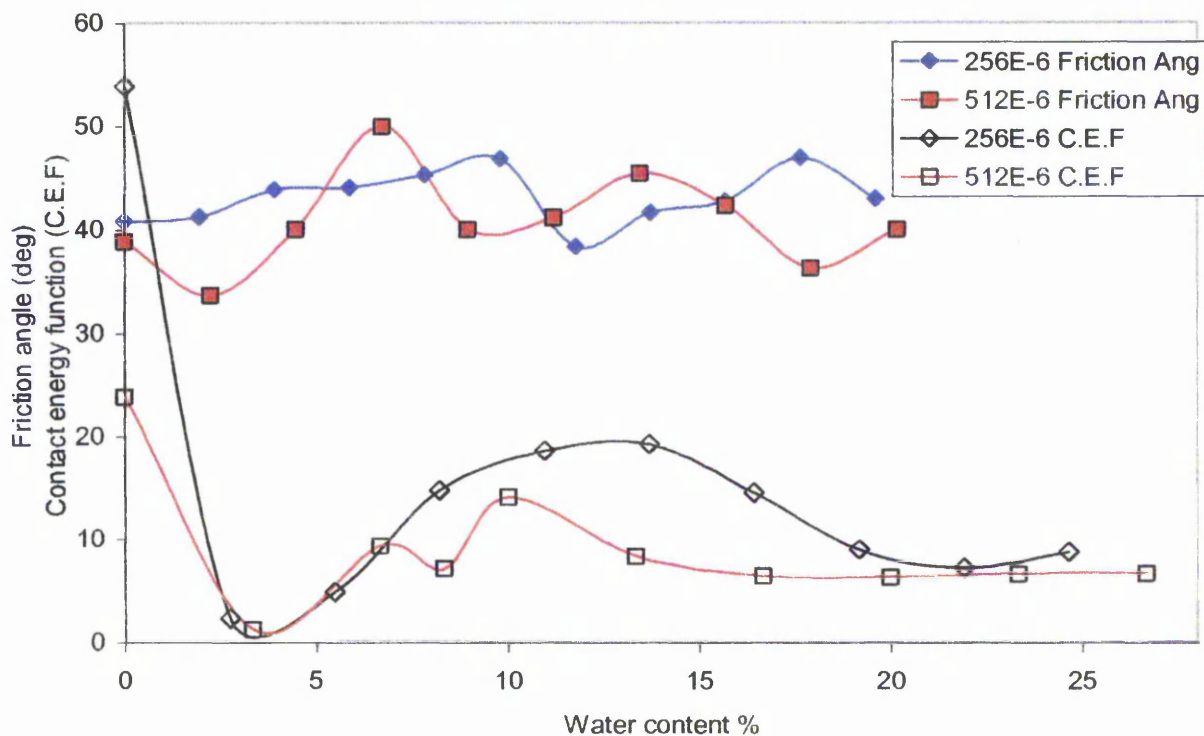


Fig 67. Friction angle and contact energy function against the water content for two samples of sharp sand with different particle diameter.

5.8 Ring shear investigation

A ring shear apparatus measures the residual shear, which is the shear force generated during continuous sliding and should not be confused with the peak shear force measured by a standard shear box experiment. The basic principles of the ring shear have already been explained in Chapter 3. In this section the effect of water content and particle size on the frictional force is investigated for a solid-granular interaction.

The changes in the frictional force between solid-granular interfaces for wet and dry granular samples have been investigated. Granular materials were prepared with 20% water content over a range of grain sizes to provide the wet samples. Dry samples of the same grain size were also tested. The bottom section containing the granular material

was set to rotate at a constant speed and the residual shear strength was measured, while the applied load was increased at three-minute intervals. Figure 68 shows the friction angle against the particle size for wet and dry samples of both sharp sand and Leighton Buzzard sand. The results confirm that wet sample produces a reduction in the friction force, which may account for the reduction in the acoustic energy shown in Figure 65 using the probing system. There does not appear to be any functional relationship between the particle size and the friction angle. The sharp sand samples show a peak in the friction angle, but there is only a small change in the friction angle associated with the Leighton Buzzard sand samples.

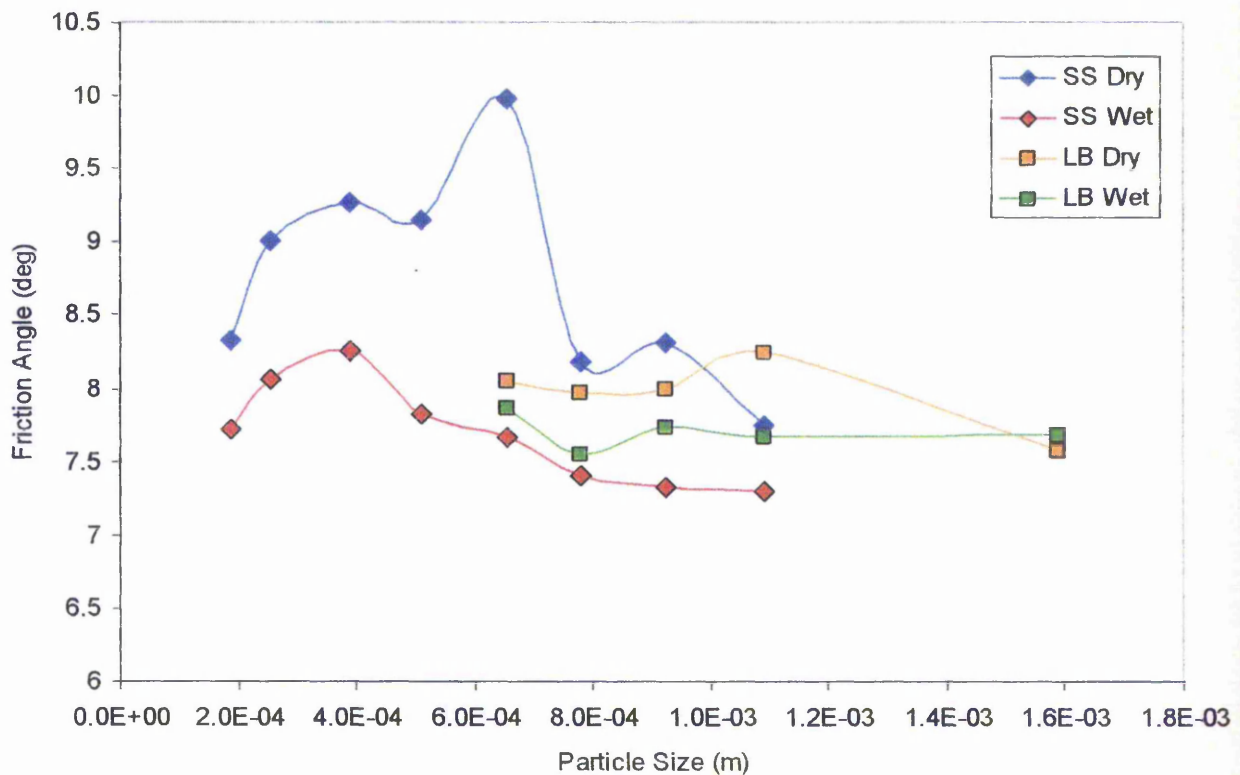


Fig 68. Residual shear friction angles against the average particle diameter data shown for wet and dry samples of sharp sand and Leighton Buzzard sand

The acoustic emission generated by the solid-granular interaction associated with the ring shear machine was investigated to determine the effect of the shear force on the acoustic parameters. The same AE measuring equipment was used on the ring shear machine and the AE sensor was attached to the top of the solid surface, which forms one half of the friction pair. The acoustic signal generated by the ring shear machine produced a number of large acoustic pulses, which did not occur using the probing system. The ring shear machine constrains the granular material within tight boundary conditions, limiting the bulk deformation of the granular material caused by loading and consequently results in larger particle stresses. Therefore, it is postulated that the large AE pulses are likely to be caused by particle crushing as a consequence of larger particle stresses that occur during sliding.

Wet granular samples did not generate a strong acoustic signal using the ring shear machine and the results obtained were severely affected by electrical noise. Therefore, monitoring the acoustic emission generated by wet granular samples could not be investigated.

The results in Figure 69 show the count rate against the applied vertical force. Under no loading conditions the count rate is large due to the high frequency noise. Increasing the load causes a reduction in the count rate, which is similar to previous experiments using the probing system. However, unlike the results obtained from the probing system the count rate does not reach a stable steady state. Therefore, the characteristic count rate could not be determined and a relationship between the characteristic count rate and the particle size could not be established. It can be seen that there is no direct relationship between the applied load and the count rate. Considering that the shear force is directly

proportional to applied load it can also be concluded that there is no relationship between the shear force and the count rate.

It was visually observed when separating the steel disk from the granular sample that some of the granular material was stuck to the steel disk, which indicates part of the shear plane was not at the sand-steel interface. The adhesion to the disk was more prominent using the smallest grain size and the amount of adhesion reduced considerably as the grain size increased. Investigations using the probing system have shown that the count rate is dependent on the number of contacts formed between the probe tip and the granular material. Therefore, a shear plane within the sub layers of the granular material would affect the number of asperity interactions on the surface of the top plate, which in turn affects the characteristic count rate. It was also observed that some fine powder was mixed with the granular samples after a period of shearing providing evidence of particle crushing.

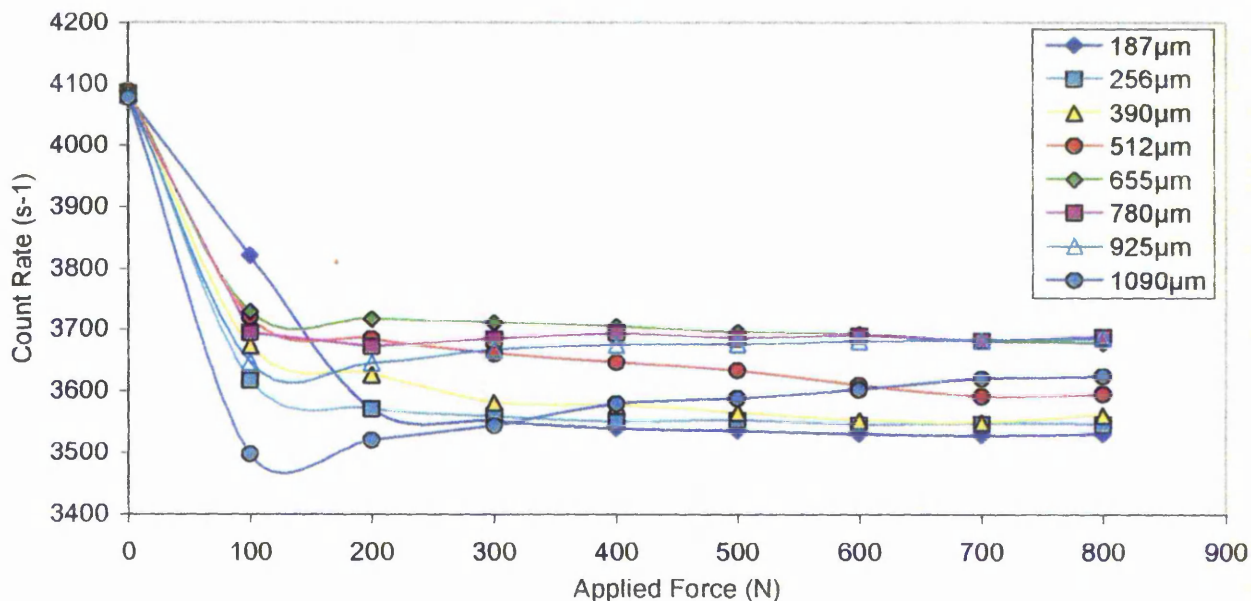


Fig 69. The average count rate against the applied vertical load using a ring shear experimental apparatus, for Leighton buzzard sand samples.

The experiments were repeated using Leighton Buzzard sand samples and the results are shown in Figure 70. In this case the results show a small reduction in the count rate due to increasing particle size. There was also evidence of grain crushing highlighted by the presence of finer particles following a period of shearing. Furthermore, there did not appear to be any signs of particle adhesion to the top plate, which occurred using the sharp sand samples.

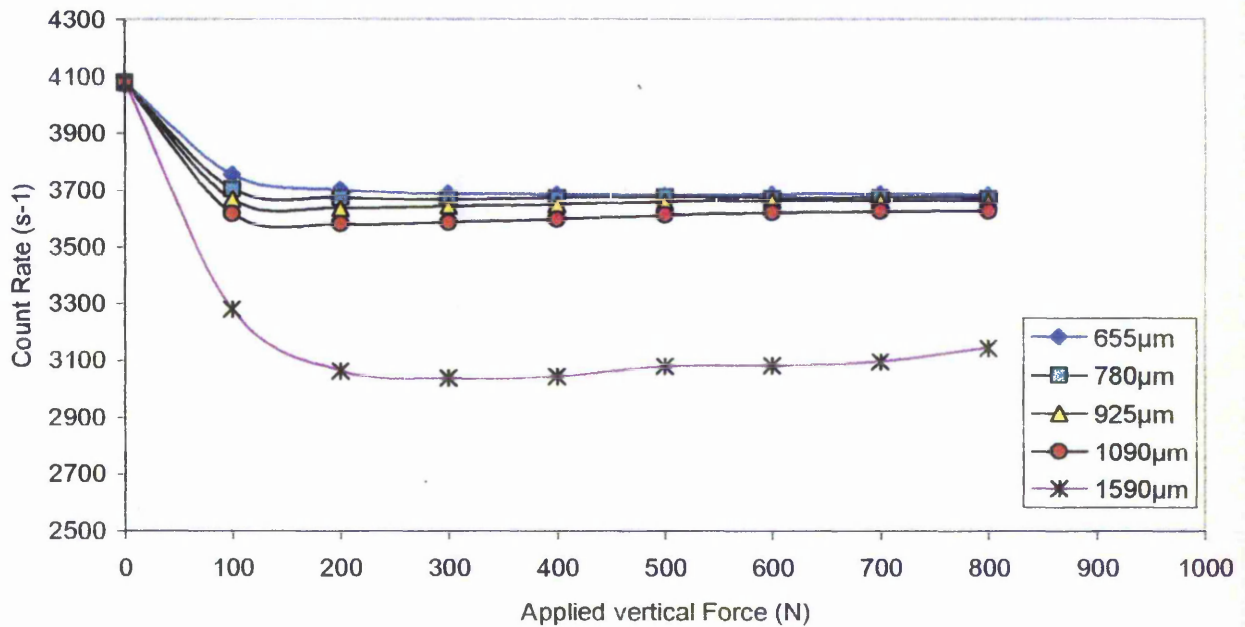


Fig 70. The average count rates against applied vertical load using a ring shear experimental apparatus, for Leighton buzzard sand samples.

Results obtained from the probing system (Figure 65) highlighted that the acoustic energy was severely affected by the water content. It was suggested that the change in acoustic amplitude due to the addition of water resulted from a reduction in the friction force. Figure 68 confirmed that the addition of water reduced the friction force and therefore the effect of the shear force on the acoustic energy has been considered. Figure 71 shows the average acoustic oscillation energy against the shear force using

sharp sand samples. The oscillation energy appears to increase almost linearly with the shear force, although there is no clear pattern between the gradient and the particle size.

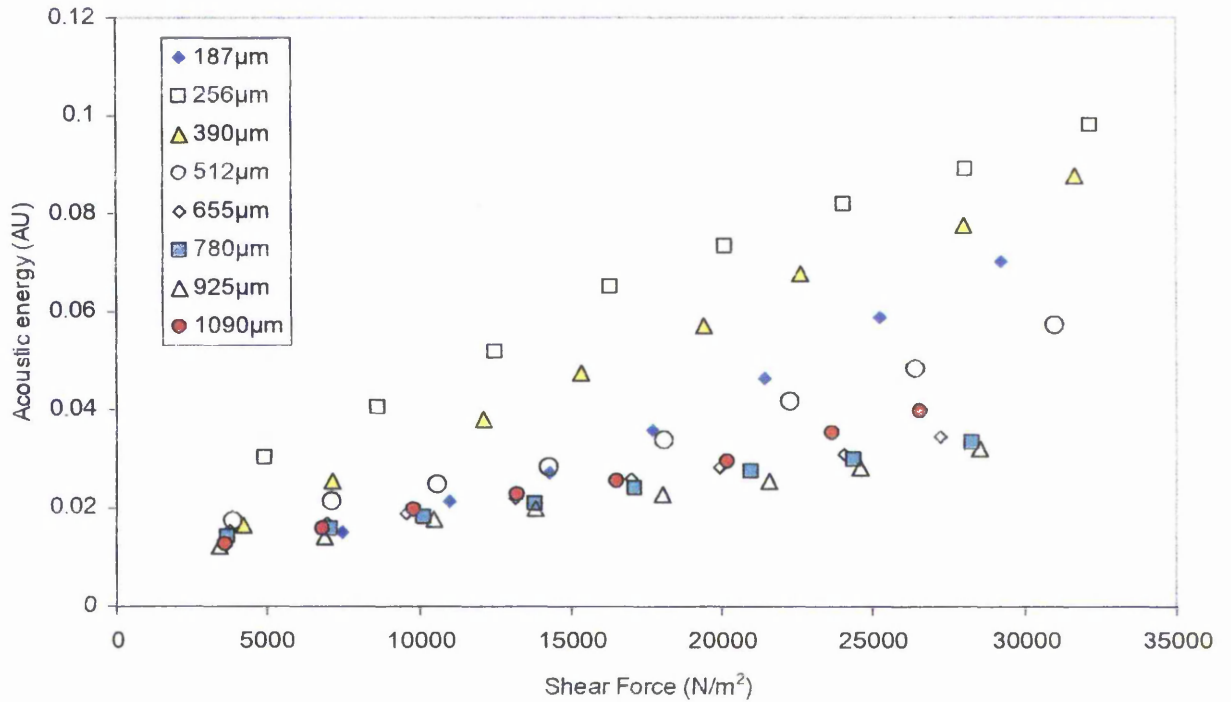


Fig 71. Average oscillation energy against the shear force using sharp sand samples in a ring shear machine.

Figure 72 shows the acoustic oscillation energy against the shear force using Leighton Buzzard sand samples. The results show that an increase in the particle size for this type of sand produced an increase in the oscillation energy. It can be seen that the changes in the oscillation energy due to an increase in the shear force is not linear and that a power law relationship may exist. Larger particle sizes produced an increase in the acoustic energy, although this change was not demonstrated by their corresponding friction angle. The results generally suggest that the particle size does have an effect on the acoustic energy but the effect of the particle size on the friction angle is negligible.

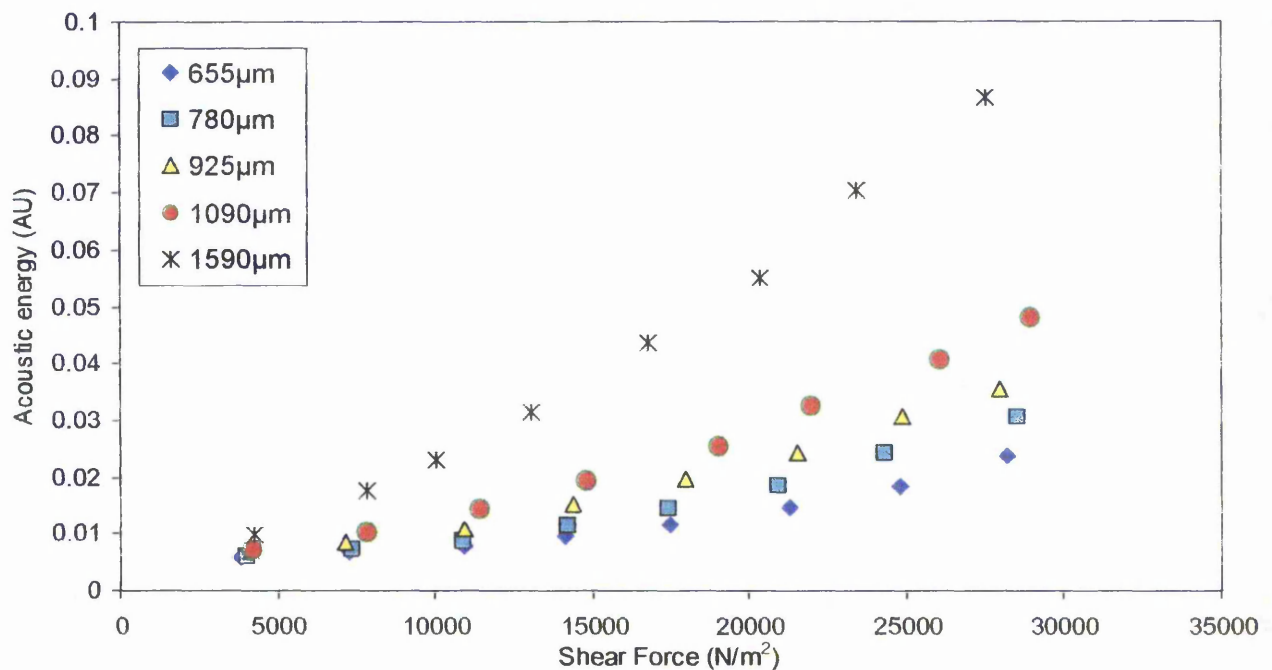


Fig 72. Average oscillation energy against shear force using Leighton Buzzard sand samples in a ring shear machine.

The results have shown that the acoustic oscillation energy is affected by an increase in the shear force as a result of increasing applied load. However, the change in the shear force due to particle size does not produce a similar change in the oscillation energy. The results have also shown that the addition of water causes a reduction in the shear force, which consequently reduced the amplitude of the acoustic signal.

6.0 Discussion

In this chapter the results obtained will be discussed considering the information gathered from the literature review as well as the equations derived in the theoretical consideration.

6.1 The Count Rate

The results associated with the count rate parameter are discussed in this section. The interaction of the friction pair materials is considered to determine what actually affects the count rate.

The results in Figures 26a, 31, 33, 34 and 37 all show that the count rate produces an S-shape curve due to an increase in the applied load. The data was divided into three sections, which highlighted two significant changes in the data. In section 1 there was only a small change in the count rate due to increasing load. The change in the count rate was small due to the fact a threshold was applied to the acoustic signal and the strength of the signal generated by the friction pair needed to be large enough in amplitude for any counts to be detected. In section 1 the amplitude of the friction-generated signal was smaller than the amplitude of the system noise, which was purposely below the applied threshold and therefore no counts were detected. The line separating sections 1 and 2 was termed the threshold line as it represented the point where the friction generated signal was large enough in amplitude for acoustic counts to be detected. Results did show that the position of the threshold line was dependent on both the sliding velocity and the applied load.

Data within section 2 suggested a power law relationship existed between the applied load and count rate. For granular materials the index value of the power law was determined to be approximately 2 using four different sliding velocities (Figure 27). Sarychev and Shchavelin [73] proposed a power law relationship between the count-rate and the applied force (Equation 31), and the index value was stated to be less than 1. The power law relationship proposed by Sarychev et al is associated with the frictional interaction of solid bodies and does not consider the solid-granular interface involved in this project. However, the results obtained from the abrasive paper experiments does consider the interaction of two solid bodies and produced an index value of approximately 1.4 for the data within section 2. It can be concluded that the results obtained within section 2 does not obey the power law relationship suggested by Sarychev and Shchavelin.

The line separating sections 2 and 3 highlighted a change in the power law relationship between the applied load and the sliding velocity. Considering the abrasive paper experiments shown in Figure 32, the index of the power law relationship for data within section 3 had a value of approximately 0.3, and agrees with the general rule suggested by Sarychev and Shchavelin.

Obtaining data within section 3 using a solid-granular friction pair was restricted due to difficulties involved with investigating a large range of applied loads. An unusual method of processing the count rate data was developed, which allowed the data highlighted by section 3 to be interrogated at lower loading conditions. However, changing the threshold also changed the shape of the curve produced from plotting the count rate against the applied load. An increase in the applied load caused the count rate

to approach a steady state, and the value the count rate approached is termed the characteristic count rate. It is the characteristic count rate that is related to the data within section three obtained using a standard thresholding method.

The count rate is a measure of the number of oscillations above a predefined threshold and the characteristic count rate can be simply considered a steady state frequency. Therefore the characteristic count rate does not provide any information that is directly related to the amplitude. The interaction of the friction pair generates an acoustic signal, which to simplify, produces a continuous frequency of oscillations with variable amplitude. Therefore the signals generated by granular materials of different particle size produced a unique steady state count rate or frequency of counts.

It is postulated that the characteristic count rate is always developed by a solid-granular friction pair, even at very small loads and that an increase in the applied load only affects the amplitude of the signal. Therefore, the increase in count rate within section 2 of the S-shape curve results from an increase in the amplitude of the characteristic signal and the change in the count rate would provide information relating to the distribution of the oscillation amplitudes associated with the generated characteristic signal.

Baranov et al [74] used an assumption that stated the count rate parameter was directly proportional to the number of asperity contact spots formed per unit time. In the case of solid bodies Tabor [48] stated that the real area of contact is proportional to the applied load, which is dependent on an increase in the areas of contacting asperities as well as the formation of new asperity contacts during loading. Considering the abrasive paper

experiments, two solid elastic bodies were in contact and therefore the number of contact spots formed would be influenced by the applied load. However, granular materials do not behave like an elastic solid. Any object applying a force on a granular material will cause the particles to form a closer packing arrangement at the point of the applied force. Any further increase of the force applied by this object will not directly increase the number particles that are in contact with the object. The applied force will be transmitted through the particles in actual contact with the object to the next plane of particles, which will also rearrange to form a closer packing arrangement [45]. Furthermore the movement of the particles will not always be in the direction of the applied force as the particles that fill smaller voids in a mono-layer will push their neighbouring grains aside. Therefore the forces acting on the particles due to an externally applied force are also dependent on the geometrical constraints, which were considered by Jewell [27, 28] for shear box investigations. Geometrical constraints include boundary walls as well as surrounding particles, which also restrict the movement of the particles during the deformation of a granular material. It can be considered that the number of particles in contact with the probe does not directly increase with increasing load, but instead produces a similar amount of particle-probe contacts during probe penetration. Therefore, the displacement of the probe causes a volume change (dilation) of the granular structure surrounding the probe rather than deform the grains in contact with the probe tip. Consequently, using granular materials of controlled grain size contained within large boundary conditions compared to the object applying the force provided a method for investigating the number of contacts generated between the probe tip and the granular material.

Results shown in Figures 44 -55 all show that the characteristic count rate reduces as the particle diameter increases. As larger particles produce fewer particle-probe contacts a reduction in the characteristic count rate would be expected. It was shown in Figure 47 that an increase in the density caused an increase in the characteristic count rate. An increase in the density would also increase the number of contacts, although pushing the probe into a loose granular material would also compact the particles to form a dense packing arrangement at the probe tip. Consequently it may be argued that the density may not have an effect on the characteristic count rate as the density will change due to probe penetration forming a similar number of contacts. However, the result in Figure 47 agrees with Josserand et al [44] who stated that the rate of compaction is a function of the initial density. Therefore a denser material will compress to a denser state compared to a loose granular material under a given load and hence the difference in the characteristic count rates.

The effect of water content on the characteristic count rate is small only producing a slightly larger variation of the characteristic count rate. The larger variation in the characteristic count rate may have been due to the effect of the water content on the density, but the results are inconclusive. The addition of water to the granular sample caused the particles to become more cohesive and the voids between particles will contain an amount of fluid, which may affect the density of the granular sample. Any density variations will affect the accuracy of characterising the particle size, which was highlighted in Figure 65.

The results associated with the characteristic count rate have provided convincing evidence that suggests the count rate is directly affected by the number of particle

contacts formed between the probe tip and the granular material. Therefore, the results obtained agree with Baranov et al [74] who stated that count rate is proportional to the number of contact spots formed per unit time as well as Akay [68] who stated that corrugated surfaces produce impulsive contact forces at the corrugation frequency. Furthermore Brinscoe et al [70] presented results where the spectral content of a friction generated signal appeared to be unaffected by the contact pressure except for an increase in the overall acoustic energy.

The general power law relationship suggested by Sarychev and Shchavelin [73] (Equation 30) does not apply to the characteristic count rate produced by the solid-granular friction pair considered in this project. However, the abrasive paper investigations did show an increase in the count rate with increasing applied force, and suggests that a power law may exist between them, although any further investigations of this relationship was beyond the scope of this project.

It can be concluded that the characteristic count rate is only affected by the number of contacts formed between the probe tip and the granular material. Therefore, it was possible to characterise granular materials of controlled grain size using an empirical function that related the characteristic count rate parameter to the average particle diameter.

The aim of this project was to develop a method of characterising soil structures using the acoustic emission generated by a drilling process. Research carried out in this project has shown that the count rate is related to the number of contacts formed between the probe tip and the granular material, which suggests that there is potential

for using the count rate parameter to identify any changes in the soil layers. However, there would be many practical implications due to the fact that actual soil structures are not carefully graded into different particle sizes. Therefore further work would be required to focus on the particle distributions, which are associated with typical soil structures. The results have also highlighted methods of characterising particle size at small applied loads, which in practical terms means that the size of drilling equipment can be reduced.

The change in the acoustic energy due to increasing load shown Figure 26b produced a similar S-shape curve to that of the count rate. The similarities between the count rate and the acoustic energy parameters were highlighted in Figure 29, where it was seen that a linear relationship existed between them. The linear relationship between the count rate and the acoustic energy was independent of both the applied load and the sliding velocity, which indicates that the count rate and the acoustic energy are proportionally affected by the loading conditions and sliding velocity in the same way. Consequently, for a given solid-granular friction pair within a certain range a universal relationship exists between the count rate and the acoustic energy.

The particle size had an effect on the universal linear relationship between the count rate and the acoustic energy. It was seen in Figure 30 that the gradient of the universal linear relationship changed due to an increase in the particle size, although there was no functional relationship between the gradient and the particle size. It can be argued that, for friction pairs with similar material properties, there is no need to monitor both the acoustic energy and the count rate for acoustic data within the region where the universal relationship applies.

A similar linear relationship between the count rate and the acoustic energy was found using the frictional interaction between the probe tip and the abrasive paper, shown in Figures 36 and 38. In this case the different grades of abrasive paper did not affect the gradient of the linear relationship, which may be due to the amount of wear the abrasive paper suffered during each test. Each grade of abrasive paper became worn very quickly so that after testing, identifying the difference in the surface roughness for each abrasive grade was difficult. Furthermore, the different grades of abrasive paper produced very similar characteristic count rate values, indicating that the effect of wear produced a similar number of contacts for each abrasive grade, based on the assumption that the count rate is proportional to the number of contacts formed per unit time.

The abrasive paper investigations highlighted that the linear relationship between the count rate and the acoustic energy was finite and it did not apply for large applied loads or sliding velocities. The universal linear relationship does not hold when the count rate approaches steady state as the count rate does not increase in the same proportion to the acoustic energy, shown in Figures 35 and 36 by a change in the gradient.

6.2 The Acoustic Energy

It can be considered that the change in the acoustic energy while the universal relationship holds is due to a function of both the number of oscillations above the applied threshold and their individual amplitude. The fact there is a linear relationship between the count rate and the acoustic energy means that the average energy per oscillation is constant, which can be determined from the gradient of the linear relationship. Therefore, an increase in the amplitude of each oscillation is balanced by

new oscillations with smaller amplitude crossing the applied threshold. When the count rate reaches a steady state the acoustic energy is not affected by a change in the number of oscillations, which was shown by an increase in the average energy per oscillation. Therefore, change in the acoustic energy was mainly due to an increase in the amplitude of the characteristic signal and it was within this region that the acoustic energy was investigated.

It was seen in The Leighton Buzzard sand and the sharp sand samples produced power law exponent values between 1.1 and 1.6 (Figures 54 and 55), although there did not appear to be any functional relationship between the index value and the particle size. Equation 40 was based on the assumption that the acoustic energy is proportional to the potential energy generated due to the elastic deformation of contacting asperities. The equation states that the power law relationship between the contact force and the acoustic amplitude has an index value of $2/3$. Therefore, the power law relationship between the contact force and the acoustic energy would have an index value of $4/3$, as the acoustic energy is proportional to the signal voltage squared. The power law curves fitted to data produced exponent values in the region of $4/3$, although there was some variation.

It was observed that the relationship between the acoustic energy and the applied load could be adequately described by a linear relationship. Table 2 highlighted that there was very little difference between applying a power law relationship or a linear relationship. Therefore, it was concluded that applying a linear relationship between the acoustic energy and the applied load was sufficient for the range of data considered in the investigation.

Equation 40 involves the force at a single asperity contact and the estimated average contact force was considered in Figures 57 and 58. The average oscillation energy was used as the acoustic parameters as it focuses more closely on the acoustic energy produced by a change in the signal amplitude rather than the increase in energy due to the effect of more counts being registered. The linear trend lines fitted to the data showed that an increase in the particle size caused a reduction in the gradient. Therefore at a given contact force the energy decreases as the particle size increases. The change in the gradient due to particle size was not linear as it did not agree with the power law stated in Equation 40, although in general terms the equation does state that the acoustic amplitude does decrease with increasing particle size.

At a given average contact force the total potential elastic energy generated depends on the sum of all the particle-probe contacts. To simplify it is assumed that all asperity contacts are deformed by the same average contact force. Granular materials with a smaller average particle size will produce more particle-probe contacts and will consequently increase the total acoustic energy for a given contact force as there are more asperity contacts at the same elastic potential. Changes in the bulk density will also affect the acoustic energy due to the change in the number of particle-probe contacts formed.

Granular materials with the same average particle diameter but of different type produced a different acoustic oscillation energy at a given average contact force (Figure 59). It can be concluded that the acoustic energy is affected by the material properties of the particles. The elastic properties of two asperities in contact will influence the magnitude of their deformation. Therefore, the magnitude of the potential energy

created from the elastic deformation of the probe's surface asperities will affect the amplitude of pressure pulse caused by the release of this potential energy, which is considered the source of the strain wave propagating through the probe shaft. Harder particles increase the elastic deformation of the probe's surface asperities and will therefore increase the amplitude of the propagating strain wave. For that reason the results in Figure 59 suggests that the Leighton Buzzard sand particles are harder than the sharp sand particles. The hardness of the two types of particles could not be measured directly, but it was observed that the sharp sand particles crumbled easier than the Leighton Buzzard sand particles.

Adding water to the granular material reduced the acoustic energy generated by the friction pair, shown in Figures 64 and 65. Using a wet granular sample made it very difficult to identify any changes in the acoustic energy due to particle size, which were apparent using dry granular samples. In most cases frictional processes produce a stick-slip phenomenon [48] and the addition of water may provide some lubrication between contacting asperities. Lubrication would reduce the force needed to break the adhesive bond (the stick phase), which in turn reduces in the elastic deformation of the contacting asperities. The reduction in the amplitude of the pressure pulse reduces the amplitude of the strain wave propagating through the probe shaft. Therefore, it is postulated that any lubrication effects caused by the addition of water may account for a reduction in the acoustic energy that occurred.

6.3 The Frictional Properties of the Granular Material

In this section the results obtained from the standard shear box and the ring shear machines are considered. The discussion will primarily focus on the shear properties of the soil as well as the relationships between the shear force and the acoustic parameters.

A number of standard shear box experiments were carried out to determine the shear properties of the granular material. Two granular samples of different size were tested and the effect of water content on the friction angle was investigated. The results obtained agreed with the research carried out Kumar and Prakash [34], who stated there was no definite relationship between the friction angle and the water content. The friction angles obtained from the shear box tests were also compared to the gradients produced from plotting the average oscillation energy against the average contact force (oscillation energy function) using the probing system. The purpose of this investigation was to identify the effect of the water content on the friction angle as well as identifying whether any change in the friction angle for a certain level of water content corresponded to a similar change in the acoustic energy. The results showed there was no correlation between the friction angle and the oscillation energy function for similar levels of water content. However, it must be noted that these results were generated from two different testing procedures, which involved different friction pairs, sliding velocities and boundary conditions. The standard shear box considered a granular-granular friction pair and therefore cannot be accurately compared to the solid-granular friction pair associated with the probing system. Uesugi [56] compared rough and smooth solid surfaces interacting with a granular material, the rough surfaces caused the shear plane to occur within the granular material while the smooth surface caused a shear plane at the solid-granular boundary. A Shear planes within the granular material

causes the material to dilate but for a smooth-solid interacting with a granular material no dilatation occurs. Therefore the properties shear plane generated by the shear box and the probing system are very different and for that reason they are unlikely to produce similar results.

A ring shear machine considers a continuous steel-granular frictional pair, which provided a frictional interaction that was more appropriate to the probing system considered in this project. Dry sand samples produced a larger friction angle than the wet samples (Figure 68) and it was also possible to record the AE generated from the dry friction pair. However, wet samples showed a reduction in the friction angle, which was also accompanied by a significant loss in the AE generated by the frictional interaction. Wet granular materials are generally more cohesive than dry samples, although improving the cohesiveness of a granular material does not necessarily improve its shear strength, which was highlighted by Kumar and Prakash [34]. In fact Yoshida et al [33] stated that the internal coefficient of friction for a granular material reduces with increasing saturation and at very large saturation levels the cohesiveness will also decrease. The pore water pressure produced by the interstitial fluid reduces the interaction between surface asperities of connecting particles. Smaller frictional forces between connecting particles results in a reduction of the granular material shear strength. For a granular-granular shear plane the shear force will also be affected by particle interlocking, which causes dilatation of the granular sample during shearing, but this is not the case for the solid-granular shear plane considered in this study. No granular interlocking occurs between a granular material and a smooth solid surface and as a consequence the pore water may have a greater influence on the interacting surface asperities thus affecting on the shear force.

The residual shear force characteristics for a range of particle sizes were investigated and the results showed that there was only a small difference between the friction angles generated by each particle size. The results obtained agree with Paikowsky [55] who stated that the grain size had little or no effect on the friction coefficient for a smooth solid interacting with a granular material. Subba Rao [58] also stated that similar friction angles were produced for a smooth solid on top of a granular material regardless of the roughness characteristics of the solid interface. Therefore, it is postulated that the change in the shear force generated between the probe-tip and the granular material for different particle sizes would also be small.

The acoustic emission generated by the ring shear experiments was investigated. Due to the slower sliding velocity of ring shear machine, the acoustic signal was not continuous. Therefore it was unlikely to reach the characteristic count rate that was produced by the probing system. The count rate data obtained by the ring shear machine produced a similar shape to the results obtained by the probing system, but identifying a change in the count rate due to particle size was not clear. One issue with the ring shear apparatus is that there was some evidence of grain crushing and this was due to the large applied forces and the small boundary conditions. Unlike the probing system the granular grains in the ring shear machine were tightly constrained within a guide ring for the sliding top plate to rest on. The guide ring applied tighter boundary conditions, which meant the granular grains were not allowed to move as freely as those in the probing system. Consequently the forces applied to individual grain were larger and resulted in some particles becoming crushed. Physical evidence of particle crushing was provided when emptying granular samples from the ring shear machine at the end of

each experiment. Therefore, it is likely that particle fracture would have an effect of the acoustic emission and may account for the larger acoustic bursts that were observed during experimentation. Crushing of the larger particles would produce more asperity contacts, which would also have an effect on the count rate.

The acoustic energy recorded from the ring shear experiments was not analysed in the same way as the probing system due to the fact the count rate did not correlate to the particle size. Evidence of granular crushing meant that the number of contacts formed between the granular material and the top plate of the ring shear machine could not be estimated. Therefore the average estimated contact force could not be determined. However, the effect of the shear force on the acoustic energy was investigated. Diei [72] proposed an equation (Equation 28) that suggested a power law relationship existed between the frictional force and the AE_{RMS} . Considering that both the acoustic energy and the AE_{RMS} are functions of the signal amplitude a similar relationship would also exist for the acoustic energy. The results showed that the acoustic energy increased with increasing shear force and the results obtained from the Leighton Buzzard sand samples also suggests a power law relationship between the shear force and the acoustic energy.

It is suggested that the main difference between the probing system and the ring shear apparatus results from the large difference in the sliding velocity. The acoustic signal generated by the probing system produced a continuous acoustic signature whereas the ring shear produced discontinuous pulses of high amplitude sometimes large enough to reach saturation levels, as well as pulses of small amplitude. Large time separations between the acoustic pulses allow the transients to have a significant effect on the propagating stress waves and may cause further complexities, which may attribute to

the instability of the characteristic count rate. Whereas a faster sliding velocity (in the case of the probing system) produced a continuous acoustic signature, which is generally dominated by the corrugation frequency determined by the contact geometry of the two sliding surfaces.

6.4 Summary

The aim of this project was to develop a novel method for characterising ground structures using the acoustic emission generated during drilling interactions. In a practical soil there are many parameters that can be used to characterise the soil. A typical engineering approach for characterisation soils include the shear strength, bearing capacity, particle size distribution and saturation levels. In this study the effect of the particle size, water content and the shear force were investigated.

The results have shown that the characteristic count rate is directly related to the number of contacts formed per unit time and for graded granular materials it was possible to determine the average particle diameter. The characteristic count rate was independent of the material type, shear force and water content, which meant it was possible to identify the particle size under many conditions. However, parameters that affect the number of contacts between the probe tip and the granular material will have a small influence on the characteristic count rate. Further work would be also required to investigate particle size distributions of more practical soils.

The acoustic energy is sensitive to many parameters associated with the granular material including the density, particle size, particle type and the water content. Due to the many parameters that affect the acoustic energy it is very difficult to isolate an

individual parameter for investigation. For example, a granular material consisting of a single particle size can form an infinite amount of structural assemblies and reproducing the exact same structure for a repeated experiment is extremely difficult. Furthermore, natural soil particles are rarely the same size and have irregular shape characteristics. Consequently, it is difficult to identify any empirical relationships between the acoustic energy and the parameters of the granular material.

The results in this thesis have shown that using the count rate to determine an estimate of the number of contacts between the probe-tip and the granular material, the average oscillation energy for a single particle interaction could be investigated. The results highlighted that the average oscillation energy decreased due to increasing particle size, which was also affected by the material type. However, adding water to the granular sample severely affected the acoustic energy and it was no longer possible to identify any changes due to particle size and material type. Therefore there are some concerns associated with using the acoustic energy to investigate the parameters of real soils, which in many cases are not completely dry.

7.0 Conclusions

The development towards a novel technique for characterising ground structures using the acoustic emission generated during drilling interactions has been presented. A review of existing ground evaluation techniques has been done highlighting some of the important parameters that are obtained from site investigations. Granular materials were graded into different particle size ranges and used to provide a controlled geotechnical medium. The physical behaviour of granular systems was investigated to provide a description of their deformation and strength properties. The frictional mechanisms of solid-solid, solid-granular and granular-granular friction pairs were also discussed. Theoretical relationships associated with the generation of acoustic emission for solid friction pairs have been adapted to consider solid-granular friction pairs considered in this project. Experimental results have provided evidence that the particle size of graded granular samples can be identified regardless of the material type and the level of water content using the characteristic count rate. Further information may be obtained using the acoustic energy parameter, although this parameter is very sensitive to many variables associated with the properties of the friction pair. Therefore, using the acoustic energy to characterise actual parameters of the friction pair still provides a very complex and technical challenge.

7.1 Experimental Conclusions

A simplified drilling arrangement was constructed where a rotating probe was used to eliminate the frictional noise due to material removal and maximise the frictional interactions at the probe-tip-granular interface. A smooth probe tip surface compared to the grain size was used to promote a correct sliding interface between the granular material and the probe tip. The probe shaft was insulated to prevent shaft friction from

affecting the generated ultrasonic signal. All shaft couplings below the transfer box were removed, as the coupling interfaces caused a significant reduction in the signal amplitude, which was attributed to transmission losses. A narrow bandwidth acoustic system was used with the count rate and the acoustic energy being the monitored parameters.

Initial results monitored the count rate and acoustic energy using a standard thresholding technique, adjusted to eliminate the counts generated by the probing system's mechanical noise. Results indicated that both the count rate and the acoustic signal increased with increasing load and sliding velocity. Both the count rate and the acoustic energy produced similar curves. A correlation between the count rate and the acoustic energy highlighted a universal linear relationship, which appeared independent of loading conditions and sliding speeds. The universal relationship was affected by the particle size, although a functional relationship between the gradient of the linear relationship and particle size could not be determined.

Abrasive paper was used in an attempt to provide a controlled friction pair material. The purpose of this investigation was to determine the affects of the surface roughness on the acoustic signals, more specifically the effect of changing the number of asperity contacts. The wear incurred by the abrasive paper resulted in all grades having similar roughness characteristics and the difference in abrasiveness could not be identified. However, the results did identify that the count rate reached a steady state, which is termed the characteristic count rate.

Using a standard thresholding technique the data highlighted that the data consisted of three regions. Region 3 is considered the most important part of the data and the results showed that large applied loads or sliding velocities are required to generate data within this region. In practice large machinery would be required to produce large applied loads or sliding velocity and in many cases may not be suitable for soils with a low bearing capacity. Therefore an unusual thresholding technique was developed to attain the data within region 3 (the characteristic signal) using smaller applied loads. Adjusting the threshold at its minimum level allowed most of the characteristic signal peaks to be detected using smaller dynamical forces. The raw acoustic signal was sampled and the results provided evidence showing that the high frequency noise became superimposed on the friction generated signal with a lower frequency and larger amplitude. The superimposition of the high frequency noise resulted in the high frequency oscillations being undetected by the threshold, indicating that a lower thresholding level could be used.

Reducing the amount of force that is needed to generate the correct set of data means that in a practical situation a smaller probing machine could be developed, which would have huge cost saving benefits.

The characteristic count rate increased with decreasing particle size. A Comparison of two grain types highlighted that the characteristic count rate was insensitive to grain composition. Furthermore, the characteristic count rate was not generally affected by the water content apart from a small variation. Changes in the density did appear to cause a slight change in the characteristic count rate where denser particulates produced a higher count rate.

Monitoring the characteristic count rate using different band pass configurations showed that, lower frequency bandwidths the separation in the count rates that corresponded to different particle sizes. However, lower frequency bandwidths improved signal amplification, which is beneficial for quieter particulates. Characterisation of the particle size was still possible using a variety of band pass configurations as well as different resonant transducers. Monitoring the characteristic count rate to determine the particle size proved to be effective regardless of the acoustic arrangement, although an element of calibration would be required. Using the characteristic count rate has shown the ability to characterise particle size and highlights the potential of monitoring the acoustic emission generated during drilling as a potential profiling tool for ground condition monitoring.

Monitoring the acoustic energy within the region where the count rate reaches a steady state has shown that a linear relationship exists between the applied load and the total acoustic energy. However, there was no clear relationship between the particle size and the acoustic energy for an increase in the total applied force. Investigations focused on the average oscillation energy and the estimated average contact force. Results showed that an increase in the particle size caused a reduction in the average oscillation energy. The oscillation energy was also affected by the particle type, which was indicated by an offset in the acoustic signals generated by each particle type. However, the addition of water caused a significant drop in the signal amplitude and therefore identifying a change in the average oscillation energy due to particle size was no longer possible.

The granular friction angles were investigated using a standard shear box for two different particle types and varying water contents. The oscillation energy functions generated by the probing system for different water contents did not correlate with the friction angles associated with similar saturation conditions. However, comparing the shear box results to the probing system does not provide an accurate comparison for friction pairs considered as the shear box involved an inter-granular shear plane, whereas the probing system involved a solid-granular shear plane.

A ring shear apparatus was used to investigate the shear force characteristics for a granular-solid sliding interface. Wet sand samples produced a smaller friction angle compared to the dry samples of similar particle size, providing evidence that the addition of water reduces the frictional force. Furthermore the wet samples did not produce a strong acoustic signal, which consequently resulted in the AE being influenced by electrical noise. The count rate recorded from the dry sand samples did not correspond to the particle size as it had done with the probing experiments. This was attributed to the slow sliding velocity, granular crushing and adhesion to the rotating steel plate.

7.2 Theoretical Conclusions

The source of the acoustic emission results from the excitation of the surface asperities due to the stick-slip behaviour of associated with sliding friction pairs. Deformation of the surface asperities during an adhesive bond generates a potential energy, which is converted into kinetic energy after the destruction of the adhesive bond. The release of potential energy generates a pressure pulse at the surface of the probe tip resulting in the strain wave that propagates through the probe shaft. Each asperity contact destroyed will

produce an unsteady transient response within the probe shaft, which will also interact with transients produced from other asperity interactions. The sliding friction pair is continuous and therefore produces a continuous source strain waves within the probe shaft. The recorded AE signal results from the interaction of all these responses generated from multiple asperity interactions and consequently produces a continuous acoustic signature.

The results obtained using the characteristic count rate provided evidence that supports the assumption the count rate is proportional to the number of contacts formed per unit time as proposed by Baranov et al [74]. The general power law relationships suggested by Sarychev et al [73], do not apply to the granular-solid interaction considered in this study. Solid-granular friction pairs generated a steady state count rate, which depended on the particle size due to the influence of the particle size on the number of contacts formed between the probe tip and the granular material. The number of particle-probe contacts was estimated using a function of the probe tip nominal area and the average particle size. Results highlighted that the characteristic count rate decreased almost linearly with increasing particle size and provided evidence that the characteristic count rate is proportional to the number of contacts formed per unit time.

The acoustic energy is a function of the amplitude of the acoustic signal generated by the friction pair. The relationship between the acoustic energy and the physical interaction of the friction pair was based on the assumption that the amplitude of the acoustic signal is proportional to the potential energy generated due to the elastic deformation of a contacting asperity. The relationship states that a power law exists between the acoustic energy and the applied load, although this relationship only

considered a single asperity contact. Diei [72] also stated that a power law existed between the AE_{RMS} and the parameters of the friction pair, although in this case the index value was also a function of the material properties of the friction pair. However, the results obtained showed that a linear relationship is sufficient to describe the relationship between the acoustic energy and the applied load for a steady state count rate.

The acoustic energy is very sensitive to a number of parameters such as, the number of asperity contacts, the contact force, the particle type, the radius of curvature and the level of water content. However, changing a single parameter such as the particle size would also affect the number of contacts, the average asperity contact force for a given applied load, the shear force and the radius of curvature. Due to the many variables that affected the total acoustic energy it was very difficult to identify accurate empirical relationships between the parameters of the friction pair and the acoustic energy. Therefore a single grain contact was considered to reduce the amount variables involved. An increase in the particle size caused a decrease in the average oscillation energy at a given contact force. However, a functional relationship between the average oscillation energy and the particle size could not be determined. Furthermore, the addition of water severely affected the acoustic energy as it reduced the frictional force between the granular material and the probe tip. For that reason, it is postulated that the shear force between the individual grains and the probe tip will have an effect on the acoustic energy.

Work relating to this thesis has been published in the NDT 2001 conference proceedings [98] as well as Ultrasonics [99] (appendix 2).

8.0 Further Work

The work in this thesis shows that acoustic monitoring of a drilling process has potential to be an alternative method for ground condition monitoring. However, further research will be required to fully establish the parameters associated with real soils and their effect on the generated acoustic emission.

Further work associated with wet particulates involving the effects of pore water pressure on the asperity interactions would be required to investigate why there is a large reduction in the amplitude of the signal generated by the friction pair.

The shear stress of soils is an important parameter for Civil engineers and a method of determining the actual shear force properties of the soil would be very useful. A full investigation of the shear properties of a soil involving a range of confining pressures, saturation levels and their effect on the AE signal needs to be determined.

The affects of the granular elastic properties on the generated AE should be investigated. Using spherical grains of known elastic properties, may allow an empirically based model to be developed that could describe the frictional interaction in more detail.

In practical environments real soils are not in layers of similar grain size and will generally have a distribution of particle sizes. Therefore an investigation of the effects of different distribution of grain sizes on the AE signal could be considered.

In practice a drilling system would be more appropriate than a probing system as real soils may involve large forces to push the probe to the required depth of soil under investigation. The development of a drilling arrangement will reduce the forces need to reach certain depths making the machinery smaller. Therefore, an investigation using a drilling process would identify any implications this may have on the recorded acoustic signal.

Following a complete and thorough parameter investigation, a prototype drilling system could be designed and used in conjunction with data from a real site investigation. This would provide genuine results associated with actual soil structures that can be compared to the information provided by the acoustic signal generated by the drilling system and therefore determine if acoustic monitoring of drilling can be used as a tool for ground condition monitoring.

References

- [1] P. Sharpe, Formation assessment for maintenance and renewals planning; 'Total Route Evaluation', Proceedings of the 2nd International Conference on Railway Engineering, London, 1999, Engineering Technical Press, 39-44.
- [2] L. Rogers, J. Maguire, Structural and engineering monitoring by acoustic emission methods-fundamentals and applications, NDT 2001 Conference Proceedings, Coventry, British Institute of Non-Destructive Testing, 49-54.
- [3] R. Hill, Confidential consultancy report, Railtrack/Scientifics, 1997.
- [4] Clayton, Mathews, Simons, Site Investigation, The University Press, Cambridge, ISBN 0-632-02908-0, 1995, 16-40.
- [5] F. Harris, Ground Engineering: Equipment and Methods, ISBN 0246112395, Granada 1983, 31-33.
- [6] A.C.Meigh, Cone Penetration Testing: Methods and Interpretation, ISBN 0408024461, Butterworths 1987, 3-39.
- [7] R. Salgado, J. Mitchell, M. Jamiolkowski, Cavity expansion and penetration resistance in Sand, Journal of Geotechnical and Geoenvironmental Engineering, April 1997, 344-354.
- [8] D. Naylor, G. Simpson, R Tab, Finite elements in geotechnical engineering, Pinerage Press, Swansea, 1981.
- [9] G. Grandjean, J. C. Gourry, A. Bitri, Evaluation of GPR techniques for civil-engineering applications: study on a test site, Journal of Applied Geophysics, 45, 2000, 141-156.
- [10] M. Fritzsche, Detection of buried landmines using ground penetrating radar, Proceedings of the SPIE 2496, 100-109.

References

- [11] K. Singh, R. Chouhan, Exploration of underground strata conditions for a traffic bypass tunnel using ground penetrating radar system – a case study, *Geotechnical and Geological Engineering*, 20, 2002, 81-87.
- [12] A. Stokes, T. Fourcaud, J. Hruska, J. Cermak, N. Nadyezhdina, V. Nadyezhdin, L. Praus, An evaluation of different methods to investigate root systems architecture of urban trees: in situ; ground penetrating radar, *Journal of Arboriculture*, 28, 1, 2002, 1-9.
- [13] British Standard 5930 (1981) Code of Practice for Site investigations, British Standards Institution, London.
- [14] R. F. Craig, *Soil Mechanics*, Chapman and Hall 1997, ISBN 0419224505, 1-35.
- [15] H. M. Jaeger, S. R. Robert, P. Berhringer, The physics of granular materials, *Physics Today*, April, 1996, 32-38.
- [16] A. Kwan, C. Mora, Effects of various shape parameters on the packing of aggregate particles. *Magazine of Concrete Research*, 2001, 53, no 2, 91-100.
- [17] L. Vanel, E. Clement, Pressure screening and fluctuations at the bottom of a granular column, *The European Physical Journal B*, 11, 1999, 525-533.
- [18] M. J. Smith, *Concise Soil Mechanics*, Macdonald & Evans 1997, ISBN 0712103619, 83-102.
- [19] G. R. Mc Dowell, M. D. Bolton, On the micromechanics of crushable aggregates, *Geotechnique* 48, no 5, 1998, 667-679.
- [20] E. Aharonov, D. Sparks, Rigidity phase transition in granular packing, *Physical Review E*, V60, no 6, Dec 1999, 6890-6896.
- [21] P. Newland, B. Alley, Volume changes in drained triaxial deformation of saturated cohesive soils, *Geotechnique*, 2, no 1, 17-34.

References

- [22] S. G. Bardenhagen, J. U. Brackbill, D. L. Sulsky, Shear deformation in granular materials, *Detonation symposium Snowmass 1998*, 547-555.
- [23] P. V. Lade, Instability shear banding and failure in granular materials, *International Journal of Solids and Structures*, 39, 2002, 3337-3357.
- [24] W. P. Schellart, Shear test results for cohesion and friction coefficients for different granular materials: scaling implications for their usage in analogue modelling. *Tectonophysics*, 324, 2000, 1-16.
- [25] J. Atkinson, Non-linear soil stiffness in routine design, *Geotechnique*, 50, 5, 2000, 487-508.
- [26] H. Wolf, D. Konig, T. Triantafyllidis, Experimental investigation of shear band patterns in granular material, *Journal of Structural Geology*, 25, 2003, 1229-1240.
- [27] R. A. Jewell, Direct shear tests on sand, *Geotechnique*, 39, no2, 1989, 309-322.
- [28] R.A. Jewel, C. P. Wroth, Direct shear tests on reinforced sand, *Geotechnique*, 37, no1, 1987, 53-68.
- [29] O. Pouliquen, F. Chevoir, Dense flow of dry granular material, *C R Physique*, 3, 2002, 163-175.
- [30] A. R. Tholen, Particle-particle interaction in granular material, *Fundamentals of Friction: Macroscopic and Microscopic processes*, Kluwer Academic Publishers 1992, 95-110.
- [31] T. Mathey, J. P. Hansen, Molecular dynamics simulations of sliding friction in a dense granular material, *Modelling Simulation Materials, Science Engineering*, 6, 1998, 701-707.
- [32] L. Bocquet, W. Losert, D. Schalk, T. C Lubensky, J. P. Gollub, Granular shear flow dynamics and forces: experimental and continuum theory, *Physical Review E*, 65, 011307, 1-19.

References

- [33] Y. Yoshida, J. Kuwano, R. Kuwano, Effects of saturation on shear strength of soils, *Soils and Foundations*, 31, no 1, 1991, 181-186.
- [34] K. Kumar, R. Prakash, Pore fluid effect on shear strength on Pilani soil, 82, Dec 2001, *IE(I) Journal-CV*, 157-162.
- [35] G. Debregeas, C. Josserand, A self similar model for shear flow in dense granular materials, *Europhysics Letters*, 52, no 2, 2000, 137-143.
- [36] C. S. Chang, Y. Chang, M. G. Kabir, Micromechanics modelling for stress strain behaviour of granular soils 1: Theory, *Journal of Geotechnical Engineering*, 118, no 12, Dec 1992, 1959-1974.
- [37] T. Schanz, P. A. Vermeer, Angles of friction and dilatancy of sand, *Geotechnique*, 47, no4, 887-892.
- [38] O. Pouliquen, N. Renaut, Onset of granular flow on an inclined rough surface – dilatancy effects, *Journal of Physics*, 2, no 6, 1996, 923-935.
- [39] E. Liss, B. Glasser, The influence of clusters on stress in a sheared granular material, *Powder Technology*, 116, 2001, 116-132.
- [40] O. Petschmann, U. Schwarz, F. Spahn, Length scales of clustering in granular gases, *Physics Review, Letter* 82, 1999, 4819-4822.
- [41] J. P. Bardet, Prediction of deformation of Hoston and Reid Bedford sands with a simple bonding surface plasticity model, *Constitutive equations for granular non-cohesive soils*, Saada and Bianchini (eds) Balkema, Rotterdam, 1998, ISBN 9061917891, 131-147.
- [42] A. Goh, Non linear modelling in geotechnical engineering using neural networks, *Australian Civil Engineering Transactions*, CE36, no4, 1994, 293-297.

References

- [43] D. E. Sidarla, J. Ghaboussi, Constitutive modelling of geomaterials from non-uniform material tests, *Computers and Geotechniques*, 22, no1, 1998, 53-71.
- [44] C. Josserand, A. Tkachenko, D. Mueth, H. M. Jaeger, Memory effects in granular materials, *Physical Review letters*, 85, no17, 2000, 3632-3635.
- [45] J.H.Snoeijer, M.V.Hecke, E.Somfai, W.V.Saarloos, Packing geometry and statistics of force networks in granular media, *Physical Review E*, 70, 2004, 011301, 1-15.
- [46] M. J. Adams, *Friction of Granular Non Metals, Fundamentals of Friction: macroscopic and microscopic processes*, 1992, 183-207.
- [47] P.Brinley, *Friction and Wear: a tribology for students*, Butterworth 1973, ISBN 040800097.
- [48] F. P. Tabor, *Friction: An Introduction to Tribology*, Biddles 1974, ISBN 0435550748, 47-76.
- [49] I. L. Singer, Friction and energy dissipation at the atomic scale: a review, *J.Vac.sci.Technol.A*, 12, no5, 1994, 2605-2616.
- [50] B.N.J Persson, *Sliding Friction, NanoScience and Technology*, Springer Heidelberg 1998, ISBN 3540632964, 37-43.
- [51] L. D. Landau and E. M. Lifshitz, *Theory of Elasticity 3rd ed*, Course of Theoretical Physics volume 7, Pergamon Press 1986, ISBN 0080339174, 26-32.
- [52] B. Pugh, *Friction and wear*, Newnes-Butterworths, 1973, ISBN 0408-00097X, 69-98.
- [53] M. J. Adams, B. J. Brinscoe, L. Pope, A contact mechanics approach to the prediction of the wall friction of powders, *Tribology in Particulate Technology*, Adam Hilger, Bristol, 8-22.

References

- [54] J. F. Archard, Elastic deformation and the laws of friction, *Proc. R. Soc. A*, 240, 190, 1957, .
- [55] S. G. Paikowsky, C. M. Player, P. J. Conners, A dual interface apparatus for testing unrestricted friction of soil along solid surfaces, *Geotechnical Testing Journal*, 18, no 2, June 1995, 168-193.
- [56] M. Uesugi, H. Kishida, Y. Tsubakihara, Behaviour of sand particles in sand-steel friction, *Soils and Foundations*, 28, no1, March 1988, 107-118.
- [57] M. A. Aguirre, I. Ippolito, A. Calvo, C. Henrique, D. Bideau, Effects of geometry on the characteristics of the motion of a particle rolling down a rough surface, *Powder Technology*, 92, 1997, 75-80.
- [58] K. S. Subba Rao, M. M. Allam, R. G. Robinson, Interfacial friction between sands and solid surfaces, *Geotechnical Engineering*, 131, April 1998, 75-82.
- [59] N. Sato, Acoustic emission technology for the development of composite materials in automobile industry, 3rd International Symposium on AE Composite Materials, Paris, 42, 1989, 42-51.
- [60] D. Mba, Applicability of acoustic emissions to monitoring the mechanical integrity of bolted structures in low speed machinery: case study, *NDT&E International*, 35, 2002, 293-300.
- [61] D. Mba, R. Bannister, G. Findlay, Condition monitoring of low speed rotating machinery using stress waves: Part 1, *Proceeds of the Institution of Mechanical Engineers*, 1999, 153-170.
- [62] C. Mechefiske, J. Mathew, Fault detection and diagnostics in low speed machinery: Part 2 The use of parametric spectra, *Mechanical System Signal Processing*, 1992, 6, no 4, 297-307.

References

- [63] J. Miettinen, V. Siekkinen, Acoustic emission in monitoring sliding contact behaviour: case study, *Wear*, 183-181, 1995, 897-900.
- [64] L. Rogers, The application of vibration signature analysis and acoustic emission source location to on-line condition monitoring and anti-friction bearings, *Tribology International*, 12, no2, 1979,51-59.
- [65] E. Kannatey-Asibu, D. A. Dornfield, A study of tool wear using statistical analysis of metal cutting acoustic emission, *Wear*, 76, 1982, 247-261.
- [66] T. J. Holroyd, N. Randall, Use of acoustic emission for machine condition monitoring, *Condition Monitoring*, 35, no2, Feb 1993, 75-79.
- [67] W. P. Dong, Y. H. Joe, A. Mardapittas, Characteristics of acoustic emission in drilling, *Tribology International*, 27, no3, 1994, 169-171.
- [68] A. Akay, Acoustics of friction, *Journal of the Acoustical Society of America*, 4, April 2002, 1525-1548.
- [69] N. Hinrichs, M. Oestreich, K. Popp, On the modelling of friction Oscillators, *Journal of Sound and Vibration*, 216, no3, 1998, 435-459.
- [70] B.J.Briscoe, A.Chateauminois, J.Chiu, S.Vickery, Acoustic noise emission in a model PMMA steel fretting contact, *Tribology Series*, 39, D.Dowson Ed, Elsevier, 2001, 673-681.
- [71] C. L. Jiaa, D. A Dornfield, Experimental studies of sliding friction and wear via acoustic emission signal analysis, *Wear*, 139, 1990, 403-424.
- [72] E. N. Diei, Acoustic emission sensing of tool wear in face milling, *Journal of Engineering for Industry*, 109, 1987, 234-240.
- [73] G. A. Sarychev, V. M. Shcavelin, Acoustic emission method for research and control of friction pairs, *Tribology International*, 24, no1, 1991, 11-16.

References

- [74] V. M. Baranov, E. M. Kudryavtsev, G. A. Sarychev, Calculation of the parameters of acoustic emission when there is external friction between solids, *Russian journal of Non-Destructive Testing*, 31, no8, 1995, 569-577.
- [75] H.F Pollard, *Sound waves in solids*, Pion ltd 1977, ISBN 0850860539, 78-142.
- [76] K. Graff, *Wave motion in elastic solids*, Dover Publications, 1991, ISBN 0486667456, 75-212.
- [77] M. Redwood, *Mechanical waveguides*, Pergamon press, 1960, 135-160.
- [78] Cheeke, *Fundamentals and applications of ultrasonic waves*, CNR Press, 2000, ISBN 0849301300, 115-140.
- [79] L. Pochhammer, *Math*, 81, 324-336, (German).
- [80] C. Chree, The equations of an isotropic solid in polar and cylindrical co-ords, their solutions and applications, *Trans. Cambridge Phil. Soc*, 14, 250-369.
- [81] V. Pagneux, A. Maurel, Lamb wave propagation in inhomogeneous elastic waveguides, *Proc. R. Soc. Lond. A*, 458, 2002, 1-18.
- [82] T. Miyamoto, K. Yasuura, Numerical Analysis of an elastic waveguide with rectangular cross section by the modal method of expansion, *Electronics and Communications in Japan*, J59-B, no2, 1976, 80-87.
- [83] T. Miyamoto, K. Yasuura, Numerical analysis on isotropin elastic waveguides by mode-matching method: particle velocities and dispersion characteristics in rods of rectangular cross section, *IEEE Transactions on Sonics and Ultrasonics*, SU-24, no6, 1977, 369-375.
- [84] R. W. Morse, Dispersion of Compressional waves in isotropic rods of rectangular cross section, *Journal of the Acoustical Society of America*, 20, no 6, 1948, 833-838.

References

- [85] M. Touratier, G. Maugin, Elastic waves in heterogeneous waveguides of rectangular cross section, *Journal of the Acoustical Society of America*, 78, no5, 1985, 1806-1825.
- [86] J. Wade, An approximate theory for elastic wave propagation in multi-bar media, PhD Dissertation, Institution of Technology, Wright Patterson Airforce Base Ohio, 1970.
- [87] J. Zemanek, An experimental and theoretical investigation of elastic wave propagation in a cylinder, *Journal of the Acoustical Society of America*, 1972, 51, 265-283.
- [88] R. Talbot, J. Prezemieniecki, Finite element analysis of frequency spectra for elastic waveguides, *Journal of Solid Structures*, 11, 1975, 115-138.
- [89] T. Hayashi, J. Rose, Guided wave simulation and visualisation by a semianalytical finite element method, *Materials Evaluation*, Jan 2003, 75-79.
- [90] R. Hill, S. Forsyth, The use of finite element modelling for understanding acoustic emission phenomena, *Progress in acoustic emission: The Japanese Society for NDI*, 2000, 111-116.
- [91] I. Grabec, E. Govekar, E. Susic, B. Antolovic, Monitoring manufacturing processes by utilising empirical modelling, *Ultrasonics*, 36, 1998, 263-271.
- [92] I. Grabec, T. Kosel, P. Muzic, Location of continuous AE sources by sensory neural networks, *Ultrasonics*, 36, 1998, 525-530.
- [93] S. Bukkapatnam, S. Kumara, A. Lakhtakia, Analysis of acoustic emission signals in machining, *ASME Journal of manufacturing science and engineering*, Nov 1999, 121, 568-576.
- [94] C. B. Scruby, Instrument science technology: An introduction to acoustic emission, *Journal of Physics E. Science Instrumentation*, 20, 1987, 946-953.

References

- [95] J. G. Kavanagh, The use of acoustic emission to monitor the deformation of a soil body, PhD Thesis, The Nottingham Trent University 1997.
- [96] A. Taylor, Probe Design, Final year thesis, The Nottingham Trent University, 2002.
- [97] K. H. Head, Manual of soil laboratory testing, Vol 2, permeability, shear strength and compressibility test, 2nd edition, Pentech Press 1994, 189-218.
- [98] R.Hill, E. Lai, T.Tyler, Characterisation of geotechnical materials using friction generated ultrasound, NDT 2001 Conference proceedings, The British Institute of Non-Destructive Testing, 2001, ISBN 090313229X, 11-17.
- [99] T.Tyler, R.Hill, E.lai, Friction generated ultrasound from geotechnical materials, Ultrasonics, 42, 2004, 169-172.

APPENDIX 1.

CLASSIFICATION OF PARTICLE SIZE

APPENDIX 1

Classification of soils by particle size (based on BS1377:1995)

Particle Size	Designation		Test Procedure	
>200mm	BOULDERS		MEASUREMENT OF SEPARATE PIECES	
60mm - 200mm	COBBLES			
20mm - 60mm	COARSE	GRAVEL	SIEVE ANALYSIS	
6mm - 20mm	MEDIUM			
2mm - 6mm	FINE			
0.6mm - 2mm	COARSE	SAND		SEDIMENTATION ANALYSIS
0.2mm - 0.6mm	MEDIUM			
0.06mm - 0.2mm	FINE			
0.02mm - 0.06mm	COARSE	SILT		
0.006 - 0.002mm	MEDIUM			
<0.002mm	FINE			

APPENDIX 2.

PUBLICATIONS

Friction generated ultrasound from geotechnical materials

T.J. Tyler, R. Hill *, E. Lai

Department of Chemistry and Physics, School of Science, Nottingham Trent University, Clifton Campus, Nottingham NG11 8NS, UK

Abstract

Drilling is a process involved with product manufacturing and for civil engineers, site preparation. The usual requirement is for efficient material removal. In this study, the friction pair interaction generated by a drilling process provides ultrasound information related to parameters for the geotechnical material being drilled, where the drill bit has non-degrading ultrasonic characteristics and no essential requirement for material removal. This study has considered monitoring the ultrasonic signal generated by a drilling process, with a view to characterising the parameters of the geotechnical material being drilled and provides a novel method to identify or characterise ground structures.

Drilling of geotechnical material systems, typically involve the interaction of a rotating probe and a granular composite medium. The applied load and angular velocity are measured to determine their relevance to the ultrasonic signal. Samples of granular materials have been graded into controlled grain size ranges. Attention has been focused on determining the effects on the ultrasound signal of grain size, bulk density and the water content of the granular material. A comparison between the various granular samples of the different grain sizes, density, water content and the associated ultrasonic signal has been done. The effect of each variable, and existing theory for these effects is commented upon.

The broad aim of this research is to evaluate ultrasonic monitoring of drilling and assess its potential for real-time geotechnical ground condition monitoring applications and offer it as an alternative to existing methods.

© 2004 Published by Elsevier B.V.

Keywords: Ultrasound; Friction; Granular materials; Condition monitoring

1. Introduction

The ultrasound generated from a solid–solid friction pair has been the main focus of research concerning friction-generated ultrasound, mainly associated with rotating and reciprocating machines. A frictional process developed during relative movement between contacting materials has an inherent level of wear that eventually would result in failure. Monitoring the ultrasonic signal generated from machinery has become an alternative condition-monitoring tool, as the generated signal contains information related to the micro-condition of the friction pair. It is possible to detect when components of a machine are becoming worn and a thus reduce the risk of catastrophic failure leading to production down time. Holroyd and Randall [1] discussed the sensitivity of using acoustic emission (AE) for detecting changes in lubrication, overloading, wear and review a number of different techniques used to analyse

the acoustic signature. Further methodologies for analysing the friction generated acoustic signatures were discussed by Bukkapatnam et al. [2] and provide a novel analysis technique based on chaos theory, wavelets and neural networks. Much of the research concerning condition monitoring focuses on the changes in the signal due to wear, but some research have also focused on the parameters associated with the generated acoustic signal. Work by Diei [3] monitored the acoustic emission generated by tool wear during face milling and proposed a power function relationship between the AE_{RMS} voltage and the rate of frictional energy dissipation given by

$$AE_{RMS} = (k\eta\tau_s A_a V)^{m/2} \quad (1)$$

where k and m are constants that depend on the AE measuring system and the material properties of the friction pair, η is a function of surface roughness and elastic properties of the friction pair, τ_s is the shear strength of the interfacial material, A_a is the visible area of contact and V is the sliding velocity. The parameters η and A_a essentially define the real area of contact and

* Corresponding author. Fax: +44-115-948-6636.
E-mail address: roger.hill@ntu.ac.uk (R. Hill).

therefore, the AE_{RMS} is a function of the real area of contact, the shear strength and the sliding velocity. Results obtained by Diei's work also indicated a linear relationship between the AE_{RMS} and the sliding velocity. Jiaa and Dornfield [4] monitored the AE generated by a pin on disk experiment, highlighting that the AE is caused by impulsive shock due to asperity collisions and micro-vibrations excited by stick-slip phenomena. The research shows that the AE_{RMS} increases with load while a linear relationship exists between the relative surface velocity and the AE_{RMS} . Sarychev and Shchavelin [5] describe the frictional process and the generated acoustic emission associated with it. Two general rules were established relating the rate of counting the acoustic pulses (count rate) to the sliding speed of the friction pair and the applied load.

The general rule for the dependence of the count rate \dot{N} on the sliding velocity is in the form:

$$\dot{N} = A + Bv^X \quad (2)$$

where A and B are constants and $X \geq 1$.

A similar relationship also applies for the dependence of the load on the count rate, but the exponent $X \leq 1$. A further relationship was expressed relating the AE activity to the regime of friction in elastic contact:

$$\dot{N}_a = k \frac{N^{0.71} \theta^{0.71} A_c^{0.71}}{r^{0.90} R_a^{1.60}} V \quad (3)$$

where N is the normal load, θ the generalised elastic modulus, A_c the counter area of contact, r the surface asperity tip radius, R_a is the surface roughness and k is a coefficient of proportionality. Further work by Baranov [6] produced two models relating the frictional parameters of the friction pair to the acoustic parameters; count rate and acoustic energy. The model for the count rate is based on the assumption that the rate of counting acoustic pulses is directly proportional to the number of contact points formed per unit time. Work by Henrique et al. [7] studied particle collisions down an inclined slope and the number of acoustic events were used to monitor the number of collisions (contacts) generated when a ball was rolled down the slope. The model for the acoustic energy relates the mechanical potential energy generated during the elastic deformation of a contacting asperity to the amplitude distribution of the acoustic signal. The energy model does not take into consideration the effects of wear and is based on the AE generated due to elastic contact.

Current studies in friction-generated acoustics have shown that the acoustic signals contain information relating to the material parameters of the friction pair. The work in this study uses the acoustic signal as a tool to characterise the material properties of the friction pair. The idea for this study originates from a study by Hill [8] for Scientifics, when it became apparent that monitoring the ultrasound generated by a drilling pro-

cess had potential for ground condition monitoring. The overall aim of this work is to develop a method of characterising geotechnical materials using a typical drilling process and monitoring the ultrasound generated due to the interaction between the drill tip and the geotechnical material.

2. Experimental design

A simplified drilling arrangement has been constructed where a rotating probe is used to maximise the friction at the probe-tip-granular contact. The probe string is designed, using a suitable coupling device, so that the ultrasonic signal is transmitted from the probe tip to a stationary piezoelectric sensor. The signal is amplified by 60 dB and filtered between 250 and 500 kHz. The captured signal is therefore in the mid-ultrasonic range and relates to the transducer monitoring frequency used. A schematic diagram of the experimental arrangement can be seen in Fig. 1.

The probe rotates, while being submerged in a granular medium of controlled particle size, initial density and water content. The feed rate and angular velocity were set to a constant value and the applied load, count rate and ultrasonic energy were simultaneously monitored. The effects of the particle size, density and water content on two ultrasonic parameters (count rate and energy) have been investigated and the system aims to be a future option for ground condition monitoring.

3. Results

The effect of load on the count rate can be seen in Fig. 2a. The signal values on the left of the figure correspond to the probe tip not being in contact with the granular medium. When the probe is pushed into the granular

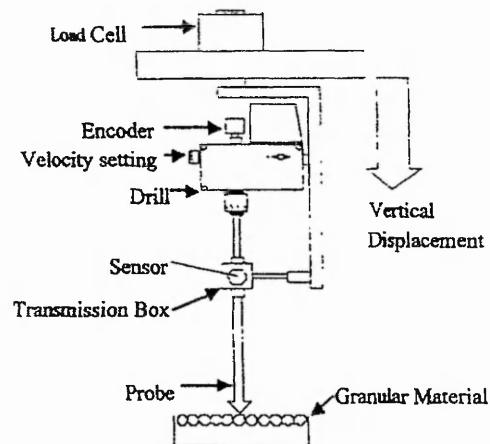


Fig. 1. Schematic diagram of the probing apparatus.

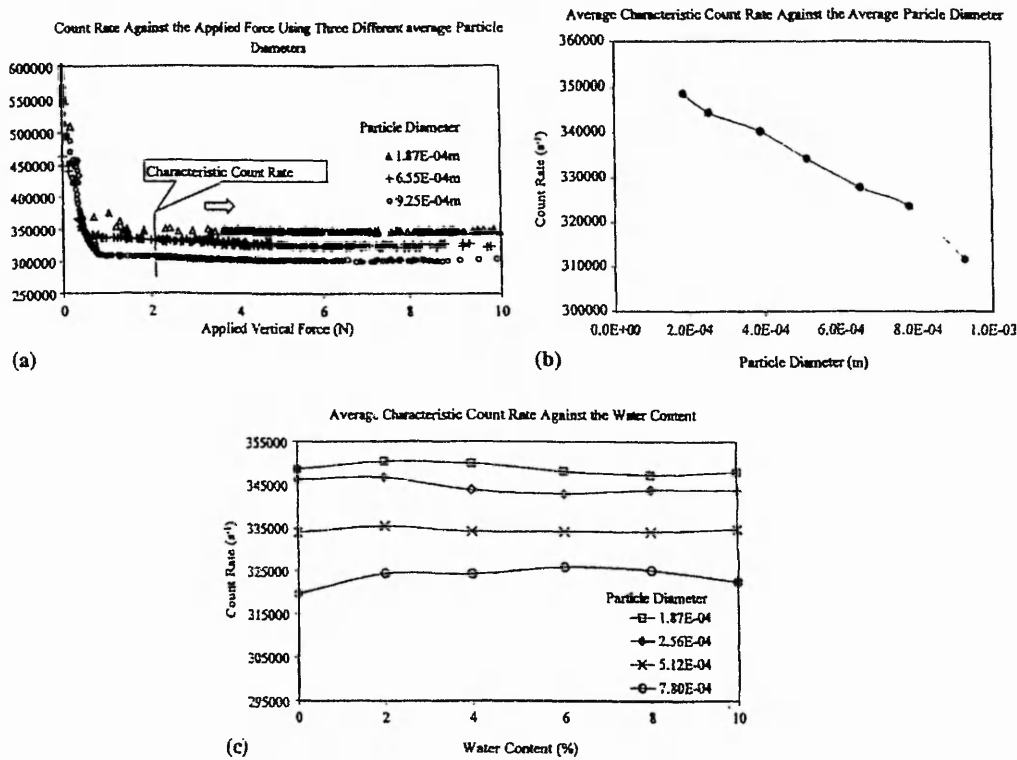


Fig. 2. (a) Count rate against the vertical applied force using three different particle sizes. Data is shown for a complete penetration to a depth of 50 mm. (b) The average characteristic count rate against the average particle diameter. (c) The average characteristic count rate against the water content of the granular sample.

material the load increases. The data highlights a stabilisation (reduction) in the count rate and is referred to as the “characteristic count rate” for a particular friction pair. The stabilisation of the count rate means that no more oscillations are being produced due to an increase in the load and therefore the signal amplitude is only subject to amplitude increase. Different grades of particulate material have been used and the characteristic count rate monitored. The results indicate that a lower characteristic count rate occurs as the average particle size is increased. Eight samples of sand were used and the characteristic count rate is compared with the particle size in Fig. 2b. Larger particle sizes produce fewer contacts and therefore the results agree with the assumption stated by Baranov et al. [6] that, the rate of counting is proportional to the number of contacts formed per unit time. The results in Fig. 2c reveal that the water content has little effect on the characteristic count rate. Four ranges of grain size have been used and the count rate is plotted against the mass percentage water content. There is a small variation in the count rate but the separation in the signals generated by the different particle sizes still exist. Results have revealed that the count rate value does not significantly change due to the addition of water and that the count rate

signal is mainly dependent on the number of contacts formed. Therefore, regardless of the water content of the sand it is possible to obtain an approximate evaluation of the average particle size.

The ultrasonic signal energy appears to be sensitive to a number of parameters including the particle size, water content, density and mineralogy. Fig. 3a shows the ultrasonic energy signal plotted against the applied force for two different initial dry densities (compacted and loose). Results indicate that the energy varies linearly with the applied load and the gradient increases with a reduction in the initial density. The effect of varying the density is more apparent when using smaller grain sizes. A change in the density using smaller particulate material will produce a larger affect on the number of probe-granular contacts generated within the apparent contact area. Lower particulate densities produce fewer contacts and therefore the pressure due to the applied force is increased and may account for an increase in the average energy per oscillation as a function of the applied force. It is expected that an increase in the particulate size would also produce an increase in the acoustic energy as a result of higher contact pressures. Fig. 3b shows the change in the average energy per oscillation due to the applied force against the average particle

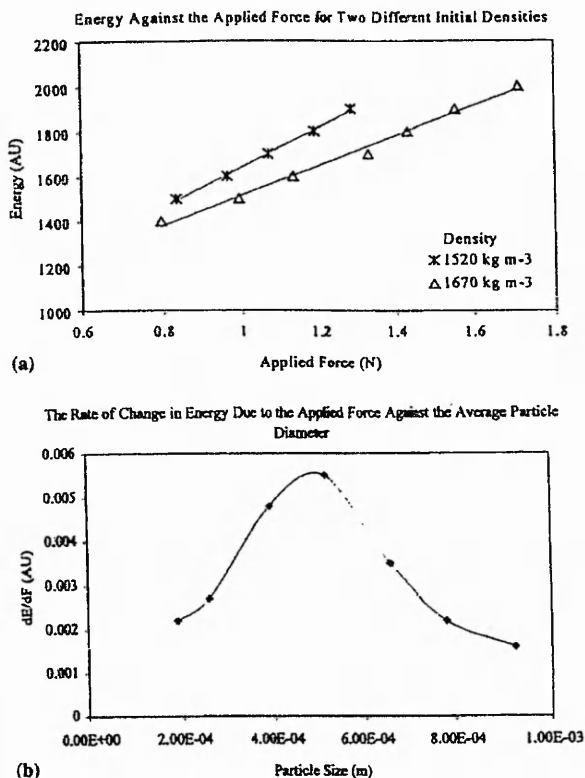


Fig. 3. (a) The energy against the applied vertical force using two initial densities (loose and compacted). A dry sand sample with an average particle diameter of 187 μm has been used. (b) The rate of change in energy due to the applied force against the average particle diameter. Using dry samples of sand with controlled grain size.

diameter. Results indicate that there is no unique relationship between this ultrasonic energy parameter and the particle size, with a peak occurring at 512 μm .

The effect of increasing the water content of the granular sample causes the sand to become acoustically quieter (a significant drop in signal amplitude). Although the sand becomes quieter, the rate of change of the ultrasonic energy due to the applied force is not affected by varying the level of water content in a wet sample but there is a noticeable difference in the gradient when comparing a dry sample with a wet sample.

4. Conclusions

Results have shown that when probing into granular materials, using a constant sliding velocity the count rate becomes stable (characteristic count rate). The characteristic count rate is affected by a change in the

number probe–granular contacts and therefore provides a method for characterising the particle size. The water content of a granular sample has little effect on the characteristic count rate and data agrees with the assumption stated by Baranov et al. [6] that the count rate is proportional to the number of contacts formed per unit time. However, the data does not agree with the general rule suggested by Sarychev and Shchavelin [5], as the characteristic count rate does not depend on the applied force. Results provide positive evidence that monitoring the characteristic count rate has potential as a tool for identifying the layers of different particle size in ground structures regardless of the moisture content.

The ultrasonic energy signal is sensitive to a variety of parameters including the load, sliding velocity, particle size, density, water content and mineralogy. Results have indicated that the contact pressure, which is affected by altering the density and particle size, affects the acoustic energy signal. However, a continuous increase in the ultrasonic energy due to larger particle sizes, which was expected, did not occur. It is possible that larger particles produce larger particle-probe contact areas thus reducing the contact pressure at a single contact spot but further work is needed for this to be established. It is clear that the ultrasonic energy contains information relating to the parameters of the friction pair but further investigation is required to fully understand the contribution of each parameter associated with the generated acoustic signal.

References

- [1] T.J. Holroyd, N. Randall, Use of acoustic emission for machine condition monitoring, *Condition Monitoring* 35 (2) (1993) 75–79.
- [2] S.T.S. Bukkapatnam, S.R.T. Kumara, A. Lakhtakia, Analysis of acoustic emission signals in machining, *ASME Journal of Manufacturing Science and Engineering* (1999) 183–207.
- [3] E.N. Diei, Acoustic emission sensing of tool wear in face milling, *Journal of Engineering for Industry* 109 (1987) 234–240.
- [4] C.L. Jiaa, D.A. Dornfield, Experimental studies of sliding friction and wear via acoustic emission signal analysis, *Wear* 139 (1990) 403–424.
- [5] G.A. Sarychev, V.M. Shchavelin, Acoustic emission method for research and control of friction pairs, *Tribology International* 24 (1) (1991) 11–16.
- [6] V.M. Baranov, E.M. Kudryavtsev, G.A. Sarychev, Calculation of the parameters of acoustic emission when there is external friction between solids, *Russian Journal of Non-Destructive Testing* 8 (1995) 569–577.
- [7] C. Henrique, M.A. Aguirre, A. Calvo, I. Ippolito, D. Bideau, Experimental acoustic technique in granular flows, *Powder Technology* 94 (1997) 85–89.
- [8] R. Hill, Confidential consultancy Report, Scientifics, 1997.

NDT 2001

**The Royal Court Hotel, Keresley, Coventry
18-20 September 2001**

Conference Proceedings

ISBN No: 0 903132 29 X

Characterisation Of Geotechnical Materials Using Friction Generated Ultrasound

R. Hill, E. Lai, T. Tyler
Faculties of Science / Engineering, Nottingham Trent University
Nottingham NG11 8NS

ABSTRACT

Frictional Processes involve the interaction of two solid surfaces (the "friction pair") and this interaction is usually considered undesirable. Due to this, much research has been dedicated to the reduction of friction, rather than using it as a tool to provide information about the processes involved within the friction contact zone. However, in the case of drilling, the friction pair interaction may provide information to determine the material being drilled where the drill bit has non-degrading acoustic characteristics. Here monitoring of the acoustic/ultrasonic signal is considered, with a view to characterising the "drillee". This paper will consider some of the factors important in this two-system interaction.

Drilling of geo-technical systems, typically, involves the interaction of a rotating probe and a granular composite medium. Various parameters, such as load and angular velocity are measured to provide information concerning their relevance to the acoustic signal. The granular material has been graded into different ranges of grain size and attention is currently focused on using the ultrasonic signal to help determine grain size information. A comparison between various granular samples and the corresponding acoustic signal has been done.

The broader aim of this research is to evaluate acoustic/ultrasonic monitoring of drilling and assess its potential for geo-technical ground condition monitoring applications and offer it as a future alternative to existing methods.

INTRODUCTION

In Civil Engineering, knowledge of the ground structure and condition is essential for many engineering applications. It is common for ground or embankment structures to suffer from long-term relaxation, but in the case of a rail track bed, the structures are subjected to periodic dynamical loading that can result in an increase in degradation. The generation of degradation highlights the need for ground condition assessment. Present techniques to characterise the ground structures use invasive or non-invasive methods [1] Invasive methods involve taking a test core and examining the physical structure. Non-invasive methods include seismic simulation or the use of ground penetrating radar. Although ground-penetrating radar is relatively well developed it can still produce images, which may be difficult to interpret.

Previous work by one of the authors [2] suggested that ultrasonic monitoring of drilling had potential for ground condition monitoring. This paper discusses some important factors needed to develop this method as a viable engineering technique for the future. The early stages of this research have been focussed on the ability to characterise the grain size of a granular geo-technical composite material (sand). The drilling operation has been simplified and is provided by a designed probe, which allows optimisation of surface interactions to increase the acoustic output required for data acquisition. The frictional process which generates the ultrasound, involves the interaction of the probe and the sand. It is known that, material properties, contact loading and sliding velocity affect frictional interactions. By using the known material properties of the probe, recording the load and sliding velocity and utilising acoustic signal parameters it is hoped that a unique relationships can be determined to characterise the material properties of the granular composite. The following sections will discuss a further development in the technique of using acoustic emission to monitor changes in the "zone of frictional contact" without having to stop the friction pair [4]. Research in this field has mainly been directed at determining failure of solids subjected to frictional forces (associated with tool life, bearing failure etc)[5]. This work uses similar principles, but monitors unorthodox friction pairs with a view to detecting physical changes of material type and not the mechanical deformation of a specific material.

THE PROBING SYSTEM

The probing system consists of a probe of fixed geometrical dimensions. The system provides a constant probe-particle contact area. The probe is set to rotate, while being progressively submersed into the granular medium at a constant feed-rate until reaching a specific depth (simulating a typical drilling process). Angular velocity is recorded simultaneously with load and acoustic emission type "count rate". The samples of granular material were initially, graded in different particle size ranges and were all contained within the same container, providing similar test conditions. The interaction between the probe and the granular material develops a frictional force. As a result stress waves are created within the probe shaft and the ultrasonic signal is recorded via a transducer mounted on the shaft, using suitable coupling devices. A change in the granular material will provide a different "friction pair" producing a change in the ultrasonic signal. By recording the changes in the ultrasonic signal it is hoped to provide information characterising the probed "drilllee".

For all experimentation, sand with controlled grain sizes has been used. In this case the sand is dry and can be considered non-cohesive (where the shape of the bulk material is determined by the surrounding boundaries i.e. container walls etc). Although a granular material can exhibit both fluid and solid characteristics, these materials behave very differently and can be considered a form of composite material [3].

Studies of granular materials have mainly been focused on the general physical properties of the materials and their behaviour under typical dynamic conditions such as internal interactions between neighbouring particles and flow along solid surfaces [3,6-9]. This research, currently involves granular dynamics because the experimental system uses a dynamic solid interaction with an initially static granular medium. Shear deformations are a result of external loads, produced by the vertical displacement of the

probe. There will also be induced flow between the rotating probe and the static sub-surface layers of the granular medium due to the inertia forces generated by the probe-granular interaction. Therefore, it is not clear how, or if, the study by Sarychev and Shchavelin is directly relevant to the more complex engineering system considered in this work. Due to this, any relationships are being investigated empirically since the problem is currently too complex for direct mathematical analysis.

SYSTEM PARAMETERS

Within the probing system there are a number of parameters that have to be considered. Changes in load and angular velocity, yield large changes in the frictional forces between the granular material and the probe thus affecting the acoustic output. Previous research in granular physics describes how an ensemble of granules in a container produces a random network of forces due to granule geometry and contact forces between granule-granule contacts and granule-boundary contacts [3,6,8]. The random nature of the granule ensemble produces a complimentary random pressure distribution. Therefore it is difficult to duplicate tests with the same loading conditions. When probing, the granular medium will deform, thus changing the structure of the granule ensemble producing a change in the pressure distribution. This provides fluctuations in the load signals, along with an inherent change in the angular sliding velocity, whereby increased loads reduce probe speed. Further clarification is needed to identify the effects of load and angular sliding velocity before it is possible to determine grain size.

Probing depth may also be an important parameter. However, as the shaft is acoustically insulated, the contact area between the granules and the probe will remain constant so that the only possible change would be due to changes in probe force as the depth increases. Although a granular system may display similar characteristics to a fluid, it does not inherit similar qualities associated with a pressure-head. The static pressure is not proportional to depth because point contacts between grains and the container walls aid in supporting the weight of the granules, which is analogous to the mechanics of an arched bridge. However, when the probe is penetrating the granular medium the load increases with depth (because material displacement must occur for the probe to penetrate). In order for this to happen the volume of the granular material must increase, and because of geometric constraints the only dimension that can change is the height. Therefore at larger depths there is more granular matter to displace thus yielding larger forces. If penetration stops, the deformation and volume change will stop, thus relieving the forces applied to the probe tip. However, due to the random nature of the pressure distribution within a granular medium it is difficult to determine a direct linear relationship with repeated tests.

Research utilising ultrasonics [4] to monitor friction contact zones between solids, provides theory relating acoustic power or "count rate" to a set of parameters involving the physical interactions within the contact zone. These parameters are; normal load, angular velocity, generalised elastic modulus, area of contact, surface asperity tip radius and surface profile. The load and the angular velocity are the only two parameters that are not a material property of the friction pair. Therefore, by determining the effects of the load and angular velocity with respect to the ultrasonic signal, a relationship can be obtained relating the ultrasonic signal to the bulk material parameters within the friction

contact zone. Initial tests assume the wear of the probe is small, due to the small loads used and therefore the material properties of the probe remain constant and any change in the output signal will be attributable to changes in the granular material being probed.

EXPERIMENTAL RESULTS

The paper by G.A.Sarychev, V.M. Shchavelin [4] focuses on the ultrasound generated due to friction between solids as a result of elastic deformation where the "count rate" is used as the acoustic parameter. The presented experimental work also uses the "count rate" as a suitable acoustic parameter. By doing this it will be possible to compare experimental results to the work by Sarychev and Shchavelin to determine if there are any associated similarities with their theory.

The first set of experiments used a constant grain size and the same probe for each test to minimise changes in the material properties during their interaction. Therefore, it is assumed that the change in the acoustic signal will result from changes in the load and the angular velocity.

Tests using a rotating probe penetrating at 50mm/minute showed that the load range was between 0-8N. It was also noticed that increased loads reduced shaft speeds. However, by reducing the feed rate the change in the angular velocity was also reduced. Therefore, by using a feed rate of 10mm/min it was possible to obtain results up to a range of 6N with only a small deviation in the angular velocity.

Figure 1 is a typical plot of the count rate against the load using a constant angular velocity and the electronic threshold set at 0.15v. From repeated tests a linear relationship was obtained whereby different velocities yielded different gradients and the y-axis intercept was dependent on the threshold setting. Although a direct relationship could not be established, the results indicated that the "count rate" is proportional to a function of the angular velocity multiplied by the load.

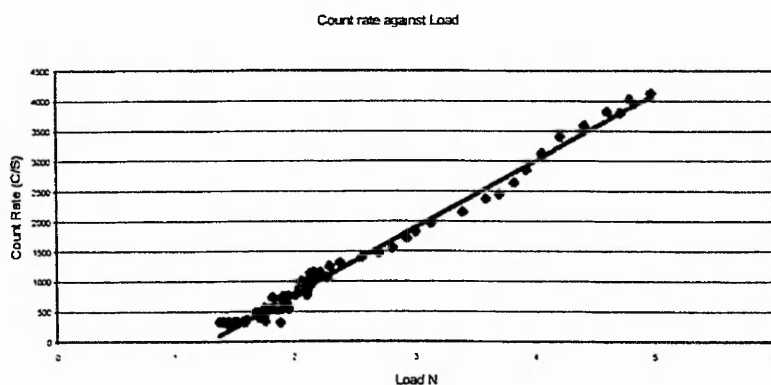
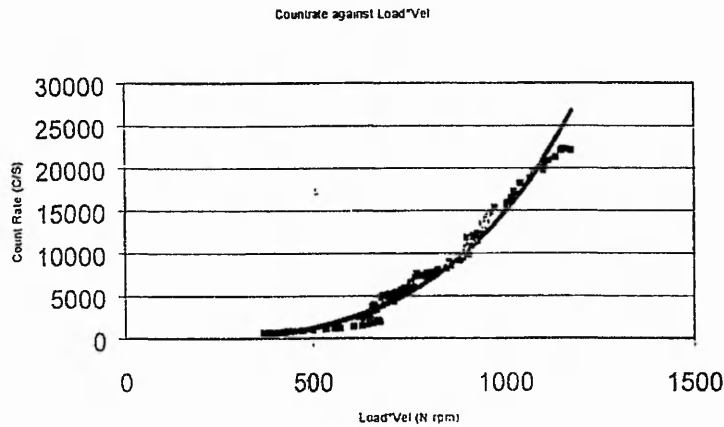


Fig 1. Typical plot of Count Rate against Load using a constant angular velocity and threshold setting

The second set of tests examined the variation of count rate against load multiplied by the angular velocity (fig 2). The results show the relationship resembles a power law function and is similar for repeated tests. The theory from reference [4] states that in most cases for different materials in contact, the dependence of the count rate 'N' on

sliding velocity generally follows the form, $N=A+BV^X$, where A and B are constants and the index $X \geq 1$. Repeated experiments gave similar results. However, the scatter of the count rate about the function line can at times be quite large and may present difficulties when trying to develop a real time system for characterising the granular material.



(Fig 2) A typical plot of Count Rate against Load*Angular velocity

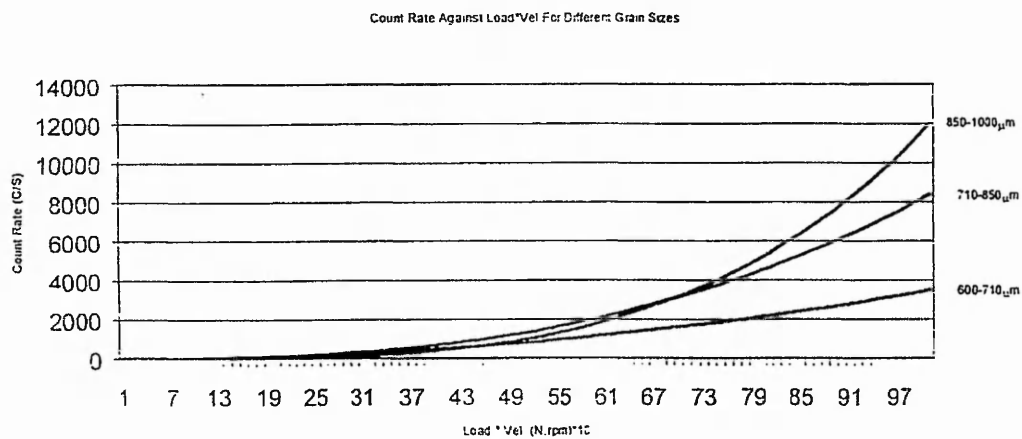


(Fig 3) Count rate against Load*Velocity using different grain sizes and the functions generated from their actual data plots.

Data was analysed to investigate the variation of count rate against the quantity “load multiplied by angular velocity” for different grain sizes. Each curve obeys a power law, related uniquely to grain size (fig 3).

CONCLUSION

The results provide evidence that ultrasonic monitoring of drilling has potential for use as a tool for ground condition monitoring. Ultrasound provides a sensitive method for detecting changes in the "drillee". By examining the whole probing cycle it is clear that the changes in the material characteristics within the frictional contact zone can be detected. It has been noted that each granular material at a given load and angular velocity combination will yield a unique output. However, developing this into a practical real time system will require a means of reducing the spread of the count rate around the function line as large outliers can produce erroneous results. Further investigation into the effects of loading and rotational speed is being undertaken. The ultrasonic signal at a certain load and angular velocity appears characteristic of a particular material being drilled, which, for this study, can be related to the grain size of the material.

References

- [1] P. Sharpe; Formation Assessment for Maintenance and Renewals Planning; "Total Route Evaluation" Proceedings of the 2nd International Conference on Railway Engineering, London 1999
- [2] R. Hill; Confidential consultancy report. (1997)
- [3] Heinrich M Jaeger, Sidney R. Nagel and Robert P Behringer; The Physics of Granular Materials, Physics Today April 1996 pp 32-38.
- [4] G.A.Sarychev, V.M. Shchavelin
Acoustic Emission Method for Research and Control of Friction Pairs
Tribology International, 24,1,(1991) pp11-16
- [5] S.T.S.Bukkapatnam, S.R.T.Kumara, A.Lakhtakia
Analysis of Acoustic Emission Signals in Machining
ASME Journal of Manufacturing Science and Eng, Nov1999 pp568-577
- [6] I.Lsinger, H.M.Pollock(eds.), Friction of Granular Non-Metals
Fundamentals of Friction: Macroscopic and Microscopic Processes pp183-207
- [7] J.T.Jenkins, M.Y.Louge
Dense Inclined Flows: Theory and Experiments Final Report, Dec 1995
- [8] T.Matthey, J.P Hansen
Molecular Dynamics Simulations of Sliding Friction in a Dense Granular Material, Modelling simul. Mater. Sci. Eng 6 (1998) pp701-707.
- [9] I.Lsinger, H.M.Pollock(eds.),
Particle-Particle Interaction in Granular Material,
Fundamentals of Friction: Macroscopic and Microscopic Processes pp95-110